2007

Characterization and analysis of hybrid electronic materials for molecular based devices

Sathish Thiruvengadam
Louisiana State University and Agricultural and Mechanical College

CHARACTERIZATION AND ANALYSIS OF HYBRID ELECTRONIC MATERIALS FOR MOLECULAR BASED DEVICES

A Thesis

Submitted to the Graduate Faculty of the
Louisiana State University and
Agricultural and Mechanical College
in partial fulfillment of the
requirements for the degree of
Master of Science in Electrical Engineering
in
The Department of Electrical and Computer Engineering

by
Sathish Thiruvengadam
B.E, Bharathiyar University, India, 2002
August 2007

To my parents and elder brother,

Arthanariswamy Thiruvengadam,

Puspha Thiruvengadam,

Venkatesh Thiruvengadam

ACKNOWLEDGEMENTS

I would like to extend my thanks to Dr. David Janes, Dept. of ECE, Purdue University, Indiana for his suggestions and support.

I extend my cordial thanks to Mr. Golden Hwaung of the Electronic Material and Device Laboratory (EMDL) in Dept. of Electrical and Computer Engineering for inspiring me to learn from circumstances and helping me in the lab. I am also grateful to my fellow students in the EMDL for the camaraderie and support you all have given to me.

Special thanks to Dr. Tom Contine, Founding Director of Andonie Sports Museum, LSU Alumni Association, for being my surrogate family here in Louisiana. I thank for all the love and emotional support you have given me during these years at LSU. You have always been there when I needed someone to vent to and when I needed a sounding board. Dr. Tom took great care of me and has considered me as a part of his own family. I am greatly indebted to him for the rest of my life. I also thank all my friends, who have helped me directly or indirectly on several different occasions.

I thank my parents and my brother for their unwavering encouragement and support through these years. Thank you for instilling in me a love of learning and for always encouraging me to do my best in whatever I tried. Above all I thank God, who has been my marshal and light all these years and will be in my future endeavors.

TABLE OF CONTENTS

v

LIST OF TABLES

LIST OF FIGURES

ix

xi

ABSTRACT

The goal of this work is to characterize and to analyze hybrid electronic materials (HEMs) using fluorescence (FL) spectroscopy and conductive probe-atomic force microscopy (CP-AFM) in order to investigate the electrical and optical properties of these materials. Currently, research efforts to characterize novel organic materials for the determination of molecular level transport properties are of great interest.[6] One of the most interesting organic materials is the porphyrin molecule, which exhibits behavior useful for memory applications.[4] Colloidal CdS quantum dots (Q-CdS) capped with *dioctyl sulfosuccinate* (AOT) and thiol functionalized porphyrin molecules are explored for their potential application to next-generation hybrid electronic systems. Q-CdS capped with AOT self-assembled on various substrates are used to study the effect of electron transport in colloidal quantum dots using FL spectroscopy. In turn, porphyrin molecules chemisorbed onto gold surfaces are used to study the phonon-electron interaction in these molecules due to their metal cations. Maximum fluorescence intensities are obtained at specific angles of incidence, such as 80° and 45° with respect to the sample, for Q-CdS and porphyrin molecules, respectively. Emission spectra of Q-CdS adsorbed onto different substrates such as gold, GaAs, and mica show a slight but systematic redshift of peak characteristics of spatially confined phonon interactions. The effects of relative quantum dot size, different substrates, and light intensity are discussed in this thesis. As the relative sizes of the quantum dots decrease, the excitation peaks are slightly blue shifted. In order to study the electron transport mechanism of a single or a few molecules in metal-molecule-metal heterostructures, the electronic characteristics of self-assembled monolayers (SAMs) of n-alkanethiols such as hexanethiol and octanethiol are investigated using CP-AFM. SAMs of alkanethiols on gold surfaces have been shown to form stable surface structures.[21] Studies have

shown that thiolated porphyrins readily self-assemble on gold surfaces.[73] The *I-V* characteristics of self-assembled monothiolated porphyrin molecules on gold substrates are measured under ambient conditions. *I-V* traces of porphyrin molecules behave sigmoidally according to the Simmons Equation for square barrier tunneling and illustrate that the electron transport mechanism through porphyrin is direct tunneling for the applied bias levels in this study.

1. INTRODUCTION

1.1 OVERVIEW OF HYBRID ELECTRONICS

Nanotechnology, from the viewpoint of solid-state electronics, is a field in which the fabrication of a device can be approached from two different methodologies—"top-down" or "bottom-up" (Figure 1.1 & 1.2). In the former approach, the drive is to retain the macroscopic properties of the materials involved while shrinking toward ever diminishing device geometries. The latter approach attempts to control individual molecules or other quantum-level structures, during the course of fabrication, for likewise realization of device functionality. This consideration of individual molecules, or assemblies thereof, has led to the use of new materials, both organic and inorganic, in this bottom-up form of fabrication. As a result, an entirely new class of nanoscale electronic structures and devices is currently under development, which themselves have created the field of *hybrid electronic materials* or HEMs.[1-3] In this thesis, we will discuss a selection of HEM structures, their characterization, and their propensity for future nanoelectronic development.
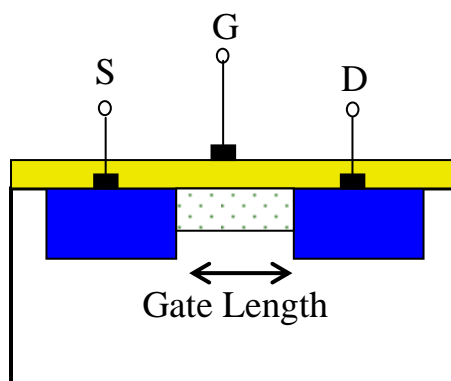
Figure 1.1: Top down methodology of fabrication showing source(S), gate (G) and drain (D) terminals in CMOS technology
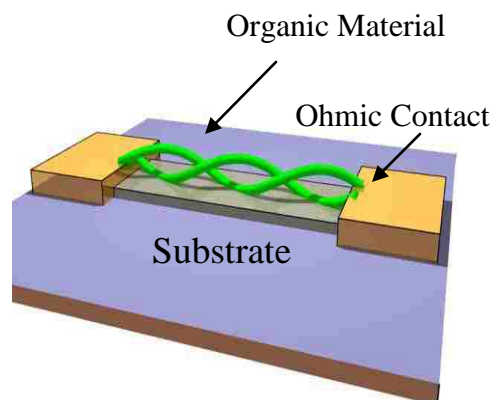
Figure 1.2: Bottom up approach utilizing self-assembly process to build molecular devices (The Harvard College – Nanoscience Program).

To begin to put this concept of HEMs into perspective within the ubiquitous realm of solid-state electronics and devices, imagine a wire in which the presence or absence of a single atom determines its electrical conductivity or a system of molecules wherein a biomolecular recognition process enables new pathways for conductivity. Now combine this molecular "system" with the now traditional inorganic semiconductor materials and metals in such a way as to be able to address these conductive pathways in an electronically useful manner (i.e.-rectification). Combinations of these, and a host of other equally diverse metal-molecule-semiconductor systems, are the fundamental components of an HEM-based, otherwise known as a *molecular electronic* (or "moletronic") structure. These unique organic-inorganic systems are opening doors to heretofore unthinkable possibilities in the nanoscale electronic arena.[4]

However, until fairly recently molecules have not played a historically prominent role in electronic devices. In fact, it was only about ten years ago that chemical applications were limited to the use of small molecules, such as silanes and germanes, as thin film precursors or as components of fabrication processes, packaging materials, and other secondary or tertiary steps.[5] Moreover, from the mid-20th century onward, the application of fundamental solid-state physics and the development of microelectronic device engineering ushered in the era of integrated

2

circuits which continues to this day. In the process, inorganic insulators, semiconductors, and metals became the basis for electronic devices and thus the microelectronics industry as a whole. Therefore, one may find little opposition to the description of molecular electronics (and the study of HEMs within it) as an emerging technology, "still in its adolescence."[6]
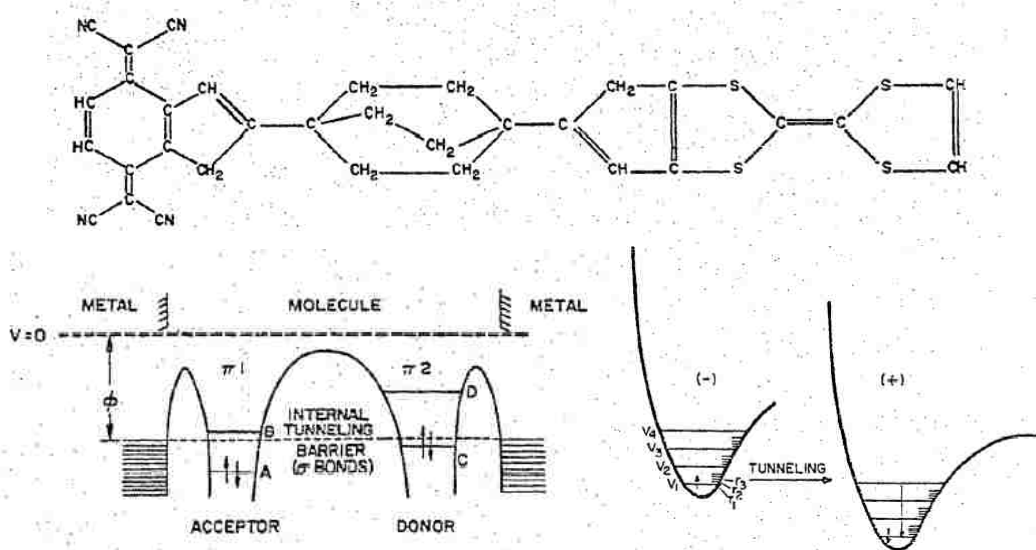
Figure 1.3: An example of a rectifying molecule, energy versus distance diagram and internal tunneling in the molecule is shown. Reprinted with permission (Appendix A1)

Yet, as with most adolescents, growth comes quickly, sometimes painfully, sometimes sporadically, but comes nonetheless, and molecular electronics is no exception. For decades, researchers in the biological and chemical sciences have studied how tasks are performed by organic molecules within biological systems, such as the storage and transfer of both energy and electrons. An early, and now considered seminal attempt to bring the aforementioned concepts to the realm of electronic devices is found in the 1974 publication by Aviram and Ratner.[7] Their work laid the foundation for the first serious consideration of using single molecules as the active elements in hybrid electronic structures. Effectively, their work was a starting point for the discussion of the molecular nature of "electronic" materials compared to the established

3

understanding of condensed matter material properties. Aviram and Ratner envisioned the idea of "molecular rectifiers"[7] which is distinct from the modern applications of organic/hybrid electronics based on bulk materials. This paper discusses theoretically the possibility of constructing a very simple hybrid electronic device, a rectifier, based on the use of a single organic molecule (Figure. 1.3). However, as was quickly realized, true molecular rectification is highly non-trivial, and their concept was indeed a brave proposal for its time.[8]

The Aviram-Ratner model was probably the first comprehensive, albeit theoretical, example of unimolecular quantum transport and its applications. However, it was also intimately connected with other electron transfer theories and related experiments which had already been (and were still being) successfully developed in parallel. In fact, the first charge and energy transfer studies in molecules actually began in the 1940's by Robert Mulliken and Albert Szent-Gyorgi in relation to the so-called donor-acceptor systems.[7,9] Charge transfer was made tangible by the proposal of Aviram and Ratner in 1974 to use a Mulliken-like electron donor-acceptor molecule as a molecular diode, generalizing *molecular conduction* into *molecular electronics*. Thus, work of this nature began to answer the call by Feynman[10], in his famous 1959 lecture "*There's Plenty of Room at the Bottom,*" for chemists, engineers and physicists to unite to build structures from the molecular level up. In short, the theory of "molecular rectification" was influential in turning the attention of researchers to the possibility of engineering single molecules to function as elements in information-processing systems.

Fundamental to all of the aforementioned is the study of those "materials" which might be used to construct a molecular electronic device. Therefore, with interest remaining steady in the course of time, particularly brisk progress in HEMs has been made in the last decade owing to successes on the experimental front.[11] More sophisticated tools such as scanning tunneling microscopy (STM) and atomic force microscopy (AFM) have enhanced the ability of HEM

4

researchers to image and to contact single molecules. On the "electronics front," we can now obtain current-voltage characteristics which may be used to determine molecular functionality and the potential for electronic device development.[12-16] No longer just a scientific curiosity, molecular electronics in general (and HEMs in particular) has been the driving force behind one of the most exciting interdisciplinary efforts in nanosciences.[17] It embraces many traditional disciplines, such as materials science and chemistry, but fundamentally relies and is built upon electronic device characterization, a mainstay of physical electronics and electrical engineering research. Yet beyond the frenzy of research excitement of late (Figure. 1.4), one may still ask, "Why do we need hybrid electronics, and what makes quantum transport at these length-scales so challenging?" The answer to the first part of this question is motivated by the technological needs forced by the exponential miniaturization trend of traditional semiconductor-based electronics. The now ubiquitous Moore's Law[18] is the metric by which this trend has been monitored since the 1960's. This "Law" clearly indicates the need for research into alternative means by which to meet ever-increasing technological and consumer - driven demands made of electronic systems.

Although HEMs and molecular electronic devices should, by no means, be considered "replacements" or the final answer to the question of "what next" beyond Moore's 2020 prediction, these materials show promise for playing an effective and necessary niche role in terms next-generation nanoelectronics.[6] The answer to the second question is a bit more complex, yet nonetheless "measurable" in terms of successfully reached milestones. In spite of the various challenges, molecular electronics thrives due to the series of fundamental issues it poses and which continue to reveal sound answers through active research. Of these, one of the most important has been the reproducible manifestation and observation of quantum transport when electrons transverse a single molecule at a constant rate.[20] In fact, these quantum-level

observations and how they are influenced by the external environment (i.e.- electric field, air, temperature) exemplifies the essence of nanoscale HEM research—that is, what happens when the truly small joins the truly large—and is at the heart of this materials characterization-based thesis.
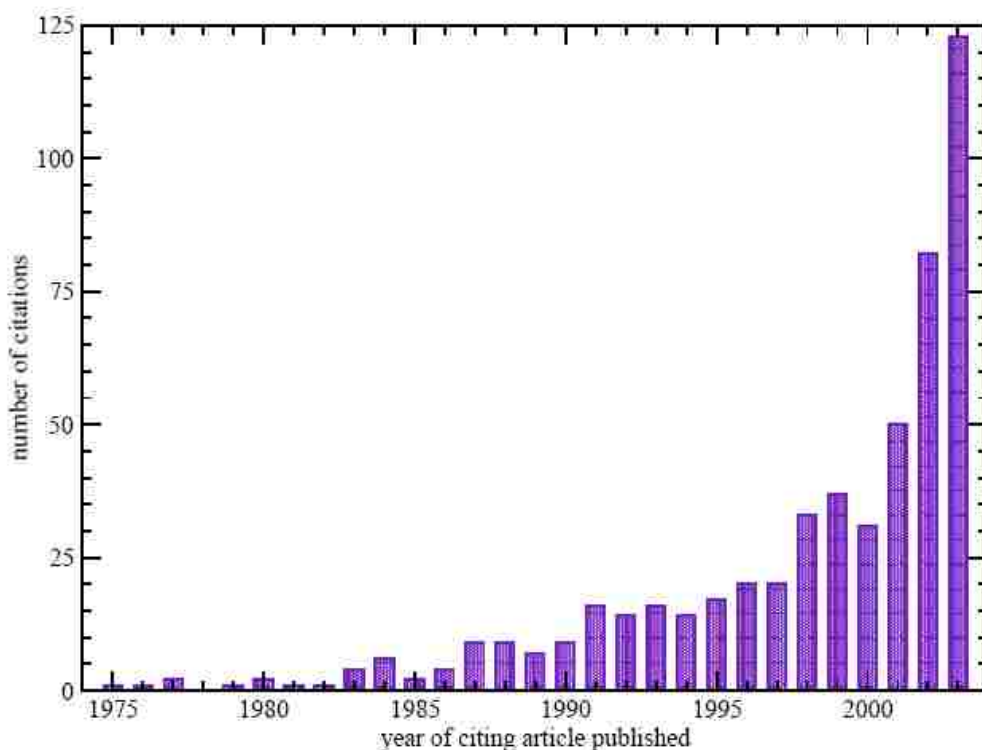
Figure 1.4: An indicator of the evolution of molecular electronics is provided by the number of citations per year to the seminal Aviram-Ratner study[7] during the last three decades[8] . Reprinted with permission (Appendix A2)

Finally, our work in HEMs is built upon a range of milestones, some of which have been already discussed, dating back to the 1920s. These "markers" along the path of using combinations of organic and inorganic materials for the realization of electronic device functionality are described, in summary, in Table 1.1. Of particular note are the characterization of n-alkyl thiol monolayers on gold[21], optical properties of colloidal CdS quantum dots[22], metal-

molecule junctions and charge transport across monolayer molecules[23], effect of light irradiation on molecules as photodiode[24], charge retention capability of organic molecules as molecular memory cell,[25] and the study of electronic properties of a molecule when it is wired in a circuit[26]. Within the last fifteen years or so, we have had a resurgence of unimolecular electronics. With the help of direct measurements of electronic behavior of single molecules or Langmuir-Blodgett (LB) monolayers which are known as "self-assembled monolayers" (typically thiols on gold), the study of single molecules is made tangible. Finally, we are able to "touch" molecules! The key to success was to touch a molecule either by a scanning tunneling microscopy (STM) tip, by a conducting atomic force microscopy (AFM) tip, or by making delicate sandwiches between inorganic metals and organic monolayers (or self-assembled monolayers) that do not "fry" the organic layer.

1.2 RESEARCH GOAL AND THESIS OVERVIEW

The goals of the research presented in this thesis are as follows:

1. To focus on understanding electron transport through a single molecule or a few molecules at a time.

2. To study the electrical conductivity through organic molecules using conductive probe atomic force microscopy (CP-AFM). The force on the molecule and the distance between the tip and the substrate is controlled using AFM.

3. To determine the electrical and optical properties of hybrid electronic materials suitable for nanomolecular based electronic devices.

In chapter 2, a historical perspective as well as discussion of background theory and characterization methods for self-assembled monolayers (SAMs) is given. This chapter brings the work of this thesis into context with the current state of the art of molecular-scale electronics. The foundations of hybrid electronics are examined, including tailorability of

molecules (both synthetic and surface chemistry), current transport mechanisms, experimental

methods, and analytical characterization of hybrid materials as potential electronic components.

Table 1.1: List of historical timelines and milestones in the field of hybrid electronics.

Timeline	Historical Milestones
1928	Theory of the alpha decay of a nucleus via tunneling by George Gamow
1940s	Study of charge transfer in molecules with respect to "donor-acceptor" systems by Robert Mulliken and Albert Szent-Gyorgi
1944	Electron Spin Resonance, first observed in Kazan State University by the Soviet physicist Yevgeniy Zavoyskiy
1950s	Bernanose and coworkers first produced electroluminescence in organic materials (OLED) by applying a high-voltage alternating current (AC) field to crystalline thin films of acridine orange and quinacrine.
1959	"There is plenty of room at the bottom" by Feynman
1965	Moore's Law - The number of transistors on an integrated circuit for minimum component cost doubles every 24 months by Gordon Moore
1974	Molecular Rectifiers based on a single organic molecule by Avi Aviram and Mark Ratner
1978	Single chain amphiphiles such as alkyl phosphates, alkyl sulfates and fatty acids can self-assemble into bilayer membranes if they contain 10 or more carbons in their hydrocarbon chains discovered by Hargreaves and Deamer.
1981	Scanning probe microscope invented by Gerd Binnig and Heinrich Rohrer at the IBM laboratory in Zurich.
1988	Theoretical prediction of single molecule field effect transistor by Avi Aviram
1990's	Semiconductor quantum dots, break junctions, nanowires, carbon nanotubes, nanopores.
2000's	Organic thyristor, molecular memories, molecular switches, molecular photodiode, conductive atomic force microscopy

In chapter 3, characterization of the optical properties of hybrid electronic materials

such as functionalized colloidal cadmium sulfide quantum dots and porphyrin based-molecules

using fluorescence spectroscopic measurements are discussed. A brief background theory of

fluorescence spectroscopic techniques is given. The results of the fluorescence measurements on these hybrid materials are provided, followed by conclusions, and suggestions for future research.

In chapter 4, the study of electron transport through porphyrin based molecules using conductive probe-AFM is discussed. An overview of AFM as well as some background theory of contemporary work involving conductive – AFM is provided. Results of electron transport mechanism through alkanethiols and porphyrin based molecules are presented, followed by conclusions, and suggestions for future research.

2. BACKGROUND THEORY AND MECHANISM OF SELF-ASSEMBLED MONOLAYER (SAM) CHARACTERIZATION

2.1 HISTORICAL PERSPECTIVE

An understanding of the place of self-assembled monolayers (SAMs), as studied in this thesis and in the field of hybrid electronics in general, begins with a look at a novel electronic device concept from the mid 1970's. At that time, during the early development of integrated circuit technology, an intuitive work by Aviram and Ratner presented the idea of using molecules to carry out tasks normally reserved for solid-state electronic devices, such as energy storage and charge transfer. As per their proposal, a simple rectifier could be created using a single organic molecule.[7] This *molecular rectifier* consisted of both donor and acceptor pi bonded systems separated by a sigma bonded tunneling bridge. The response of such a molecule to an applied electric field, along its axis, would not allow current to bypass equally well in one direction as in the other—thus exhibiting a nonlinear rectifying behavior. Although intriguing, Avarim and Ratner's "device" would remain a theoretical concept for the next twenty years, while over the next quarter century innovations in processing techniques created higher density, smaller feature sizes, and ultimately faster silicon-based transistors.

With the development of "traditional" (inorganic semiconductor based) electronic devices and circuits, and concurrently, the Moore's Law driven race to decreasing dimensions, breakthroughs in methods by which to better resolve smaller feature sizes also emerged. These methods, which included the invention of scanning tunneling microscopy[27] (STM) in 1981 and powerful variations such as atomic force microscopy[81] (AFM), provided the means by which work in the single-molecule domain could be realistically considered. It was, in fact, the development of characterization techniques, possibly even more than the creation of any

particular device, which set the stage for work beyond Avarim and Ratner's original concept.

Nonetheless, after the mid-seventies, several variations on the theme of molecular-based electronics emerged from the study of purely molecule-to-molecule electronic transport mechanisms to more hybrid (organic-inorganic) combinations of submicroscopic and nanostructured materials and devices. Concurrent investigations by chemists, physicists, materials scientists, and of course, electrical engineers, make it challenging to specify a chronological timeline for the discoveries that have led to the use of SAMs. However, there are certain milestones common to the interdisciplinary research efforts that eventually combined to form the field of hybrid electronics. These notable discoveries, as considered from the electrical engineering perspective, were briefly discussed in Chapter 1.

Currently, there is significant interest in the synthesis of novel hybrid submicroscopic or nanostructure materials due to large differences found in their properties, which could, in turn, lead to new technological applications. These materials, of which SAMs are a significant part, have great potential for addressing some basic issues about dimensionality, space-confined transport phenomenon, and applications. In the next decade or two, molecules might be increasingly used not only as precursors for bulk electronic materials but also as the active electronic components. Motivating this is the fact that the current very large scale integrated circuits paradigm, based on CMOS technology, is difficult to extend to ultra-dense integrated circuit feature sizes smaller than 10 nm. This is mainly due to the sensitivity of silicon field-effect transistor parameters and the high cost of fabrication. A potential complementary process to CMOS technology is hybrid electronics, where molecular-based circuits are fabricated using hierarchical assembly processes. Molecules by their nature operate at the nanometer scale in which individual atoms and functional groups can be controlled through synthetic chemistry. As such, it is important to study the characteristic properties and the conduction behavior of

molecules and small clusters while searching for a device in which quantum mechanical phenomena are the basis for operation instead of a detrimental side effect. Moreover, making molecular-scale electronics into a functioning structure will demand revolutions in circuit architecture, design, and fabrication technologies along with a deep understanding of conduction and electronic interactions in single molecules. The aforementioned criteria are, in fact, the major motivation behind the field of molecular-scale electronics[29].

Finally, from these multi-dimensional beginnings hybrid electronic materials (HEMs), specifically where SAMs are involved, are the basis for many of today's molecular electronic devices. Various electronic device applications have been already designed and synthesized that have electronic characteristics tailored for applications in bulk devices.[6] In this work, the critical study of molecular transport phenomena is based upon an understanding of hybrid configurations involving SAMs and the materials upon which these monolayers are formed (to be discussed.) On that note, the discussion that follows will address the fundamentals of SAM based phenomena.

2.2 SELF-ASSEMBLED MONOLAYERS

Self-assembled monolayers (SAMs) are ordered molecular structures formed by the adsorption of an active surfactant on a solid surface (Figure 2.1). Taking advantage of intramolecular, intermolecular, and interfacial forces, it is possible to design ordered 2D and 3D polymolecular architectures. For reproducibility, atomic level flatness (or as close as possible) is needed for the base of support upon which the monolayer forms. For this reason careful selection and preparation of the substrate is very important. Once a flat substrate surface is achieved, then atoms and molecules can attach to surfaces in two ways—physisorption (physical adsorption) or chemisorption (chemical adsorption).
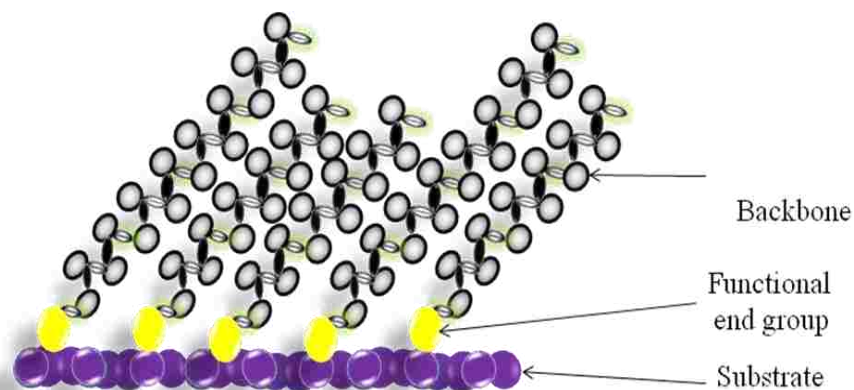
Figure 2.1: An array of molecules self-assembled on a flat substrate surface.

2.2.1 Physisorption

Physisorption is the adhesion (also called adsorption) of a thin layer of molecules to a surface without the formation of a chemical bond, either molecule-molecule or molecule-substrate. The binding is mainly due to the interplay of weak attractive forces (predominantly Van der Waals and electrostatic which exist over long ranges) and hard core repulsions. Physisorption is an exothermic process, and its enthalpy can be measured by monitoring the rise in temperature of a sample with known heat capacity during the process of adsorption or desorption of the adsorbate. The enthalpy of physisorption is low (approximately 20 kJ/mol), and this small enthalpy change is insufficient to cause bond breaking. So a physisorbed molecule retains its identity, albeit perhaps distorted by the surface. Physisorption is a reversible process, and the adsorption involved can also take place in multilayers. We have used samples of physisorbed molecules both on conductive and insulating substrates in this thesis as will be discussed in Chapter 3.

2.2.2 Chemisorption

Chemisorption is the adsorption of molecules to a surface through the formation of a chemical bond, as opposed to Van der Waals forces. The type of interaction is strong; covalent

bonds form between adsorbate and surface. The enthalpy of chemisorption (ranging from 50 kJ/mol to 800 kJ/mol) is higher than that of physisorption.
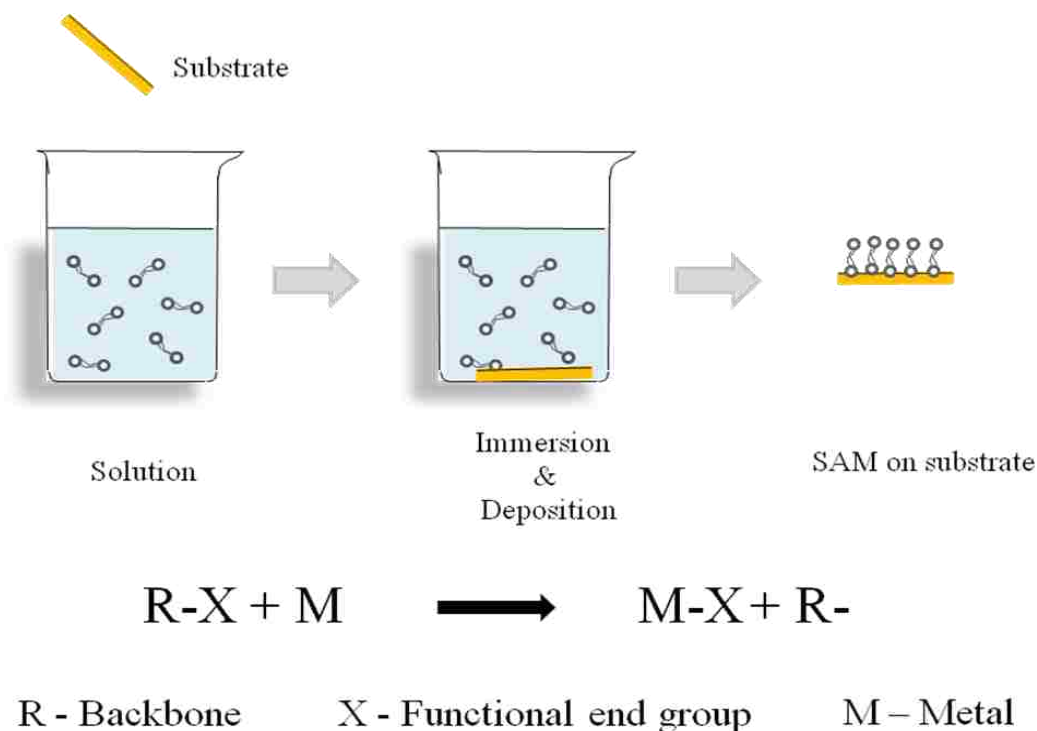
Figure 2.2: A schematic representation of self-assembly of molecules by immersing a substrate (e.g. metal – gold) into a solution of the surface-active material consisting of backbone R and functional group X. The end group reacts chemically with the metal and the material, spontaneously forming a 2D assembly.

SAMs can be formed spontaneously by immersing an appropriate substrate into a dilute solution as formed by dissolving an active surfactant into an organic solvent. This method is shown in Figure 2.2. (Another method involves sublimation of the molecular adlayer in vacuum but is beyond the scope of this thesis.) SAMs will spontaneously orient toward the substrate surface and form an energetically favorable ordered layer while the surface active head group of the molecule chemically reacts with and chemisorbs onto that substrate (Figure 2.3). By this process different types of SAMs can be created such as organosilicon on oxidized surfaces, alkanethiols on Au, Pt, GaAs; colloidal quantum dots of CdS on Au; and porphyrins on Au.[4, 30-35]

14
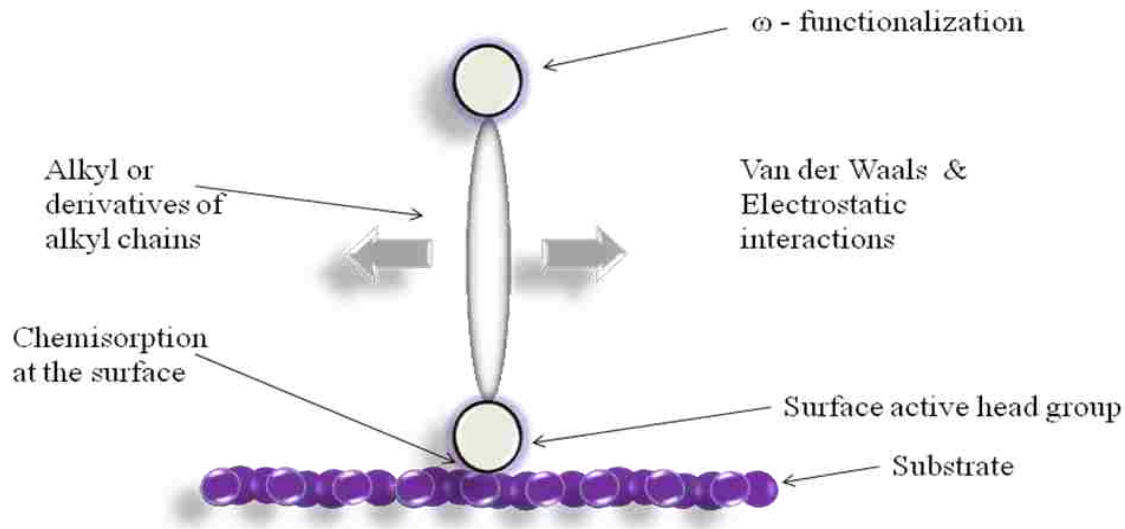
Figure 2.3: A schematic showing chemisorption reaction of a surfactant on a substrate.

2.2.3 SAM Formation and Utilization

In order to best understand how to exploit the process of chemisorption for the formation of SAMs as they apply to hybrid electronic materials and devices, a deeper look into the self-assembling surfactant molecule itself is needed. The latter is typically composed of three (3) parts as follows:

1. A head group enhances chemisorption to the substrate (exothermic process) and anchors the molecule to the substrate surface. The strong molecule-substrate interactions result in attaching the head group to a specific site on the surface through chemical bonding. This is the molecular equivalent of an alligator clip. The bonding can be covalent (e.g. Si-O-Si on oxidized surfaces), covalent and slightly polar (e.g. Au-S for alkanethiols on gold), and ionic. Due to substrate-head group interaction, molecules try to attach to every available binding site on the surface and tend to pack in one beside the other.

2. Alkyl or alkyl derived chains play a vital role in the packing density of the molecules. Short-range dispersive Van der Waal forces become effective when the distance between

15

adjacent molecules is very small. In turn, the molecules tend to reorganize due to these interactions between the alkyl chains. If the alkyl chain is substituted with any other polar bulky function, then long-range interactions are predominant.

3. Omega (ω) – functionalization is the terminal end group which opens up the possibility of successive anchoring or chemical reactions.

These three components are the basis for the chemisorbed SAM structures as studied in the work of this thesis.

While there are various potential self-assembling alligator clips, one of the most common and well characterized uses sulphur as the headgroup for thiolates (R -S$^-$) adsorbed to Au(111) surfaces.[36,37] Implementation of molecular-scale electronics depends upon being able to address individual or small numbers of molecules. The key issue is to find a way to assemble molecules in a repeatable fashion and develop methods to test these molecules. To resolve individual molecules electronically, one has to attach electrodes on either side of the molecules. One way of establishing the contact between the molecule and the electrode is self-assembly. The ability to position and to pattern molecules selectively on a surface with molecular precision is an important factor to be considered. This simple process with its intrinsic error-correction advantage makes SAMs inherently manufacturable and thus technically attractive and cost-effective. In addition, SAMs can be designed and engineered to provide extremely high functional density. On the other hand, in order to perform highly complex functions as those of current integrated circuits, a self-assembly strategy that enables easy formation of complex patterns to "program" the structures and (electrical) properties of materials at nanometer levels needs to be developed.

Conformation and monolayer assembly of pentiptycene-derived α, ω-alkanethiol has been reported, and the relative inter-chain interaction and packing densities depend on the

conformation of the molecules.[35]   In the deposition process of self assembled monolayers (SAMs), orientations of molecules are solely random. The orientation of the molecules depends upon various issues. The thiol (-SH) group is attached to the Au (111) surface, and the alkyl (-CH) group is on the top surface, i.e. the SAM is terminated by an alky group. In alkanedithiols three different orientations are possible depending upon the bonding between the thiol and metal surface, shown is Figure 2.4.
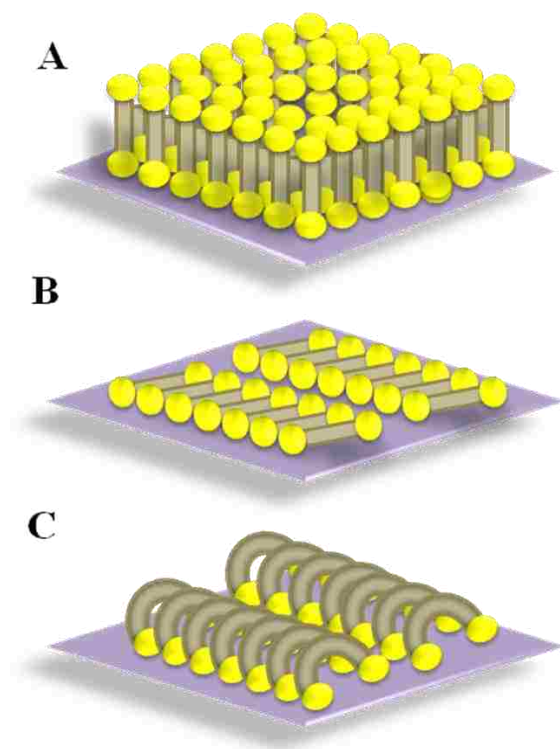
Figure 2.4: Schematic representation of three distinct orientations of alkanedithiols on the metal surface corresponding to (A) stand-up position, in which the thiols are bonded to metal surface followed by alkyl chain and further thiol is the terminal group, (B) lie- down orientation in which both the thiols are bonded to the metal surface in a flat fashion, and (C) the looped monolayer assembly structure where both thiol ends are bonded to the metal surface and the alkyl chain forms a loop.

Monolayer assemblies on n-alkyl thiols ($CH_3(CH_2)_nSH$) adsorbed onto polycrystalline gold from dilute solution have been characterized by optical ellipsometry, infrared (IR) spectroscopy and electrochemistry.[21] The IR spectroscopy and ellipsometric data indicated that the long-chain thiols are a densely packed crystalline-like assembly with fully extended alkyl chains tilted from the surface normal by 20-30° (Figure 2.5). As the chain length decreases, the structure becomes increasingly disordered with lower packing density and coverage.

.
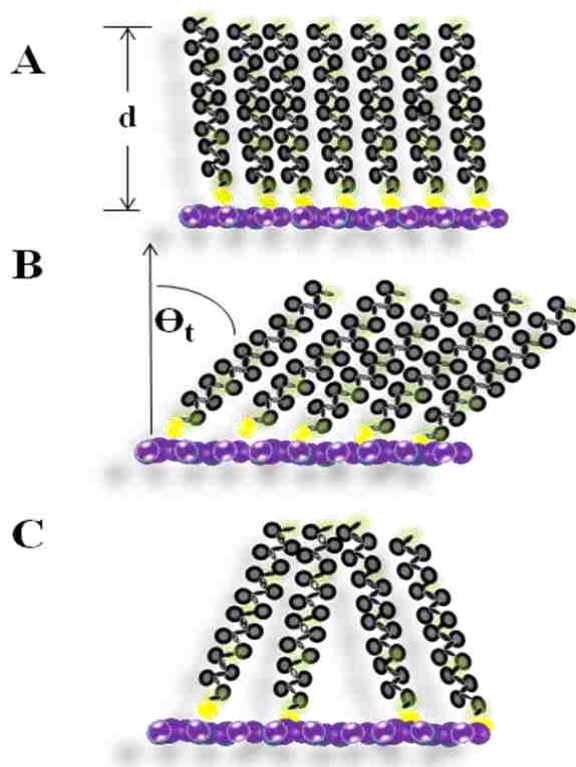
Figure 2.5: Schematics of an organized monolayer assembly: (A) closely packed arrangement of alkyl chains oriented normal to the substrate surface of a chain length, d; (B) closely packed arrangement of head groups with tail uniformly oriented at an angle Θ_t from the surface; and (C) closely packed arrangement of head groups with a distribution of tilted tail groups.

Molecules can be measured from either pure monolayer or mixed monolayer SAMs. Mixed monolayer is formed by the co-adsorption of different molecules, and the surface coverage can be varied by varying the concentrations.[26,36,37] Depending upon the ability of

18

adsorption, the molecules may not pack as well around the adsorbate. This could lead to great disorder in SAM formation. Nonetheless, disordered molecules can be adsorbed at lower concentration along with ordered monolayers. This could possibly disturb the control over the location of the molecules and disturb the order and/or quality of the film.

Molecular exchange is more prone to happen at the defect sites, substrate vacancy islands, and substrate step edges as the molecules are less constrained than the surrounding matrix. Exchange processes can be controlled by the type and the density of defects. Taking advantage of this, molecules of interest can be inserted in the defect sites of SAM, called directed self assembly (discussed in Chapter 4). Due to lack of space, the molecule of interest would approximately get inserted and then be forced to stand up normal to the surface

However, for all points that can be considered with respect to the formation and ultimate utilization of SAMs, alkanethiols form excellent host matrices due to their ability to self-assemble. The dynamics of formation, which allow control of film quality and post-adsorbing processing, are well understood. Alkanethiols are chemically inert and have low electrical conductivity. Conductive probe-atomic force microscopy (CP-AFM) has been used to characterize the electron transport, current-voltage (*I-V*) properties, and breakdown voltages of insulating SAMs.[26] As the assembly, chain length, and chemical functionality of alkanethiols can be tailored, they have been used as a model systems for electron transport measurement through molecules.[38] With this background measurement of alkanethiol SAMs, we can explore the electronic properties of embedded molecules.

2.3 SAM CHARACTERIZATION

Monolayers formed through self-assembly can be characterized in order to determine their composition and structure (including defects) as these are significant in the study specific electronic properties of the material. Characterization of self-assembled monolayers helps to

ensure the presence of particular molecules on the substrate surface which could be used for building further molecular-scale devices. We use the following five techniques in this thesis to characterize the self-assembled monolayers:

2.3.1 Ellipsometry

Ellipsometry is a versatile and powerful optical technique for the investigation of the dielectric properties (complex refractive index or dielectric function) of thin films. Ellipsometry as a technique extended into many different fields, from semiconductor physics to molecular-scale electronics, both for research purposes as well as industrial applications. Ellipsometry is a very sensitive measurement technique and has exceptional capabilities for thin film metrology. As an optical technique, spectroscopic ellipsometry is non-destructive and contactless. Specifically, in an ellipsometric experiment, electromagnetic radiation is emitted by a light source and linearly polarized to then pass an optional compensator before impinging upon a sample (Figure 2.6). The reflected/transmitted radiation passes an optional compensator and a second polarizer, which is called analyzer, and falls into the detector. Typically, ellipsometry is carried out in the reflection mode, and the change in polarization is measured upon reflection of the light.
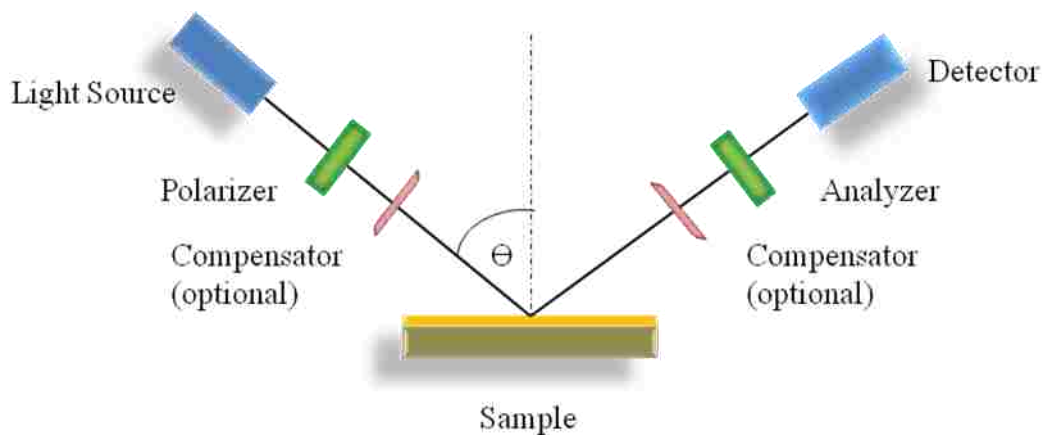
Figure 2.6: Schematic setup of a typical ellipsometric measurement.

20

Ellipsometry is commonly used to characterize film thickness for single layers or complex multilayer stacks ranging from a few angstroms or tenths of a nanometer to several micrometers with excellent accuracy. The name "ellipsometry" stems from the fact that the most general state of polarization is elliptic. This technique has been known for almost a century and has many standard applications today. It is mainly used in semiconductor research and fabrication to determine properties of layer stacks of thin films and the interfaces between the layers. However, ellipsometry is also becoming more interesting to researchers in other disciplines; determination of the thickness of organic thin films as well as self assembled monolayers.[20,21,37,39] We have used ellipsometry to determine the thickness of organic molecules, the reproducibility of SAMs, and to ensure the presence of specific molecules on the substrate surface in order to prepare for future device fabrication using these substrates.(Appendix B)

2.3.2 Reflection Absorption Infra Red Spectroscopy

Infrared (IR) spectroscopy is widely used to identify molecular adsorbates that form on metals in the course of surface chemical reactions. Because IR spectroscopy is one of the few surface sensitive probes that provides molecule-specific information without disturbing the chemisorbed state, there is great interest in extracting as much structural information from the spectra as possible. As a molecule sits on a surface, it will vibrate. Such vibrations can be studied by shining infrared light onto the surface. If the molecule has a dipole moment, that is one end of the molecule has a positive charge and the other end a negative charge, then the molecule can absorb infrared light but only at certain fixed frequencies. Hence, an infrared spectrum of light reflected from the surface will show absorption peaks which are characteristic of the molecule and its method of bonding to the surface. This is the basis of the reflection absorption infrared spectroscopy (RAIRS) technique. Vibrations can only be detected if the

vibration is perpendicular to the surface. Detection of the infrared spectrum is generally accomplished using the FTIR (Fourier Transform Infra Red) technique.

The adsorption of several thiols on a gold surface has been characterized by IR spectroscopy.[21,36,37,39] Octanedithiol (ODT) and nonanedithiol molecules on bare GaAs have shown sharp peaks at relatively low wave numbers (2918 and 2850 cm^{-1} for the CH_2, antisymmetric and symmetric stretches, respectively), which indicate highly ordered and crystalline monolayers.[30] Porphyrin based self-assembled monolayers of thin films on silicon have shown the presence of phenyl ring vibration at 1605 and 1396 cm^{-1} as well as additional vibration at 1450 cm^{-1} for carbon-nitrogen (C-N) bond and two strong characteristic bands at 1635 and 1593 cm^{-1} for N-substituted pyridyl groups.[40] We have used RAIRS in this thesis to investigate the adsorption of certain thiol groups (-SH) to the gold surface, and this will be discussed in Chapter 4.

2.3.3 X-ray Photoelectron Spectroscopy

X-ray Photoelectron Spectroscopy (XPS) is a quantitative spectroscopic technique that measures the empirical formula, chemical state, and electronic state of the elements that exist within a material. It is a surface chemical analysis technique that can be used to analyze the chemistry of the surface of a material. XPS is based on the photoelectric effect where the concept of the photon was used to describe the ejection of electrons from a surface when light impinge upon it. XPS spectra are obtained by irradiating a material with a beam of X-rays while simultaneously measuring the kinetic energy and number of electrons that escape from the top 1 to 10 nm of the material being analyzed. For XPS, Al K-alpha (1486.6eV) or Mg K-alpha (1253.6eV) is often the photon energy of choice. These photoelectrons have energies up to 1500 eV and typically have a characteristic range between 3 and about 8 atom layers (1 to 3 nm). Other X-ray lines can also be chosen such as Ti K-alpha (2040eV).

The XPS technique is highly surface specific due to the short range of the photoelectrons that are excited from the solid. The energy of the photoelectrons leaving the sample is determined using a CHA (Concentric Hemispherical Analyzer), and this gives a spectrum with a series of photoelectron peaks. The binding energy (BE) of the peaks is characteristic of each element. The peak areas can be used (with appropriate sensitivity factors) to determine the composition of the material's surface. The shape of each peak and the binding energy can be slightly altered by the chemical state of the emitting atom. Hence XPS can provide chemical bonding information as well. *XPS is not sensitive to hydrogen or helium*, but can detect all other elements. The binding energy for H or He is in the range of MeV whereas the other atoms has energies in terms of eV. XPS must be carried out in UHV (Ultra High Vacuum) conditions. A typical XPS experimental setup is shown in Figure 2.7.
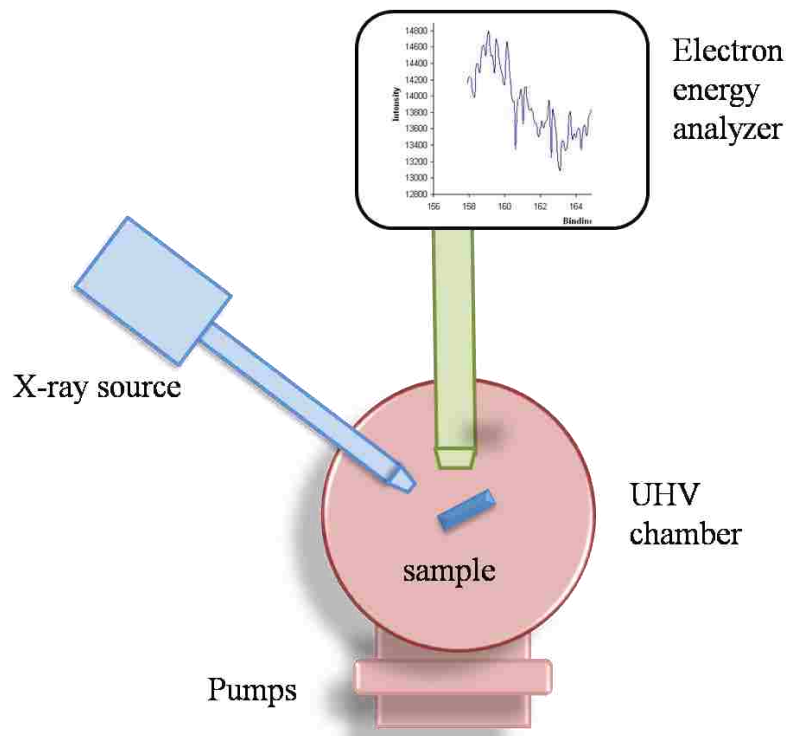
Figure 2.7: Schematic setup of a typical XPS experiment.

XPS has been used extensively in thiol SAM characterization to determine the chemical environment of sulphur atoms (i.e., whether they are bound to surface).[41] Structural and chemical properties of mixed self-assembled monolayers by coadsorption of symmetric and asymmetric disulfides on Au(111) are characterized by XPS. The results show that the C/Au ratios in mixed SAMs of disulphides are slightly less than those of thiols when their surface compositions are equal.[36] Nanoscopic molecular junction incorporating a series of rigid thiol-terminated norbornylogs are characterized to determine the film orientation.[39] The sulphur exists in three different states—bound (BE~161.8 eV), unbound (BE~163.5 eV), and oxidized (BE~167.8 eV). Covalently bound self-assembled porphyrin monolayers show a characteristic change in their electronics spectrum along with a signature in XPS.[40] Also, electronic states of L-cysteine (Cys) adsorbed on gold as thiolate have been investigated.[42] XPS is used here to investigate the orientation of thiolated monolayers adsorbed on gold and will be further discussed in Chapter 4.

2.3.4 Atomic Force Microscopy

The Atomic Force Microscope (AFM) is a very high-resolution form of scanning probe microscope with demonstrated resolution of fractions of a nanometer, much better than the optical diffraction limit.

AFM is one of the foremost tools for imaging, measuring, and manipulating matter at the nanoscale. It is being used to solve processing and materials problems in a wide range of technologies affecting the electronics, telecommunications, biological, chemical, automotive, aerospace, and energy industries. The materials being investigating include thin and thick film coatings, ceramics, composites, glass, synthetic and biological membranes, metals, polymer and semiconductors. AFM is being applied to studies of phenomena such as abrasion, drafting, dip pen writing, nano-structure fabrication, indenting, and lithography. AFM not only images

(Figure 2.8) the surface in atomic resolution but also measures the force at the nano-Newton

scale. AFM is also discussed in more in detail in Chapter 4.
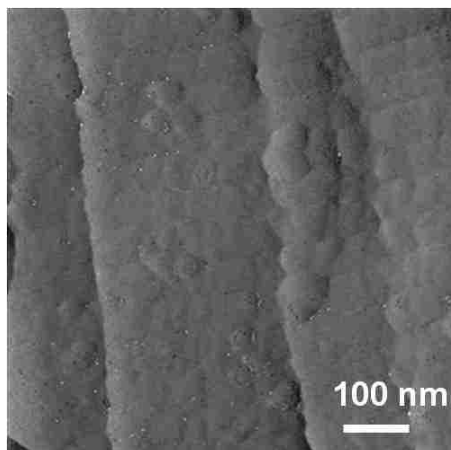
Figure 2.8: An AFM scan of thin collagen membrane. Reprinted from [98]. (Obtained by S. Thiruvengadam, Dept. of ECE, LSU via a Pacific Nanotechnology, Inc. Nano-R AFM as housed in the department's Electronic Material & Device Laboratory)

2.3.5 Fluorescence Spectroscopy

Fluorescence spectroscopy is a technique (another form of electromagnetic spectroscopy)

which analyzes fluorescence from a sample. (Spectroscopy (Appendix B), in general, is a

characterization technique which provides a means by which to study the interaction between

radiation (electromagnetic or particle) and matter and to measure this interaction.) A light

source, usually ultraviolet light, is used to excite the electrons in molecules of certain

compounds. This causes the molecules to emit light with different energy, typically lower than

the incident light, and in the visible range. A hot body emits radiation due to its high

temperature and is said to exhibit incandescence. However, all other forms of light emissions are

called luminescence. Molecules are said to have various states referred to as energy levels.

Fluorescence spectroscopy is primarily concerned with electronic states and vibrational states.

In general, the material being examined will have a ground state (a low energy state level) of

25
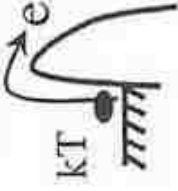
interest and an excited energy state with higher electron energy. Each of these electronic states has vibrational energy states which are involved in the emission process. The phenomenon of fluorescence spectroscopy is discussed more in detail in Chapter 3.

2.4 Overview of Electron Transport Mechanisms in Molecules

2.4.1 Forms of Electron Transport

Transport in single molecules or in monolayers of molecules placed between two metal electrodes is expected to be very different from transport in bulk structures, mainly due to the inherent small size of the molecules. For electron transport studies in molecular-based structures, it is important to know the terminology. The highest occupied molecular orbital (HOMO) and the lowest unoccupied molecular orbital (LUMO) are similar to the valence and conduction band in solid state materials, respectively, but with discrete energy levels caused by quantization effects in constricted dimensions of the molecule. The difference in HOMO and LUMO is referred to as the energy band gap (E_g). Given the fact that molecules are much smaller than the mean free path of electrons in typical metals (~ few nanometers at room temperature), bulk resistivity (due to the interactions of electrons with lattice vibrations and impurities of the system) is not a valid concept. This implies that the resistance of a system in which a molecule or monolayer of molecules is attached to the electrodes does not originate from the inelastic scattering of the electrons at the Fermi energy with the phonons of the molecule. Usually, the molecule is considered as a potential barrier through which electrons tunnel coherently and, to first order, basic theory neglects inelastic scattering in the molecule altogether. One of the main sources of resistance is the interface between a metal surface and the molecule, usually called "contact resistance". The contact resistance also depends upon the character of the bond between the molecule and the electrodes (strong or weak force) as well as the geometry of the contact.

Table 2.1: Potential conduction mechanisms; Reprinted with permission (Appendix A3)

Conduction mechanism	Characteristic behavior	Temperature dependence	Voltage dependence	Schematic band diagram
Schottky emission	$I \sim T^2 \exp\left(\dfrac{-q\left(\Phi - \sqrt{\frac{qV}{4\pi\epsilon d}}\right)}{kT}\right)$	$\ln\left(\dfrac{I}{T^2}\right) \sim \dfrac{1}{T}$	$\ln(I) \sim V^{1/2}$	
Frankel–Pool conduction	$I \sim VT^2 \exp\left(\dfrac{-q\left(\Phi - 2\sqrt{\frac{qV}{4\pi\epsilon d}}\right)}{2kT}\right)$	$\ln\left(\dfrac{I}{T^2}\right) \sim \dfrac{1}{T}$	$\ln\left(\dfrac{I}{V}\right) \sim V^{1/2}$	
Hopping conduction	$I \sim V \exp\left(\dfrac{-\Delta E}{kT}\right)$	$\ln\left(\dfrac{I}{V}\right) \sim \dfrac{1}{T}$	$I \sim V$	
Fowler–Nordheim tunneling	$I \sim V^2 \exp\left(-\dfrac{4d\sqrt{2m}}{3\hbar V}(q\Phi)^{1.5}\right)$	—	$\ln\left(\dfrac{I}{V^2}\right) \sim \dfrac{1}{V}$	
Direct tunneling	$I \sim V \exp\left(-\dfrac{4\pi d}{h}\sqrt{2m\Phi}\right)$	—	$I \sim V$	

Depending upon the geometry of the molecule as the barrier height (single-well or multi-well), different transport mechanisms (non-resonant vs. resonant tunneling) are possible. Charging effects (Coulomb blockade regime) are taken into consideration depending on the strength of the coupling between the metal-molecule interfaces. The inelastic contributions to current are expected to play a minor role in the low bias regime in simple tunneling junctions, whereas they have a vital role in a system in which phonon-assisted tunneling (hopping) is the dominant transport mechanism. A variety of transport mechanisms can be found in molecular systems depending on the character of the metal-molecule interface (Table 2.1). One of the systems that has been more extensively studied in the field of molecular-scale electronics is a SAM of alkanethiols adsorbed onto gold.

Several experimental groups have reported fairly reproducible data[38,43] using a variety of techniques, ranging from nanopore experiments, in which one of the electrodes is evaporated on top of the SAM,[44,45] to conductive probe-atomic force microscopy (CP-AFM), in which the SAM is contacted with the AFM tip.[46] Typically the SAM is prepared by exposing a Au(111) surface to a solution containing the alkanethiols in organic solvents such as toluene and ethanol.[26,46] After several hours a long-range ordered SAM is formed, the monolayer is chemically adsorbed to the surface through Au-S bonding, and the alkanethiol chains are tilted by ~30° with respect to the surface normal. The top electrode contact to the molecule (AFM tip or the evaporated contact), on the other hand, is a much weaker bond. It has been found experimentally that in this system the conductance (G) depends exponentially on the length of the alkanethiol chain,

$$G = G_\circ e^{-\beta d}$$

(2.3-1)

where d is the number of methyl groups in the alkane chain, and β, the current decay constant, is found to be about 1 per methylene. The value of β depends upon the applied bias as well as the type of metal-molecule junction.[26]

2.4.2 Potential Applications for Electron Transport Mechanisms

A molecular approach toward information storage based on redox properties has been studied by several groups. Current approaches are based on the development of molecular-scale switches, which can be used both in logic and memory circuits. The basic paradigm for electronic information storage is retention of charge in a capacitor. The most straightforward approach to molecular-scale memory would be to store charge at the molecular level. Another more fundamental approach would utilize the oxidation states of individual molecules to store charge, which has the advantage that multiple oxidation states within one molecule can be addressed to access more than one bit.

One such molecule, which has already been exploited for its multi-bit possibilities, is that of the porphyrin. Anions and cations of porphyrin molecules can be formed electrochemically with the cations, which have the greater chemical stability, used as memory elements.[32] Direct electrical communication with porphyrin was accomplished by attaching the molecules to Au via a thiol linker in a self-assembly process.[47] To avoid handling free thiol groups, the investigators employed thiol protected groups which are cleaved *in situ* upon exposure to Au surfaces. Roth *et al.* have used Zn-tetraarylporphyrins bearing S-acetylthio-derivatized linkers, which form a SAM on the Au surface. No discernible reorganization was observed even after 24 hours. The studies reported herein demonstrated that porphyrin SAMs exhibit characteristics that could make them potential molecular-based memory elements given their amenability to electrochemical processing and charge retention.

Liu *et al.* demonstrated that porphyrin-based molecules bound to Si(100) exhibit redox behavior useful for information storage.[4] They confirmed that molecular memories can survive silicon device fabrication processing and real-world operation. In particular, they demonstrated that these molecules are stable under extreme temperature (400°C) and a large number of read-write cycles (10^{12}).

Koo *et al.* has studied the electrical properties of porphyrin based molecules. The current-voltage (*I-V*) characteristics were found to exhibit outstanding switching diode and tunneling diode behavior even at room temperature.[14] The I-V characteristics of Al/Al$_2$O$_3$/Zn-porphyrin Langmuir-Blodgett (LB) monolayer/Al devices measured at room temperature in air showed a typical rectification curve for a diode. Moreover, a much higher current was obtained at a positive bias rather than a negative bias. They observed decreases in currents at both positive and negative bias when the device was under the influence of an electric field.

A variety of transport mechanisms can be found in molecular systems depending on the character of the molecule and of the interface[38]. From this point, we will continue this discussion overview of electron transport mechanism by examining the platforms fabricated and analytical methods for conduction measurements. In particular we will review the experiments in which such mechanisms have been observed.

2.4.3 Device Prototypes for Electron Transport Measurements

2.4.3.1 Mechanically Controlled Break Junctions

Several groups have used a technique known as the mechanically controlled break (MCB) junction in order to obtain a pair of nanometer-scale contacts.[48] A small piece of notched metallic wire is glued onto a flexible substrate, and subjected to tensile stress by mechanically bending the substrate, after which an adjustable tunneling gap can be established. The two ends of metal wire can now be used as metallic probes, which became atomically sharp when broken.

The nano-gap can be adjusted with nanometric precision by relaxing the amount of bending imposed on the substrate through a piezoelectric element. Reed *et al.* measured benzene-1, 4-dithiolate SAMS between gold contacts, as shown in Figure 2.9. In the experiments reported by them, the molecules are adsorbed from 1mM solution of tetrahydrofuran (THF) onto the two facing gold electrodes of the break junction which were broken in solution under an Ar atmosphere.
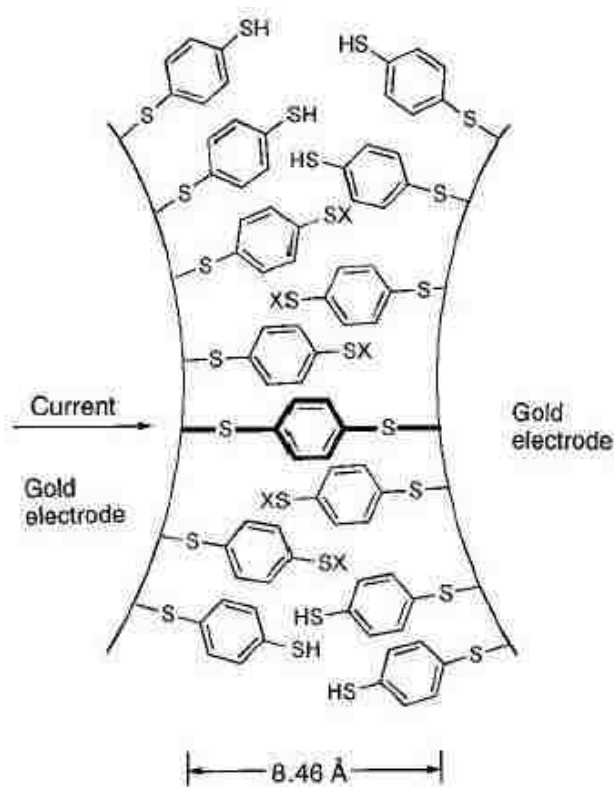
Figure 2.9: Mechanically controlled break junction measurement of benzene-1,4-ditholate. Reprinted with permission (Appendix A4)

The THF solvent was allowed to evaporate in ambient Ar atmosphere and the tips (the Au electrodes) were returned to measure the electrical properties of the molecule or molecules adsorbed on the surface. They obtained highly reproducible conductance measurements (I-V). An apparent gap of ~0.7V was observed in all cases, which could be a possible indicator of a Coulomb staircase. They also observed a single measurement that gave resistance which was

31

approximately half the value of the maximum resistance. This suggested the possibility of two noninteracting self-assembled molecules in parallel.

Researchers at Forschungszentrum Karlsruhe clearly demonstrated electron transport through a single molecule (or at most very few) and not a large ensemble of molecules.[49] They chose to use a lithographically fabricated MCB junction to provide an electrode pair with tunable distance. As the tunneling gap decreases, the resistance decreased exponentially, and the conductance was highly unstable at higher bias voltage. At a certain distance, the stable behavior observed was interpreted as establishment of metal-molecule-metal junction through a stable chemical bond. As long as the junction distance remained stable, the investigators were able to observe highly reproducible data. In general, asymmetric molecules always showed asymmetric I-V characteristics, however symmetric molecules showed both symmetric and asymmetric I-V characteristic behaviors.

In spite of the uncertainty of contact geometry in MCB junctions, it has proven to be an important method of characterization for organic molecules in that it has the ability to measure a single or very few molecules chemically bound to metal electrodes in an accurately controllable gap. Of the many techniques available for characterization or metal-molecule systems, MCB has proven useful to investigators interested in characterizing organic molecules.

2.4.3.2 Nanopore

Metal-molecule-metal heterostructures can be formed by a novel fabrication technique which directly measures the conduction through a small number of organic molecules.[50] These devices consist of a self-assembled monolayer of conjugated molecules sandwiched between top and bottom metallic electrodes which, in turn, provide good control over the device area and intrinsic contact stability. Researchers at Yale have developed a structure called "nanopore" to accomplish the aforementioned tasks. It is shown in Figure 2.10.

32
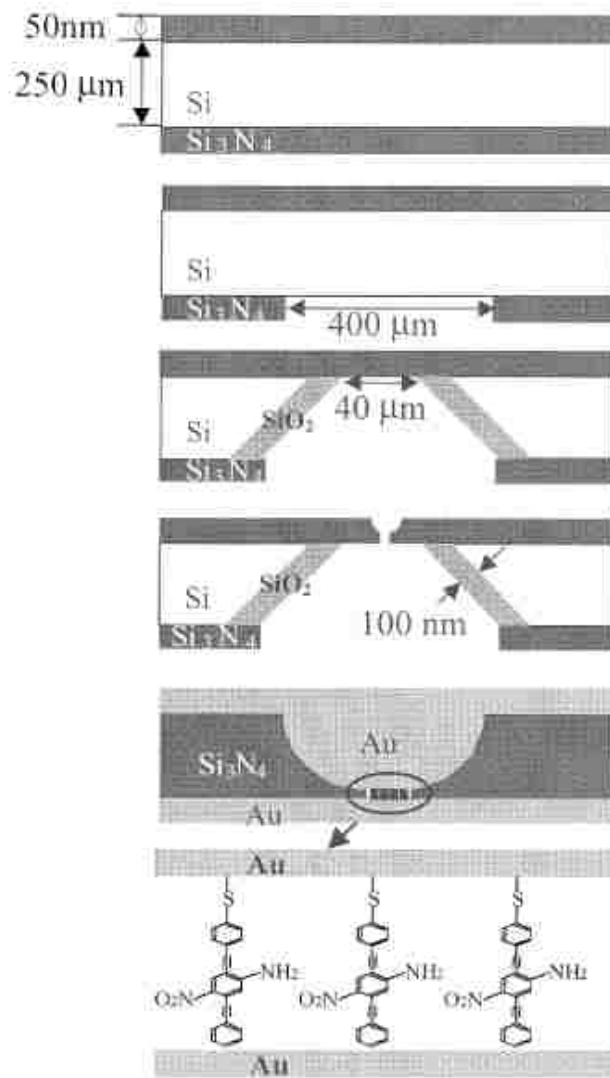
Figure 2.10: Nanopore device fabrication process. Reprinted with permission (Appendix A5)

The device fabrication starts with a high-resistivity silicon wafer with a low-stress Si_3N_4 film deposited on both sides by low-pressure chemical vapor deposition (LPCVD). By standard photolithographic processing, a sacrificial Si_3N_4 membrane (40 um x 40um and thickness ~70nm) is fabricated. Subsequently e-beam lithography and reactive ion etching were used to create a single pore with a diameter of approximately 30 nm. The bottom metal (gold) electrode was thermally evaporated, and then the entire structure was transferred into a molecular solution

(4-thioacetylbiphenyl) for deposition of the SAM layer. After the SAM formation, the structures was removed from the solution and loaded into a high vacuum chamber of 10^{-8} Torr to deposit the top electrode.

Prior to *I-V* measurements, a 10 Å layer of Ti was deposited onto the upper surface of the SAM/nanopore structure. Following this a low temperature deposition of 30 A Ti and 800 Å Au were also deposited. This low temperature deposition helps to minimize thermal damage to the SAM. Two terminal current-voltage (*I-V*) characteristics were measured in the temperature range from room temperature down to 57 K. Prominent rectifying behavior was observed with linear behavior at negative bias and exponential behavior at positive bias. Temperature dependence measurements suggested a thermally activated transport mechanism, which reveals the hopping conduction mechanism.

The same structure has been used to study molecules with nitro or amine functionalities.[25] Molecules with nitro moieties were observed to change their state of conductivity as would a molecular random access memory cell. The amine and unfunctionalized molecules do not exhibit storage behavior. Positive bias corresponds to hole injection from the chemisorbed thiol-Au contact (not the top evaporated Au contact), and the characteristics were repeatable with high accuracy. Device degradation was not observed. The activation energy E_a for this molecule was found to be approximately 80 meV.

Furthermore, nanopore was used to study the mechanism of electron transport in self-assembled alkanethiol monolayers on gold surfaces. In recent work, the deposition of the top contact was modified such that the kinetic energy of evaporated Au atoms at the surface of the monolayer was reduced, thus preventing Au atoms from punching through the monolayer. This was achieved by flowing liquid nitrogen throughout the cooling stage during the thermal evaporation process (under the pressure of $\sim 10^{-8}$ Torr). The alkanethiols showed no significant

changes in *I-V* characteristics during temperature dependence (300 to 80 K) measurements. Thus, the conduction mechanism through alkanethiol was observed to be direct tunneling[44], perhaps they assumed through-bond tunneling. Even negative differential resistance (NDR) and switches at room temperature have been reported.[52]

2.4.3.3 Crossed-wire

A simple crossed-wire tunnel junction technique was used to study oligo(phenylene ethylene) (OPE) by researchers at the Naval Research Laboratory. The work involved two crossed-wires brought into contact with precise control over the contacts.[23] Figure 2.11 shows a schematic representation of a crossed-wire tunnel junction. The investigators used 10 μm diameter wires, one modified with a self-assembled monolayer of the molecule of interest. This wire was mounted in such a manner so the other wire would cross it, geometrically speaking. One of the wires was kept perpendicular to the applied magnetic field (B). The junction gap was precision controlled using the Lorentz force generated from a small dc current (<5 mA).
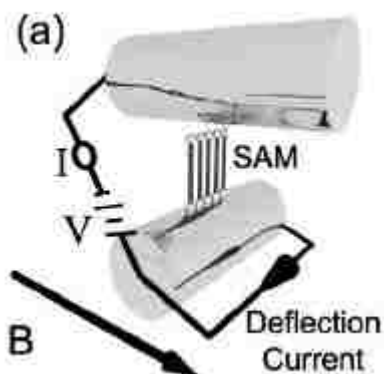
Figure 2.11: Schematic representation of a crossed-wire tunnel junction. Reprinted with permission (Appendix A6)

I-V characteristics demonstrated that OPE acts like a molecular wire under symmetric contact conditions, however it exhibits the characteristics of a molecular diode when the

connections are asymmetric. Different charge transport behaviors were observed depending upon the nature of its two metal-molecule contacts.

Despite the challenges, the discoveries as to how molecules respond to applied electric fields in both interesting and nontrivial ways are encouraging. However, even the fact that SAMs can be formed without any electronic (or optical) intervention has thus far proven to be extremely useful in the study of hybrid electronic processes. The insight that can be gained from SAMs into molecule-metal/insulator/semiconductor phenomena, at the nanoscale, will invaluable to the eventual development of next-generation atomic scale devices.

3. FLUORESCENCE SPECTROSCOPY OF HYBRID ELECTRONIC MATERIALS

3.1 INTRODUCTION

Hybrid electronic materials (HEMs) have been known to exhibit strong photoluminescence and are thus potential materials for use in electroluminescence as needed in telecommunications and information display applications. Although electroluminescence in inorganic materials was observed over a century ago, it was only half century later that electroluminescence in organic materials was observed. The last decade has seen a multidisciplinary thrust in designing stable high performance hybrid materials for electronic applications and a concurrent effort in understanding the optoelectronic transport properties of such materials.

HEMs can span the whole conductivity range from isolated molecules behaving as wide gap insulators to materials with strong collective effects behaving as metals, semiconductors, or superconductors. These collective effects often result from intermolecular interactions mediated by π-bonding networks. Because of the weak Van der Waals force, organic molecular materials have narrow bands and hence lower carrier mobilities than inorganic covalent materials. The chemical inertness of molecular materials makes them less sensitive to chemical impurities, and the absence of dangling bonds circumvents the problems associated with surface states. While there are several ways to understand the phenomenon of electron-phonon interaction, the experimental determination of electron transitions from one energy level to another level is most directly verified by fluorescence spectroscopy.

Fluorescence spectroscopy (FL) is often used to understand analyte (molecular) binding and its dynamics. The emission of light can be categorized as either incandescence or

luminescence. The term luminescence refers to various forms of light emission and involves a radiative transition which, in turn, lowers the energy of a molecule by the emission of a photon. In order for the process of luminescence to exist for any period of time, energy must be supplied to the system to maintain an excited state population. Based on the source of energy, different forms of luminescence exist. However, we will focus this discussion on the type of luminescence that is of analytical importance, i.e. photoluminescence. In photoluminescence, the excited state is produced by the absorption of light. Further, the luminescence process can be categorized as fluorescence or phosphorescence. If the electron spin states of the two energy levels are the same, the process is referred to as fluorescence.

Fluorescence provides information about analyte properties as well as about the solvent or environment surrounding the molecule. FL has several analytical advantages over other spectroscopic measurements such as absorption spectroscopy. The inherent advantages of FL techniques are the selectivity and sensitivity of the measurements. For a given fluorosphore, both the absorption and emission occur at specific wavelength ranges. Hence, the selectivity arises from the fact that a fluorophore has specific wavelengths of absorption and emission. The sensitivity of the technique arises from the fact that emission is a measure of low light levels above a theoretically zero background which enhances the detection limit. Recently, many fluorescent small molecules (organic dyes/ quantum dots) have been used to detect metal ions.[22,56] Quantum dots (nanocrystals) are semiconductor particles that have all three dimensions confined to the nanometer length scale. As a result of quantum confinement, quantum dots have unique optical and electronic properties significantly different from bulk materials.

In our work, functionalized Q-CdS capped with AOT and porphyrin based-molecules are examined using the fluorescence spectroscopy technique. Three differently sized Q-CdS capped with AOT and self-assembled on different substrates such as metal, semiconductor, and insulator

are used to investigate the phenomenon of electron transport in the quantum dots. In turn, porphyrin molecules chemisorbed onto gold surfaces are used to study the phonon-electron interaction in these molecules due to their metal cations. Our preliminary research shows that the maximum fluorescence intensities are obtained at a specific angle of incidence, such as 80° and 45° with respect to the samples, for Q-CdS and porphyrin molecules, respectively. Emission spectra of Q-CdS absorbed onto different substrates such as gold, GaAs, and mica show a slight but systematic redshift of peaks characteristic of spatially confined phonon interactions. The effect of relative quantum dot size, different substrates, and light intensity are reported in this thesis. Simultaneously, a gradual blue shift of excitation peaks is observed as the relative size of the quantum dots decreases. The fluorescence properties of porphyrin molecules are successfully reproduced from chemisorbed porphyrin on gold substrates.

Therefore, photoemission experiments that probe the electronic structure of nanocrystals are indispensable if one wishes to gain insight into the electronic structure-property relationship. Compared to traditional (inorganic) electronic materials, relatively few studies have been carried out on *hybrid* electronic materials to date. Techniques such as photoluminescence and fluorescence spectroscopy are of immense value in probing the optoelectronic structure of hybrid samples.

3.2 BACKGROUND THEORY

Since the study of fluorescence in organic materials, there has been a multidisciplinary driving force behind the investigation of hybrid materials for electronic applications, particularly in an effort to understand the optoelectronic transport properties of such materials. Our research is motivated by a range of milestones which act as pointers toward the goal of creating HEM-based devices. Some of the significant milestones of optical (or optoelectronic) spectroscopy for

Q-CdS and porphyrin based-molecules, as they pertain to the study of electronic characterization, are discussed in this section.

3.2.1 CdS Quantum Dots

Semiconductor Quantum dots (QDs) have been the subject of great scientific and technological interest because of their remarkable electronic and optical properties and potential for a wide range of applications.[54-56] QDs are semiconductor nanocrystallites which represent a general class of materials (mesoscopic), that span the physical domain between bulk materials and molecular compounds, with sizes ranging from 2-10 nanometers (10-50 atoms) in diameter. Interesting and strongly size-dependent optical and electronic properties arise in these materials when the quantum dot is small compared to the length scale of the electron-hole pair, the exciton Bohr radius. In this regime, known as the confinement regime, the electron and hole wave function experience three dimensional quantum confinement due to the physical boundaries of the quantum dot itself. The confinement induces quantization of the bulk electronic bands such that quantum dots, sometimes called "artificial atoms", have discrete electronic transitions that shift to higher energies with decreasing size. The confinement increases the kinetic energy of the carriers, thus resulting in an increase in band gap as the confinement increases (size decreases). When the size of the semiconductor approaches the size of the Bohr radius, the electron energy levels are no longer continuous but are discrete.

QDs are smaller than the Bohr radii for the semiconductor materials. Since the charges cannot be separated by a distance larger than the size of the particle, they are confined to be closer than the Bohr radius, which is manifested as a change in energy. In other words, it takes a significant amount of energy (~ 10.2 eV) to confine an exciton. The required energy is manifested in an apparently larger band gap. Another way of saying this is that if a particular semiconductor absorbs light at a band gap energy of 900 nm, for example, then that

semiconductor will absorb light at a smaller wavelength (i.e. a higher energy) if it were to shrink down to quantum dot sizes. It will also emit light at shorter wavelengths. As the particle gets smaller and smaller, so do the absorption and emission wavelengths. Their composition and small size give these dots extraordinary optical properties that can be readily customized by changing the size or composition of the dots. As the emission frequency is dependent on the band gap, it is therefore possible to control the output wavelength of the QDs with precision.

The most popular choices of QD materials are CdSe and CdS. Their bulk bandgaps are 1.7 eV for CdSe and 2.4 eV for CdS (corresponding to absorption onsets at ~720 nm and ~520 nm, respectively), which means that their absorption energies are tunable throughout the visible region. These QDs can be synthesized using various methods such as lithography, epitaxial growth, and colloidal synthesis.[57,58] Quantum dots incorporate the most sought-after characteristics, such as multiple colors and brightness, of either fluorescent dyes or semiconductor light emitting diodes (LEDs). Several research groups have explored the properties of CdS QDs .[22,59] For example, Mews *et al.* studied the structural and spectroscopic properties of CdS/HgS/CdS quantum-dots quantum wells (QDQW).[60] They used hole burning (HB) and fluorescence line narrowing (FLN) spectroscopy to investigate the homogeneous optical properties for absorption and emission and observed the expected optical features. The homogeneous optical measurements demonstrated that epitaxially grown nanocrystals fabricated by wet chemistry methods can alter the intrinsic electronic properties of colloidal semiconductor QDs.

The QD surface is usually covered with organic ligands, which make the particles soluble and prevent aggregation. Sookal *et al.* investigated the preparation of CdS/dendrimer nanocomposites and characterized their unique physical and optoelectronic properties.[61] They used dendrimers as the stabilizing host for CdS QDs and found that the photoelectronic

properties of CdS clusters were sensitive to synthesis conditions, including dendrimer type, solvent type, and the concentration of dendrimer and other solutes. The CdS/dendrimer nanocomposites subsequently undergo slow aggregation in solution. Upon excitation with light at a wavelength of 340 nm, the nanocomposites in methanol solution manifested strong photoluminescence (PL) with emission maxima at about 450 nm. They presumed that the stable optoelectronic property of these nanocomposites was due to continued stabilization of the CdS clusters by the dendrimer host.

Bakkers *et al.* used intensity modulated photocurrent spectroscopy (IMPS), a time resolved optoelectrical method to study the excited-state dynamics in CdS quantum dots (Q-CdS) adsorbed onto gold electrodes.[62] The aqueous Q-CdS were adsorbed as a monolayer on a bare gold electrode as well as on hexanedithiol or nonanedithiol SAM on gold. They observed the optical transfer function and found that the thermally activated process (or thermal release of charge carriers) was not involved, since the transfer function was also independent of temperature in the range 274 – 334 K. However, they noticed low tunneling rates which were due to excited-state relaxation within the particle because of the participation of a long-lived excited state. They showed that tunneling rates can be directly determined from the tunneling sequence. These tunneling rates indicated that the particles were not bound to the surface by a sulfur-gold interaction but by the stabilizing polyphosphate chains.

To investigate Q-CdS as a potential electronic material, it is necessary to understand the electron transport mechanism in these quantum dots. Hole levels and excited states in CdS nanocrystals have been investigated by Li *et al.* using a hole effective-mass Hamiltonian for the Wurtzite structure.[63] They calculated the hole energies for different sizes and found that the optically passive state will become the ground hole state for small Q-CdS of radius less than 69Å. They computed the exciton states of Q-CdS including the Coulomb interaction between

the electron and hole and suggested that one can measure the exciton transition energies as function of the exciton ground-state energy. They proposed that the dark exciton would be more easily observed in the Q-CdS than that in Q-CdSe. The size dependence of the resonant Stokes shift was predicted to be slightly larger than that of Q-CdSe.

Rakovich *et al.* scrutinized the temperature dependence of the absorption, PL and PL excitation (PLE) spectra, of two kinds of Q-CdS composites—CdS doped glass films and matrix-free films of close-packed Q-CdS.[64] Their work was devoted to comparing these two quantum dots. They used the Maxwell-Garnett model to analyze absorption spectra and from this inferred the e-h pair state energy as well as obtained evidence of a strong absorption in the glass matrix containing CdS. A Gaussian fit was used for the estimation of QD full width at half-maximum (FWHM) for each temperature. From the PL intensity and temperature dependence they concluded that a photo-generated hole was captured on an acceptor-type trap before radiative recombination with a confined electron. They explained the origin of the Stokes shift between the absorption and emission peaks. The temperature coefficients of the optical transition energies for both QDs were similar, while smaller for the CdS/glass films. This may be due to different boundary conditions for the thermal expansion of CdS crystallites.

The electron transitions between different energy levels in hybrid materials (Q-CdS) are studied through optical methods such as fluorescence spectroscopy and Raman scattering. For example, Balandin *et al.* reported the Raman scattering polarization study of arrays of Q-CdS self-assembled by an electrochemical technique.[31] The dots were synthesized using electrochemical deposition of CdS into a porous anodized alumina film with an average diameter of 10nm. They used an Ar ion laser to excite at 514 nm corresponding to the energy E~2.4eV, which is lower than the band-gap energy for CdS. They observed a pronounced peak around 3000 cm^{-1} which was attributed to intersubband transition within the conduction band CdS dots.

43
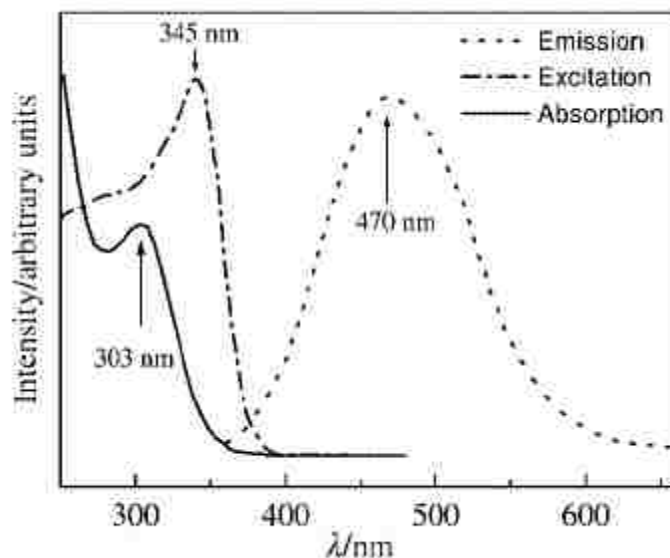
Figure 3.1: UV-VIS and fluorescence spectra of an aqueous solution Q-CdS. Reprinted with permission (Appendix A8)

Similar studies reported by Sapra *et al.* synthesized Q-CdS passivated with cysteine ester, which has potential applications in biological sensors.[65] They showed that the cysteine ester capped Q-CdS are more effective compared to other thiols and shift the mid-gap surface-state dominated fluorescence closer to the band edge. Q-CdS/cysteine ester was prepared by a one-pot solution phase technique. The UV-VIS absorption spectra of an aqueous solution of the nanoclusters exhibited a fairly sharp excitation peak at 303 nm (4.1eV), with the bandgap ≈3.6 eV (Figure 3.1). This blue emission of Q-CdS shows the possibility of using these structures as fluorescent biological probes.

As discussed earlier in this section, QDs covered with ligands are soluble and avoid aggregation. To enhance the band gap emission, a shell with higher band gap energy is usually used to coat the surface of the luminescent QDs. For example, Chen *et al.* investigated water-soluble luminescent Q-CdS capped with polyphosphate, L-cysteine, and thioglycerol.[22] They found that the ligands had a profound effect on the luminescence response of Q-CdS to

physiologically important metal cations. In our research, I chose to work with Q-CdS capped

with *dioctyl sulfosuccinate (AOT)*. Of the twenty naturally occurring amino acids, only cysteine

(HS-CH$_2$-CH(NH$_2$)-COOH) contains a mercapto substituent, making this chiral amino acid

interesting for studying adsorption on gold surfaces. The mercapto or thiol group (-SH) binds to

gold with high affinity, and a rich literature on the adsorption of self-assembled thiol monolayers

on gold surface exists.[66,67] Ogawa *et al.* demonstrated that a layer of AOT capped Q-CdS on an

electrode can be prepared by incorporation into self-assembled dithiol monolayer on gold.[68]

Q-CdS, a direct band gap material (II-VI), can be used in the fabrication of optoelectronic

devices such as solar cells, laser light emitting diodes, photoconductors and other optical devices

based on its non-linear properties. It has wide biomolecular applications such as selective ion

probes, fluorescence labeling, and targeting cancer cells.

3.3.2 Porphyrin Based Molecules

Conjugated organic materials are known to exhibit strong photoluminescence ever since

1963, with the pioneering work of Pope *et al.*, who reported observing the phenomenon of

electroluminescence in single crystal anthracene.[69] Helfrich *et al.* at the National Research

Council of Canada performed ground-breaking work in further understanding

electroluminescence in such materials.[70,71] Practical applications did not result from this early

work because of the large driving voltages and the poor charge injection into single crystals.

After several radical efforts in this field, polymeric semiconductors which could be cast as thin

films were developed and led to the fabrication of organic field effect transistors.[72] Shen *et al.*

made the tangible achievement of electroluminescence in conjugated organic thin films based

light emitting devices, which could be tuned for three-colors.[2]

In recent years, there has been a thrust to design stable high performance molecular based

information storage and a concurrent effort in understanding the electronic and optical transport

properties of such hybrid materials. One of the molecules being investigated for molecular-scale electronics is porphyrin-based molecules.[73-77] Porphyrins are fascinating compounds with biological significance and widely occur in nature including hemes and chlorophyll, to name a few. They are responsible for oxygen transport and storage in living tissues. Heme containing proteins, including cytochromes, serve as an electron carrier in the electron transport chain and are involved in photosynthesis. The basic structure of a porphyrin consists of four pyrrole units connected by four methane bridges (Figure 3.2). It is an aromatic system and obeys Huckel's Rule for aromaticity in that they posess $4n+2$ π electrons which are delocalized over the macrocycle. For the primary photoprocesses in photosynthetic organisms, a renewed interest in artificial systems (based on chlorophyll derivatives) influenced the creation of synthetic porphyrins, whose physical and chemical properties can be readily tailored by varying their metal and/or their organic framework. One such attempt was made by Kampas *et al.* from the Department of Energy and Environment, Brookhaven National Laboratory. They found that the Al-porphyrin interface was photoactive and varied the substituents of porphyrin as well as screened the photoresponses of a large number of porphyrin derivatives.[78]

Strickland *et al.* investigated the rate and equilibrium binding to DNA polymers. Interaction of porphyrin and its derivatives with DNA were studied by equilibrium dialysis and stopped-flow dissociation kinetics as a function of $[Na^+]$.[79] These studies allowed them to assess the selectivity and the importance of charge interactions in influencing the binding. The UV-visible spectrum of the highly conjugated porphyrin macrocycle showed intense absorption at around 400 nm and weaker absorption at higher wavelengths (450 to 700 nm). Variation of the peripheral substituent on the porphyrin ring often causes minor changes to the intensity and wavelength of this absorption. Insertion of metal or protonation of two of the inner nitrogen

atoms into the porphyrin cavity also changes the visible absorption spectrum. These features can be helpful in determining certain features like charge storage in porphyrin.
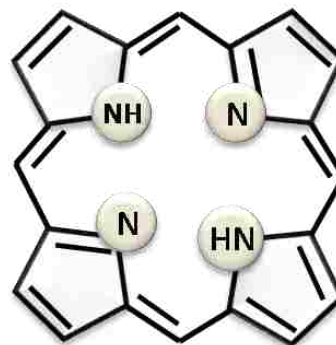
Figure 3.2: Schematic representation of pyrrole ring and porphyrin molecule.

The porphyrin ring is very stable to concentrated acids, and itself can act both as an acid and a base. Strong bases such as alkoxides can remove the two protons (pKa ~16) on the inner nitrogen atoms of a porphyrin to form a dianion. It can undergo a variety of chemical reactions typical of aromatic compounds. There are two general approaches to obtain a desired porphyrin—(1) by modification of a naturally occurring porphyrin, or (2) by total synthesis. Although convenient, modification of naturally occurring porphyrins poses great limitations on the choice of peripheral substituent because certain substituents cannot be modified easily. In most cases, such limitations can be overcome by total synthesis, which involves the synthesis of the pyrrole subunits having the required substituent.

Koo *et al.* examined porphyrin derivatives for the possibility of reduction and oxidation (redox) states as molecular-scale memory or logic circuits. The device fabrication process using Zn-porphyrin Langmuir-Blodgett (LB) films was described, and the electrical properties of these

devices were obtained. The cyclic voltammetry and *I-V* characteristics of Zn-porphyrin LB film was found to exhibit outstanding switching diode and tunneling diode behavior at room temperature.[14] The electrical performance of the devices were greatly determined by the electrode materials used.

Molecular based information storage uses a collection of redox-active molecules attached to an electroactive surface in which information is stored in the discrete redox states of the molecules.[32] Porphyrins have been used as the active elements for two main reasons as follows: (1) Redox potentials of stable π-cation radicals of the porphyrin can be tuned by synthetic design; (2) The charge retention time of porphyrin-based information-storage elements are long (minutes) compared with that of the conventional semiconductor based dynamic random access memory (tens of milliseconds). Monomeric porphyrins exhibit two accessible cationic states,[76] whereas triple-decker architecture exhibits as many as four states.[77]

Molecular components as functional elements in place of semiconductor-based devices must compete under the extreme conditions required for processing and operating a practical device. Porphyrin-based molecules bound to Si(100) exhibiting redox behavior useful for information storage have been studied.[4] These molecular elements were stable under extreme temperature (400° C) for extended periods (~1 hour), and did not degrade under large numbers of read-write cycles (10^{12}). The cyclic voltammetric (CV) behavior of a porphyrin monolayer, formed on a micrometer-scale, photolithographically patterned, and hydrogen passivated Si(100) substrate (due to covalent bonding between Si-O-C), was observed. The robustness of the system was illustrated by performing repeated cycles of oxidizing the electrically neutral monolayer and reducing the resulting positively charged monolayer to its electrically neutral state. As a result, the thermal stability and read-write cycling information indicated that a porphyrin-based information storage system was extremely robust.

As discussed earlier, porphyrins absorb certain wavelengths of visible light strongly, and the close molecular packing in self-assembled porphyrin arrays offers the possibility for intermolecular transfer or delocalization of the excitation energy. For example, nanorods displaying an intriguing array of photoconductive behavior were demonstrated using nanometer-sized photoelectronic devices fabricated with SAM of porphyrinic materials.[80] Schwab *et al.* illustrated that the porphyrin nanorods were insulating in the dark, and upon illumination with 488 nm light, the nanorods became photoconductive. They formulated a qualitative conductivity model which addresses the conduction in terms of excitation of electrons from HOMOs to LUMOs.

From the examples and milestones, such as the aforementioned, with respect to the nanoelectronic properties of both porphyrin-based molecules and colloidal Q-CdS, that we were motivated to conduct the fluorescence (FL) spectroscopy characterization study that is the topic of this chapter. However, prior to the discussion of our results, it is useful to understand FL and how it can be best applied to hybrid electronic materials.

3.3 FLUORESCENCE SPECTROSCOPY

Fluorescence (FL) spectroscopy or Fluorimetry or Spectrofluorimetry is a type of electromagnetic spectroscopy which analyzes florescence from a sample. Fluorescence refers to the process where the molecular absorption of a photon triggers the emission of another photon with a longer wavelength. The energy difference between the absorbed and emitted photons ends up as molecular vibrations or heat. Usually the photons are absorbed in the ultraviolet range, and the emitted light is in the visible range. However this depends on the absorbance curve and Stokes shift of the particular fluorophore. Fluorescence spectroscopy can be used to identify and analyze fluorescent compounds at very low concentration (in the parts per billion range) while providing information about structure, formulation, and stability. Both solid and

liquid samples can be analyzed using fluorimetry. Fluorescence spectra are produced when ions or molecules absorb electromagnetic radiation at short wavelengths (higher energy) and are capable of radiating at longer wavelengths (lower energy). Besides uniquely identifying fluorescent compounds, these spectra provide information on the structure of fluorescent substances.

3.3.1 Fluorescence Process

Molecules have various states referred to as energy levels. FL spectroscopy is primarily concerned with electronic states and vibrational states. In general, molecules being examined will have a lower energy state, called the "ground electronic state," and a higher energy state, called the "excited electronic state." Each of these electronic states has various vibrational states. Photons of light are small "packets" of energy, each with energy proportional to their frequency ($h\upsilon$), and these can be absorbed by molecules, with the molecule gaining the energy of the photon, or emitted by molecules, with the photon carrying some of the energy of the molecule away.

In FL spectroscopy, the molecule is first excited, by absorbing a photon of light ($h\upsilon_{Ex}$) from its ground electronic state (S_o) to one of the various vibrational states in the excited electronic state ($S_1^{'}$). Having absorbed energy and reached one of the higher vibrational levels of an excited state, the molecule rapidly loses its excess of vibrational energy by collision and falls to the lowest vibrational state of the excited electronic state (S_1). From this level, the molecule can return to one of the various vibrational levels of the ground electronic state (S_o) again, emitting its energy ($h\upsilon_{Em}$) in the form of fluorescence (Figure 3.3). As molecules may drop down into any of the vibrational levels of this ground state, the photons will have different energies, and thus different frequencies. The difference in energy ($h\upsilon_{Ex} - h\upsilon_{Em}$) is called the Stokes shift, which is fundamental to the sensitivity of the fluorescence technique. Therefore, by

analyzing the different frequencies of light emitted in FL spectroscopy, the structure of these different vibrational levels can be determined. One transition, which from the lowest vibrational level in the ground state to the lowest vibrational level in the excited state, is called the 0-0 transition and is common to both the absorption and emission phenomena. On the other hand, all other absorption transitions require more energy than any transition in the fluorescence emission. The shape of the emission spectrum is always the same, despite changing the wavelength of the exciting light because the emission fluorescence always takes place from the lowest vibrational level of the first excited state.
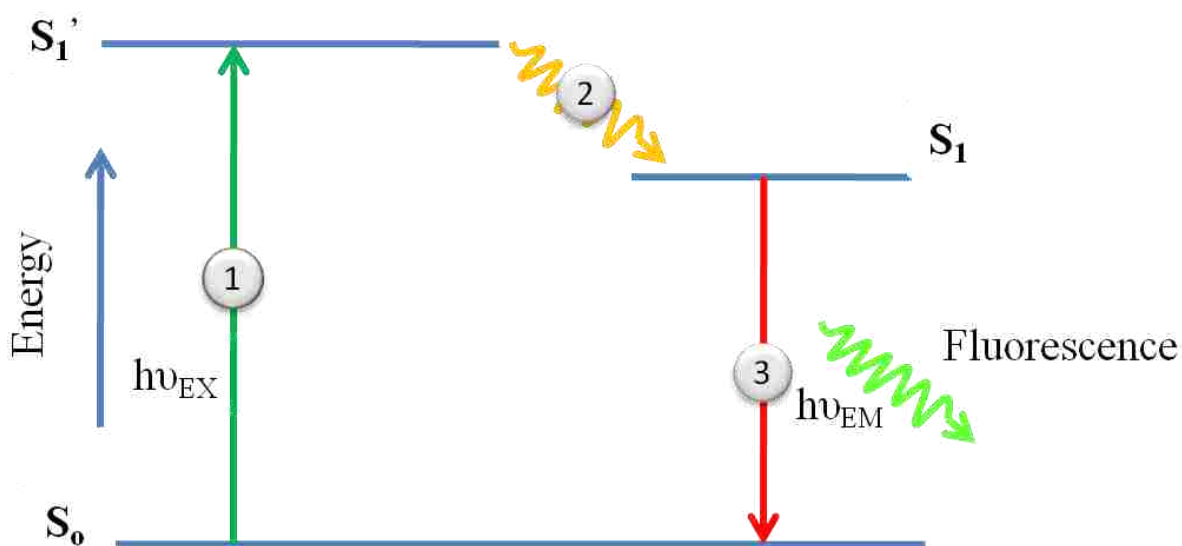
Figure 3.3: Jablonski diagram illustrating the process involved in the creation of an excited electronic singlet state by optical absorption and subsequent emission of fluorescence. Stage 1: Molecule is excited by absorbing a photon of light ($h\upsilon_{Ex}$) from its ground electronic state (S_o) to excited electronic state (S_1). Stage 2: Molecule rapidly loses its excess of vibrational energy by collision and falls to the lowest vibrational state of the excited electronic state (S_1). Stage 3: Molecule returns to ground electronic state (S_o) again, emitting its energy ($h\upsilon_{Em}$) in the form of fluorescence.

3.3.2 Fluorescence Spectra

The FL emission process is purely cyclical and the same fluorophore can be repeatedly excited and detected, unless the fluorophore is irreversibly destroyed in the excited state which is known as photobleaching. A single fluorophore can generate several detectable photons and this is the cause for the high sensitivity of fluorescence detection techniques. A plot of emission intensity against wavelength is known as the emission spectrum. If the wavelength of the exciting light is varied, and the emission from the sample is plotted against the wavelength of the exciting light, this display is known as the excitation spectrum. While varying the excitation wavelength if the intensity is kept constant, then the plot obtained by plotting emission intensity against exciting wavelength is known as the corrected excitation spectrum. With certain exceptions, the FL excitation spectrum of a single fluorophore in dilute solution is identical to its absorption spectrum. In turn, the emission spectrum is independent of the excitation wavelength, due to the partial dissipation of excitation energy during the excited-state lifetime. The emission intensity is proportional to the amplitude of the FL excitation spectrum at the excitation wavelength.

3.3.3 Fluorescence Detection

FL intensity is quantitatively dependent on the parameters defined by the Beer–Lambert Law such as the product of the molar extinction coefficient, optical path length, and solute concentration — as well as upon the fluorescence quantum yield of the dye, the excitation source intensity, and the fluorescence collection efficiency of the instrument. In dilute solutions or suspensions, FL intensity is mostly linearly proportional to these parameters. This linearity can often extend over a relatively broad concentration range, especially for fluorophores with high quantum efficiencies.

All fluorescence instruments contain the basic items such as a source of light, a sample holder, and a detector. In addition, we need the capability to tune the incident light wavelength and to manipulate the detector signal. To achieve these analytical purposes, either filters or monochromators are used in the fluorescence instrumentation (Figure 3.4).

3.3.4 Applications of FL Spectroscopy

FL spectroscopy is widely used to investigate the electron-phonon interaction in complex compounds such as semiconductors, organic and inorganic materials. For example, cysteine ester passivated CdS nanoclusters fluorescing in blue region has been reported.[65] Further, CdS/ZnS stabilized in sol-gel derived silica matrix are reported as blue semiconductor nanocrystal laser.[59] This ensures the possibility of using these quantum dots as fluorescent biological probes. The electroluminescence of any material creates an exciting opportunity for reengineering of the optical, electronic, and thermal properties of many technologically important hybrid materials through modification of their electronic states. For example, organic multilayer white light emitting diodes based on thin films of organic materials are reported.[91] These spectroscopic techniques are used to understand the quantum phenomenon compared to bulk materials.

FL spectroscopy is also being widely used to investigate the fluorescence properties pertinent to the biochemical, medical, chemical fields with respect to analyzing organic compounds. For example, FL spectroscopy investigation of structural, organization, and orientation of membrane proteins has been reported.[92] Some of the important approaches included in these studies are depth of penetration of membrane proteins and peptides employing fluorescence quenching, site-directed labeling, and the wavelength-selective fluorescence approach. Conformational study of peptide derivative models exhibiting helical conformation revealed through FL spectroscopy are reported as potential atheroprotective agents.[93]
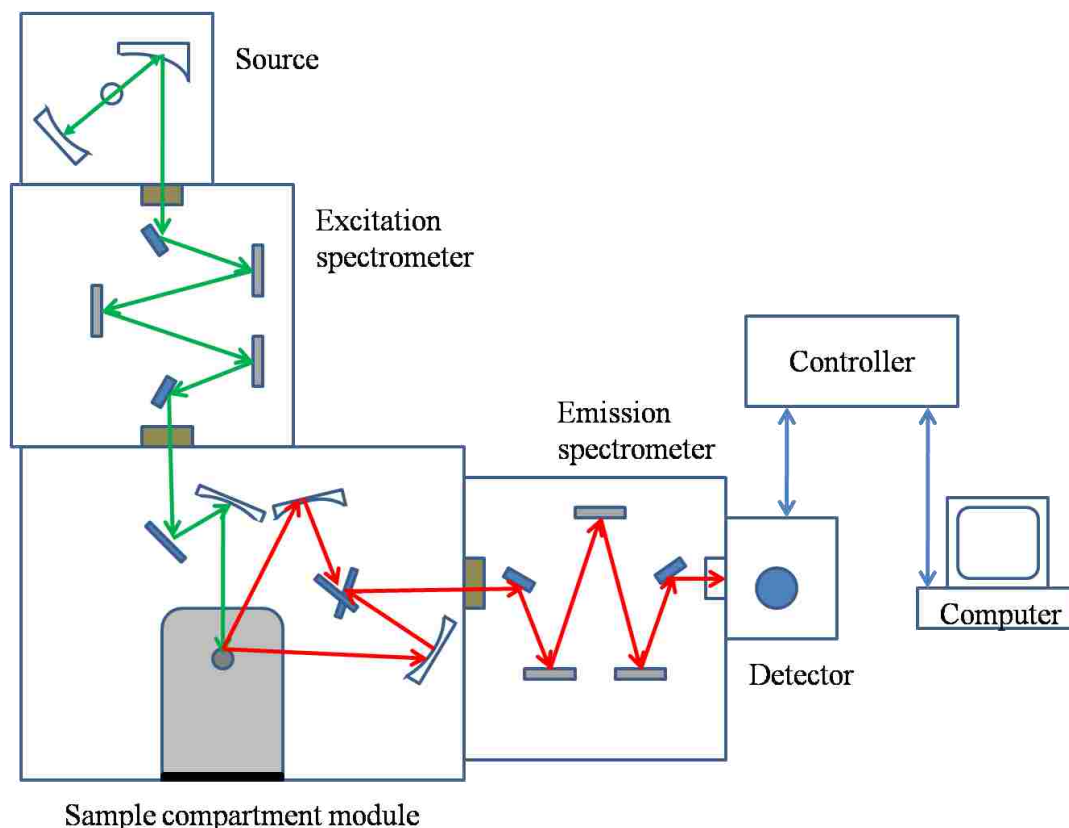
Figure 3.4: Schematic representation of a fluorescence spectroscopy instrument [19].

3.4 EXPERIMENTAL DETAILS

3.4.1 Chemicals and Materials.

For our work high-purity water (Millipore purification system) was used in the preparation of all solutions. All chemicals were reagent or spectrographic grade and were used as received. Two primary forms of samples such as colloidal Q-CdS and porphyrin based-molecules for examination by FL were prepared. The colloidal Q-CdS capped with AOT were provided by Professor Isiah Warner, Dept. of Chemistry, LSU, by way of Dr. Warner's postdoctoral assistant, Dr. Mark Lowry. AOT capped Q-CdS dissolved in heptane with varying particle sizes between 1–5 nm (relative size obtained from absorption spectrum depending upon the heptane concentration) were deposited on different substrates such as gold on glass, mica, and GaAs. Using a micropipette, 3 µL of Q-CdS solution was dropped onto the substrates and

54

allowed to evaporate in air. The monolayer was formed by physisorption of colloidal Q-CdS dissolved in heptane on different substrates. These physisorbed Q- CdS monolayers were used for the fluorescence measurements. The absorbance spectra of Q-CdS in Figure 3.5 illustrates that the higher the heptane concentration in the synthesis of AOT capped Q-CdS, the larger the particle size. The relative sizes of these dots are between 1 nm to 5 nm with heptane concentration between 20 µL to 90 µL, respectively.
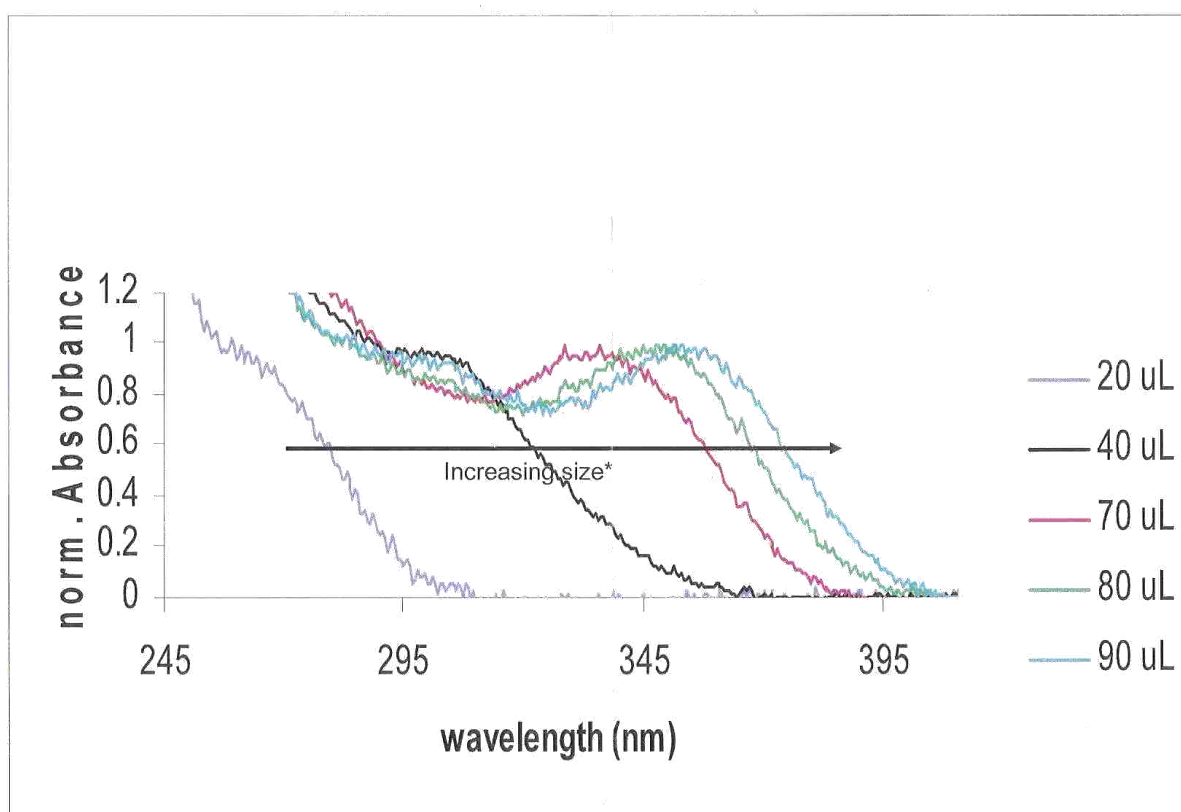
Note: Spectra taken in 90% Hexane 10% Heptane
* Relative size estimated from absorption spectra

Figure 3.5: Normalized absorbance spectrum of AOT capped Q-CdS in heptane.

Next, porphyrin monolayers are formed on gold substrates. A small amount of trityl protected monothiolated phorphyrin was cleaved ex-situ. The cleaved monothiolated phorphyrin

55

solution was prepared in toluene. Gold on mica substrates were rinsed with toluene and then dried with a stream of nitrogen before immersion. Self assembled monolayers (SAMs) were prepared by immersing gold substrates into this porphyrin solution for 12–14 hours. After immersion, the samples were removed from solution, rinsed with toluene at least three times and then dried with a stream of nitrogen.

3.4.2 Fluorescence Measurements

The experiments have been performed using a Fluorolog-3Model FL3-22 spectrofluorometer from Jobin Yvon Horiba with state-of-the-art optical components and DataMax, the driving software for Windows. Fluorolog-3 has a Xenon source of radiation to produce photons, and the beam of light is filtered by an excitation spectrometer (double-grating monochromator) which allows a single wavelength of light to reach the sample. In the sample compartment, the sample responds to the incoming radiation. The transmitted radiation can be collected at two different modes such as front face (FF) and right angle (RA). In RA mode, the transmitted signal slightly displaces the sample from its normal position and directs the transmitted light into the collection optics with a mirror mounted at 45°. In FF mode, the light is collected at an angle of 22.5^o. RA mode is widely used for liquid samples and FF is commonly used for samples such as thin films, powders, pellets, microscope slides, and fibers. In FF orientation, stray and reflected light off the surface of the sample are minimized. The resulting radiation is filtered by an emission spectrometer (double-grating monochromator) that feeds the signal to a photomultiplier detector. By stepping either or both spectrometers through a wavelength region, and recording the variation in intensity as a function of wavelength, a spectrum is produced. The spectrometer components are connected to a controller which, in turn, transfers information to and from the computer. The standard sample-compartment module is a T-box, which provides efficient throughput with a choice of standard right-angle emission

collection or optional front-face emission collections. Cut-on filters are used to eliminate second-order effects of the gratings. Figure 3.6 shows the experimental setup used for the fluorescence spectroscopic measurements.
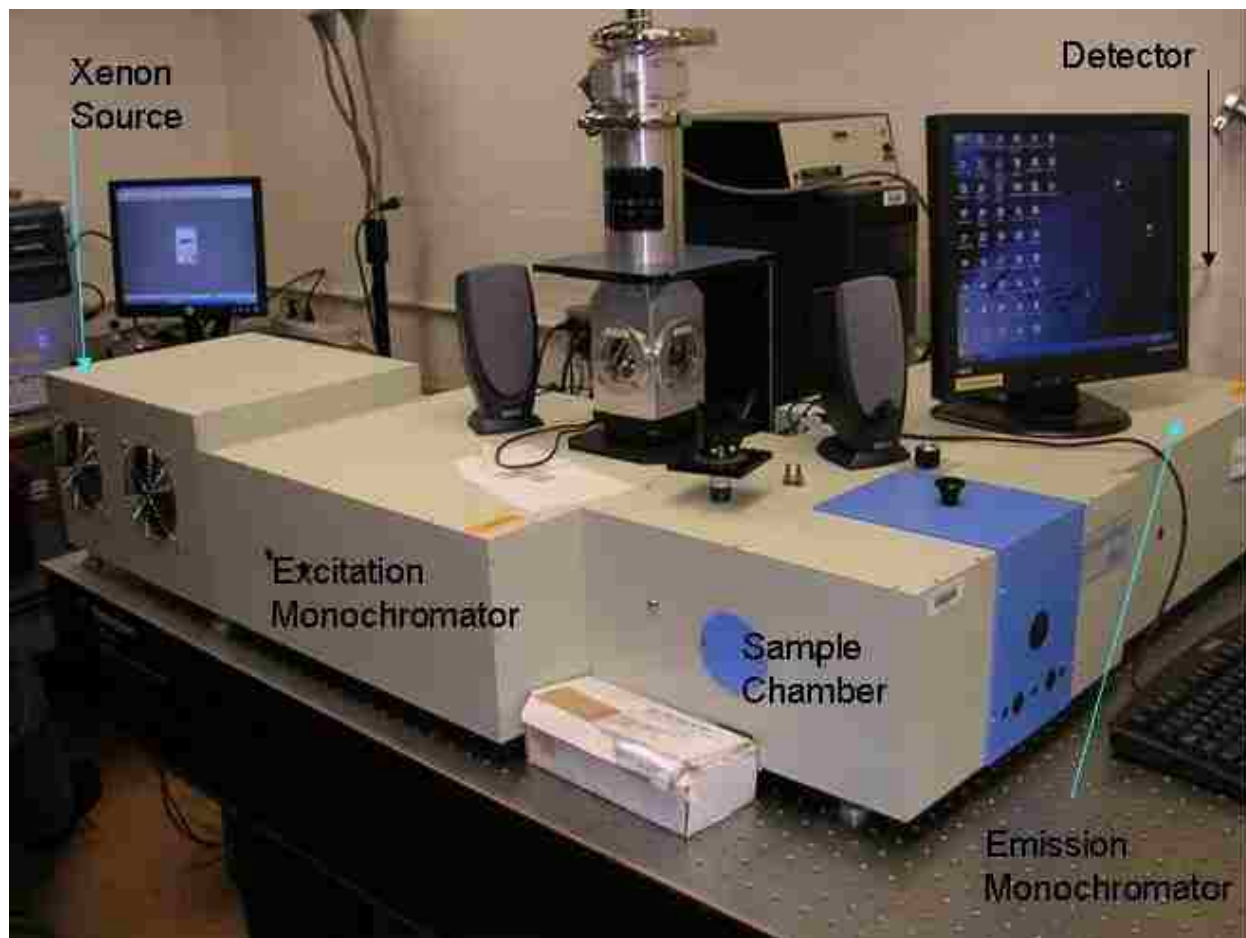
Figure 3.6: Experimental setup of fluorescence spectroscopy.

All of the fluorescence measurements of liquid samples, such as AOT capped Q-CdS in heptane and monothiolated porphyrin in toluene, are measured in RA collection mode. In turn, the fluorescence measurements on solid samples such as AOT capped Q-CdS physisorbed on Au/glass, mica, and GaAs, respectively, and SAM of monothiolated porphyrin on Au/mica are collected in FF mode. To avoid transmission reflections and scattering, the solid samples are oriented to such an angle to get maximum fluorescence emission in FF mode collection.

Figure 3.7 and Figure 3.8 shows the liquid and solid sample holders respectively. The angles of incidence for solid samples are determined as described in the following section.

Figure 3.7: Liquid sample holder and a cuvett filled with liquid sample.

Figure 3.8: Graduated base rotatable solid sample holder.

Determination of Incidence Angle

Usually, solid samples are loaded onto the solid sample holder with its plane of surface normal to the incident light, and signals are collected in FF mode. To avoid direct reflection of

light incident on the sample with a reflective background such as gold and GaAs, the sample is slightly displaced from the normal position with different possible collection angles. The resulting emission signals are compared with different collection angles, and the best of all is selected as the angle of incidence in our measurements. Figure 3.9 shows the schematic representation of angle of incidence with respect to right side of the sample, and Figure 3.10 shows the schematic representation of angle of incidence with respect to left side of the sample.
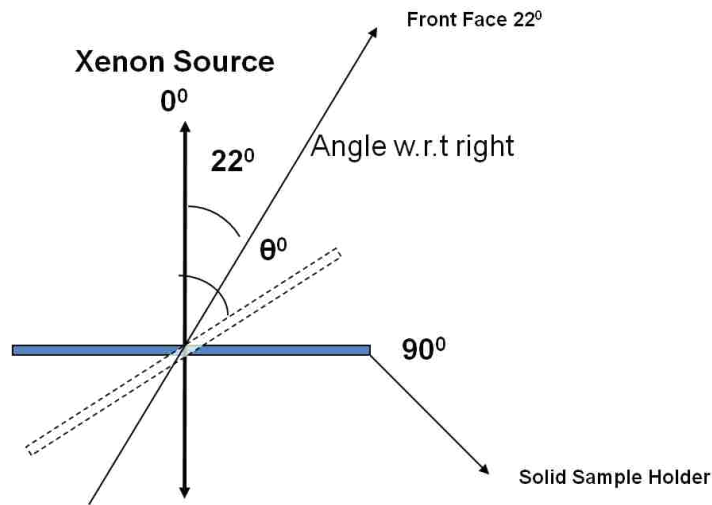
Figure 3.9: A schematic representation of the solid sample holder facing the Xenon light with its plane perpendicular to the light source. The sample holder is oriented with an angle θ between the light source and the sample surface in the first quadrant.
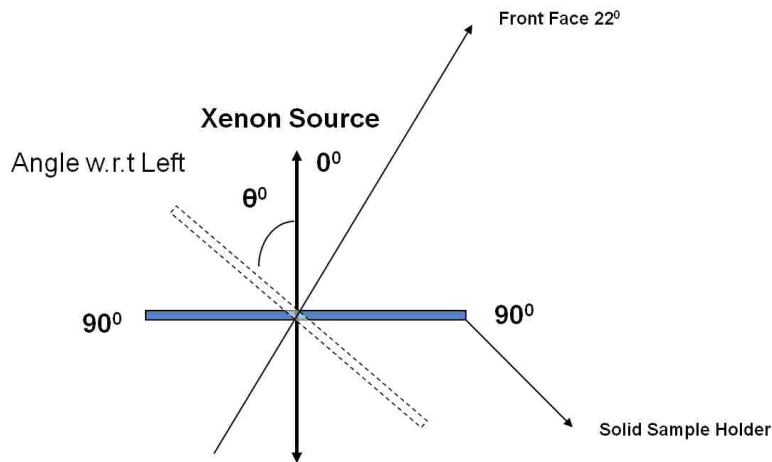
Figure 3.10: A schematic representation of the solid sample holder facing the Xenon light with its plane perpendicular to the light source. The sample holder is oriented with an angle θ between the light source and the sample surface in the second quadrant.

The angle of incidence for AOT capped Q-CdS physisorbed on gold is calculated to be 80° to the right of the sample. The same angle is used as well to obtain the fluorescence spectra of Q-CdS on mica and GaAs. The angle of incidence for porphyrin on gold is calculated to be 45° to the right of the sample as shown in Figure 3.9. With the determined angle of incidence, all the fluorescence measurements are obtained for the entire range of excitation and emission wavelength (200 nm to 800 nm), known as matrix scan. From the matrix scan, we determine the excitation and emission peaks and run the individual emission/excitation scans, respectively. I varied the excitation and emission band pass filter slit widths and analyzed the fluorescence intensity. Depending upon the fluorescence intensity, low signal to noise ratio, and higher resolution data, the slit widths are varied between 2 and 4 nm to obtain the fluorescence spectra.

3.5 RESULTS AND DISCUSSION

3.5.1 Optical Properties of the AOT Capped Q-CdS

The concentration of heptane has a significant influence on the final size of the colloidal Q-CdS. The fluorescence spectra of the AOT capped Q-CdS excited with 2 nm slit band width for three different concentration of heptane are shown in Figure 3.11. The fluorescence spectra recorded from colloidal Q-CdS are in good agreement with the literature.[65] The spectra show a clear shift of the excitation peak onset to shorter wavelengths as the concentration of heptane decreases. A primary indication of size-quantized semiconductor particles, as compared to bulk species, is a blue shift in the excitation spectrum. The CdS colloids generally have a weak broad emission ranging from 500-700 nm. This fluorescence could be attributed to the recombination of the charge carriers immobilized in traps of different energies. The functionalized Q-CdS showed long emission wavelengths and a high separation between the excitation and emission wavelengths (over 100 nm).

The emission maxima of the AOT capped Q-CdS decreases from 515nm to 488nm as the size decreases (for heptane concentration 80 μL to 40 μL). Typically, the emission maxima are shifted to shorter wavelengths with decreasing particle diameter. The excitation transitions with band gap energies (E_g) gradually shift from 3.45 eV (360 nm λ_{max}) to 3.35 eV (370 nm λ_{max}) as the relative particle size varies.
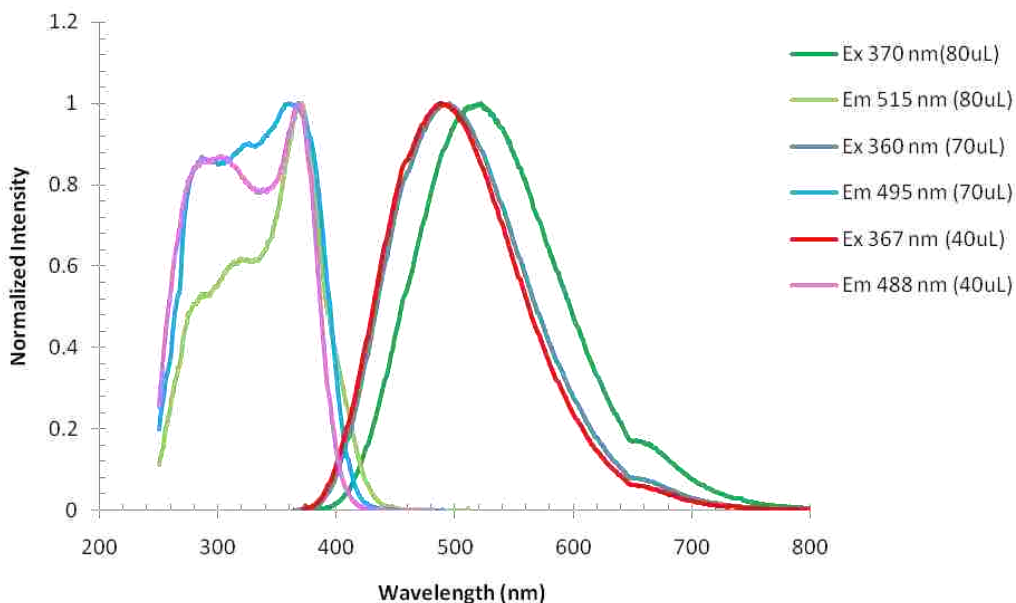
Figure 3.11: Normalized fluorescence spectra of AOT capped Q-CdS in heptane solution showing excitation (Ex) and emission (Em) peaks for selected concentrations 80, 70, and 40 uL. (Excitation /emission slit sizes : 2 nm)

3.5.2 Optical Properties of the Physisorbed AOT Capped Q-CdS

3.5.2.1 Effect of Angle of Incidence

The angle of incidence of the light source has a large influence on the fluorescence intensity. The emission spectra of AOT capped Q-CdS in 90μL heptane physisorbed on Au/glass are shown in Figure 3.12. The emission spectra of Q-CdS on Au are obtained by exciting at 350nm for different angles of incidence. As discussed earlier, the sample holder is

oriented with an angle θ between the light source and the sample surface in the both first (left side of the sample) and second (right side of the sample) quadrant. The maximum emission (Y) intensity is obtained for Q-CdS absorbed on Au excited at 350 nm with 5 nm slit width (excitation and emission width: 5/5 nm) and incidence angle of 80° right with respect to the sample (Y5/5 80Rx350). Rakovich *et al.* has reported the absorbance and photoluminescence (PL) study of CdS quantum dots.[64] The emission spectra show good agreement with the PL spectra of this literature. The spectra show a broad band in the visible range and a pronounced high energy peak in ultraviolet spectral range. The high energy peak could be due to the radiative recombination of a confined electron in a quantum dot and a hole captured at a shallow acceptor level. The exitation transition with band gap energy 3.54 eV (350nm λ_{max}) is obtained from the spectra.
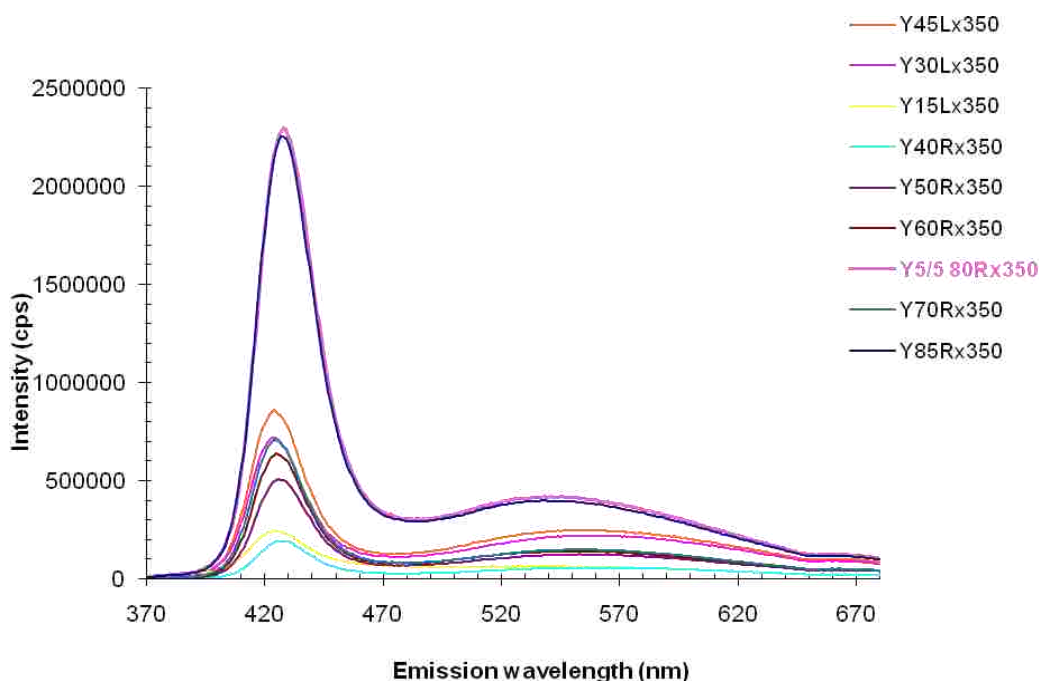
Figure 3.12: Emission spectra of AOT capped Q-CdS in heptane 90μL solution physisorbed on gold/glass substrate excited (x) at 350 nm with different angle of incidence both left (L) and right (R) as indicated. (Excitation /emission slit sizes : 5 nm)

3.5.2.2 Effect of Physisorbed Substrate

The fluorescence spectra of the AOT capped Q-CdS physisorbed on gold, mica and GaAs in 40µL, 70µL and 80µL heptane with slit size 2nm and angle of incidence at 80° right are shown in Figure 3.13, Figure 3.14, and Figure 3.15, respectively. Q-CdS absorbed on different substrates such as metal, semiconductor and insulator have the same excitation wavelength; however the emission wavelengths are red shifted. Q-CdS in 40µL heptane is excited at 360nm, and the emission peaks are obtained at 460nm, 470nm and 482nm for gold, mica, and GaAs substrates respectively. Q-CdS in 70µL heptane is excited at 365 nm, and the emission peaks are observed at 505nm, 481nm and 490nm for gold, mica, and GaAs substrates respectively. Q-CdS in 80µL heptane is excited at 370nm, and the emission peaks are observed at 525nm, 500nm and 515 nm for gold, mica, and GaAs substrates, respectively.

Figure 3.13: Normalized fluorescence spectra of AOT capped Q-CdS in heptane 40 µL physisorbed on different substrates showing excitation (Ex) and emission (Em) peaks respectively. (Excitation and emission slit sizes : 2 nm respectively)

In general, the emission spectra are broad band emissions extending over a large part of the visible region and shift to higher energies as the particle become smaller. Both electrons and holes could be trapped in shallow traps, and recombination of the donor acceptor pair might give rise to sub-bandgap emission. The shift of an electron-hole pair typically would follow the valence and conduction band edges. The large spectral width of the emission band could be caused by inhomogeneous broadening due to particle size and electron-phonon coupling.

Figure 3.14: Normalized fluorescence spectra of AOT capped Q-CdS in heptane 70 µL physisorbed on different substrates showing excitation (Ex) and emission (Em) peaks respectively. (Excitation and emission slit sizes : 2 nm respectively)

Q-CdS physisorbed on gold emits photons at shorter wavelengths compared to Q-CdS adsorbed on mica and GaAs. Q-CdS adsorbed on mica emits photons at higher wavelengths compared to particles on gold; however emits photons at shorter wavelengths compared to quantum dots adsorbed on GaAs. To investigate the stability of the samples, I took

measurements on different days and observed similar behavior with an exception of lower fluorescence intensities.

Incorporation of Au atoms into Q-CdS increases the bandgap, and emission peaks shift to shorter wavelengths. The shift in bandgap may be by an exchange of Q-CdS capped with AOT and Au during the deposition process. Integration of mica with AOT capped Q-CdS does not strongly influence the bandgap, but it serves as a recombination center situated in the bandgap. Thus a red-shifted emission is observed. The fluorescence intensity of Q-CdS adsorbed on GaAs is higher (normalized intensities are shown in the figure) compared to particles adsorbed on gold and mica. The increase in fluorescence intensity could be due to radiative recombination of a confined electron in the quantum dot and a hole captured at a shallow acceptor level of the GaAs substrate interface. Therefore, a functionalized Q-CdS adsorbed onto GaAs would be recommended for potential hybrid electronic devices. The Q-CdS/GaAs complex has maximum fluorescence emission which could be used for various optoelectronic device applications.
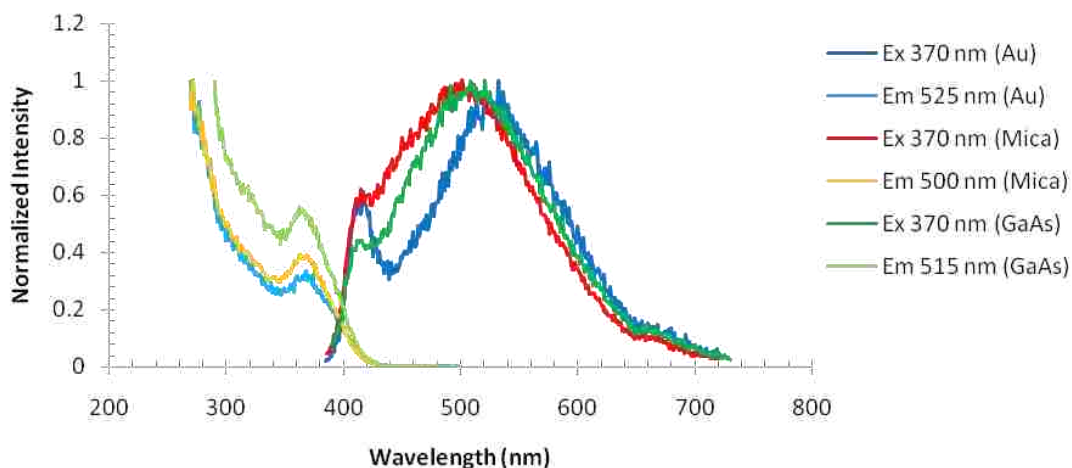
Figure 3.15: Normalized fluorescence spectra of AOT capped Q-CdS in heptane 80 µL physisorbed on different substrates showing excitation and emission peaks respectively. (Excitation and emission slit sizes : 2 nm respectively)

3.5.2.3 Effect of Slit Width and Relative Size

The fluorescence spectra of the AOT capped Q-CdS physisorbed on gold, mica, and GaAs in 40µL, 70µL and 80µL heptane with slit size 4nm and angle of incidence at 80° right are shown in Figure 3.16, Figure 3.17 and Figure 3.18, respectively. The fluorescence spectra of Q-CdS excited with two different excitation/emission slit widths 2 and 4 nm are compared and not many variations are observed. However, when the slit opening is varied from 2nm to 4nm, the Q-CdS in 40µL heptane physisorbed on gold, mica, and GaAs showed an increase in fluorescence intensities and emission peaks such as 470nm, 479nm and 483nm, respectively. Such variations are not significant in larger particles. As the relative size of the quantum dots decreases, the excitation wavelengths are blue shifted.
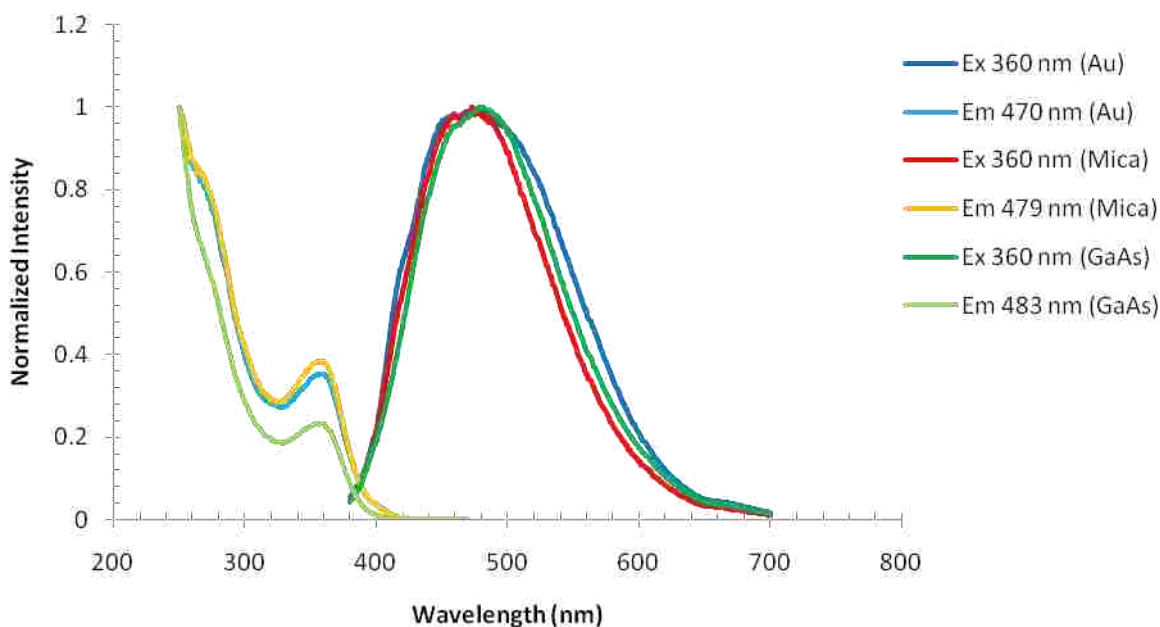
Figure 3.16: Normalized fluorescence spectra of AOT capped Q-CdS in heptane 40 µL physisorbed on different substrates showing excitation (Ex) and emission (Em) peaks respectively. (Excitation and emission slit sizes : 4 nm respectively)

As the intensity of the incident light source is increased, the sample gets ample light energy for excitation of more electrons to excited electronic states. Having absorbed energy and

66

reached one of the higher vibrational levels of an excited state as discussed earlier, the molecule rapidly loses its excess of vibrational energy by collision and falls to the lowest vibrational state of the excited electronic state. Increase in electron population in the excited state increases the rate of collision, and from this level, the molecules return to the ground electronic state in the form of fluorescence. The increase in the emission peak could be attributed to higher radiative recombination of confined electrons in quantum dot and trapped charge carriers compared to free charge carriers.
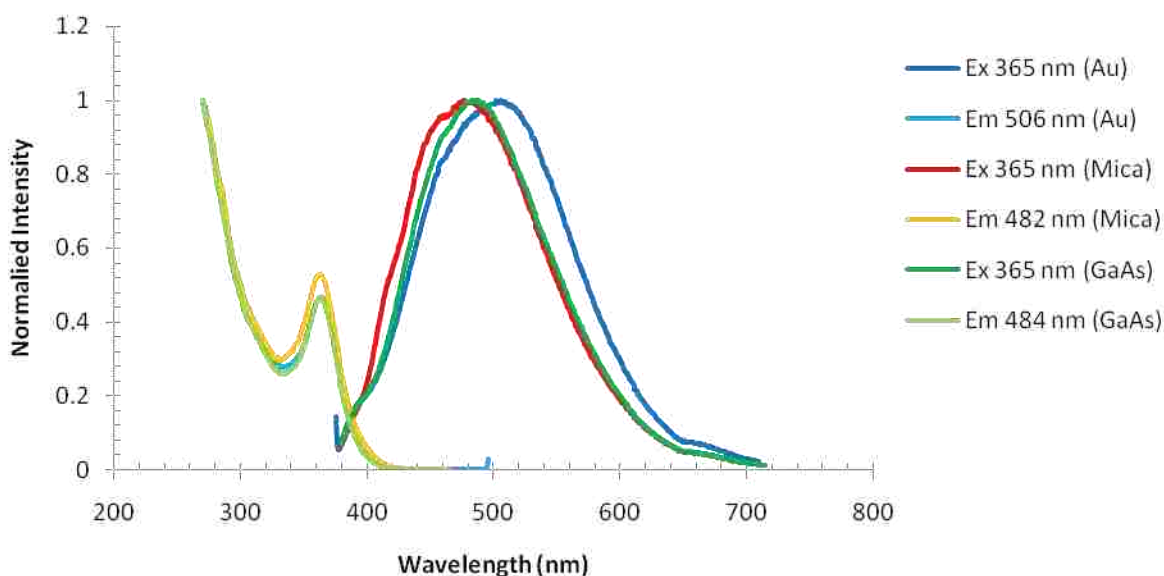
Figure 3.17: Normalized fluorescence spectra of AOT capped Q-CdS in heptane 70 μL physisorbed on different substrates showing excitation (Ex) and emission (Em) peaks respectively. (Excitation and emission slit sizes : 4 nm respectively)

The spectra show a broad band in the visible range for Q-CdS with relatively smaller sizes (heptane 40 and 70 μL), perhaps a pronounced high energy peak in ultraviolet spectral range is observed for Q-CdS with relatively larger size (heptane 80 μL). As previously mentioned, the large spectral width of the emission band could be caused by inhomogeneous broadening due to particle size and electron-phonon coupling. The high energy peak for

67

relatively larger Q-CdS could be due to the radiative recombination of a confined electron in a quantum dot and a hole captured at a shallow acceptor level.
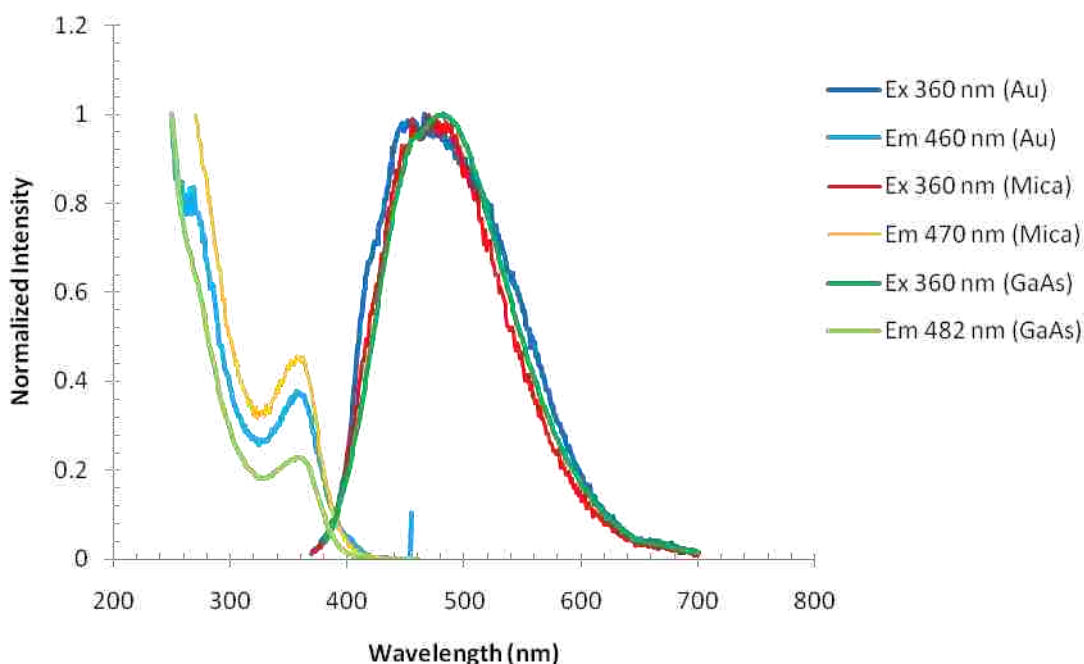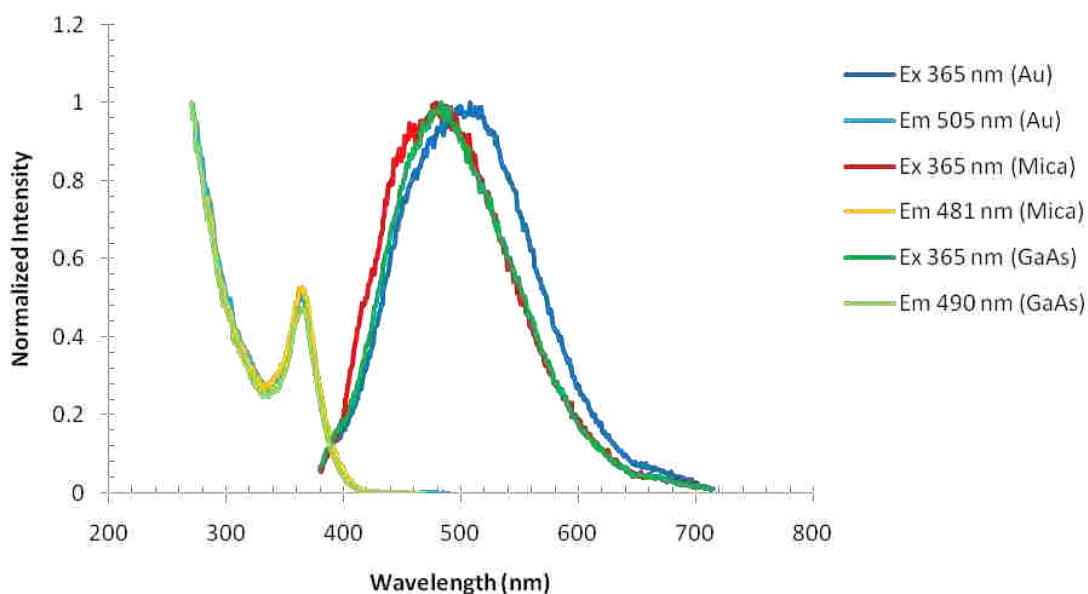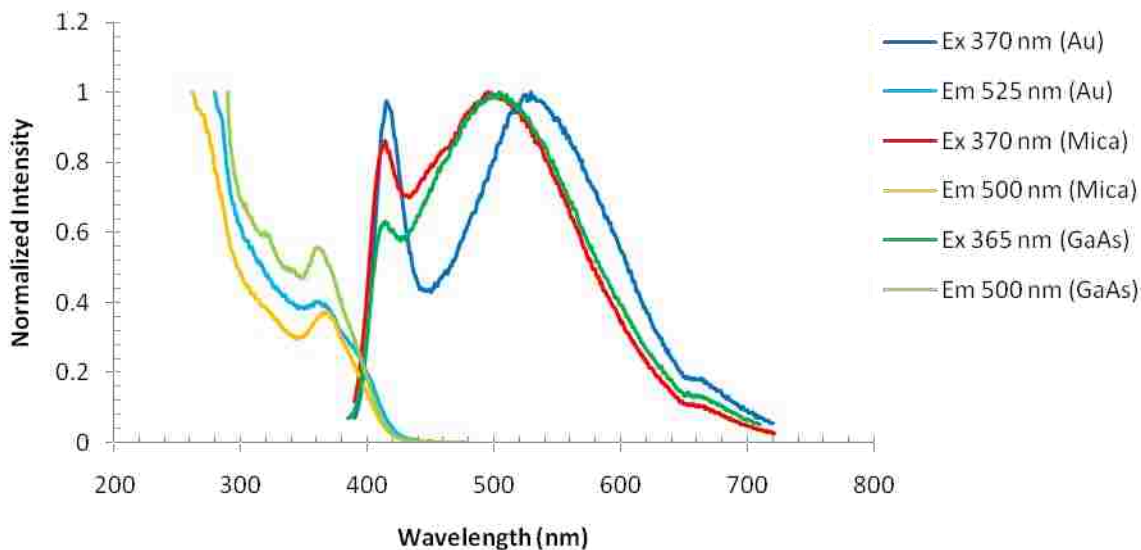

Figure 3.18: Normalized fluorescence spectra of AOT capped Q-CdS in heptane 80 µL physisorbed on different substrates showing excitation (Ex) and emission (Em) peaks respectively. (Excitation and emission slit sizes : 4 nm respectively)

The spectra show a broad band in the visible range for Q-CdS with smaller sizes (heptane 40 and 70 µL), perhaps a pronounced high energy peak in ultraviolet spectral range is observed for Q-CdS with larger size (heptane 80 µL). As previously mentioned, the large spectral width of the emission band could be caused by inhomogeneous broadening due to particle size and electron-phonon coupling. The high energy peak for larger Q-CdS could be due to the radiative recombination of a confined electron in a quantum dot and a hole captured at a shallow acceptor level.

3.5.3 Optical Properties of the Monothiolated Porphyrins

The fluorescence spectra of the monothiolated porphyrin dissolved in toluene are shown in Figure 3.19. Monothiolated free base porphyrin excited at 420nm shows two emission peaks at

662nm and 720nm. The fluorescence spectra of porphyrin molecules observed here are in good agreement with the literature.[94,95] This fluorescence could be attributed to the recombination of the charge carriers immobilized in traps of different energies. The emission spectra show a broad band in the visible range (620 to 780 nm) with two pronounced high energy peaks. The high energy peak could be due to the radiative recombination of confined π electrons in the molecule. The excitation spectra obtained for the emission wavelengths 662 and 720 nm are in good agreement to each other which reproduced the excitation peak at 420 nm. The functionalized porphyrin showed shorter emission wavelengths and a high separation (Stokes's shift) between the excitation and emission wavelengths (over 200 nm). The excitation band gap energy for porphyrin to excite an electron from conduction band to valence band is 2.95 eV (420nm λ_{max}).
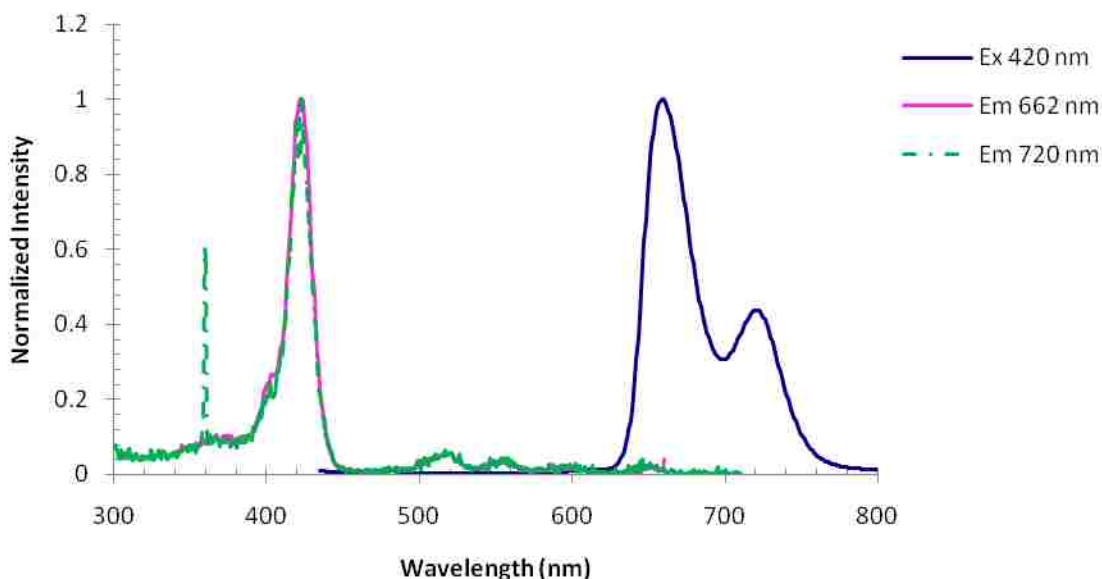
Figure 3.19: Normalized fluorescence spectra of monothiolated porphyrin in toluene solution showing excitation (Ex) and emission (Em) peaks respectively. (Excitation and emission slit sizes : 5 nm respectively)

3.5.4 Optical Properties of SAM of Monothiolated Porphyrins

3.5.4.1 Effect of Angle of Incidence

The fluorescence spectra of the monothiolated free base porphyrin were successfully reproduced from porphyrin molecules self-assembled on gold surfaces. Molecules excited at 420nm showed two emission peaks at 659nm and 720nm. The fluorescence intensity is varied with respect to the exciting angle of incidence. To avoid stray reflections and transmissions, front-face mode coupled with different angles of incidence with respect to the sample surface has been used. As discussed earlier, the fluorescence spectra for free base porphyrin chemisorbed on Au substrate excited with various angle θ with respect to the left (L) and right (R) of the sample are recorded. The maximum emission intensity has been observed for porphyrin molecules self-assembled on Au excited at 420 nm with an incidence angle of 45° right with respect to the sample as shown in Figure 3.20.
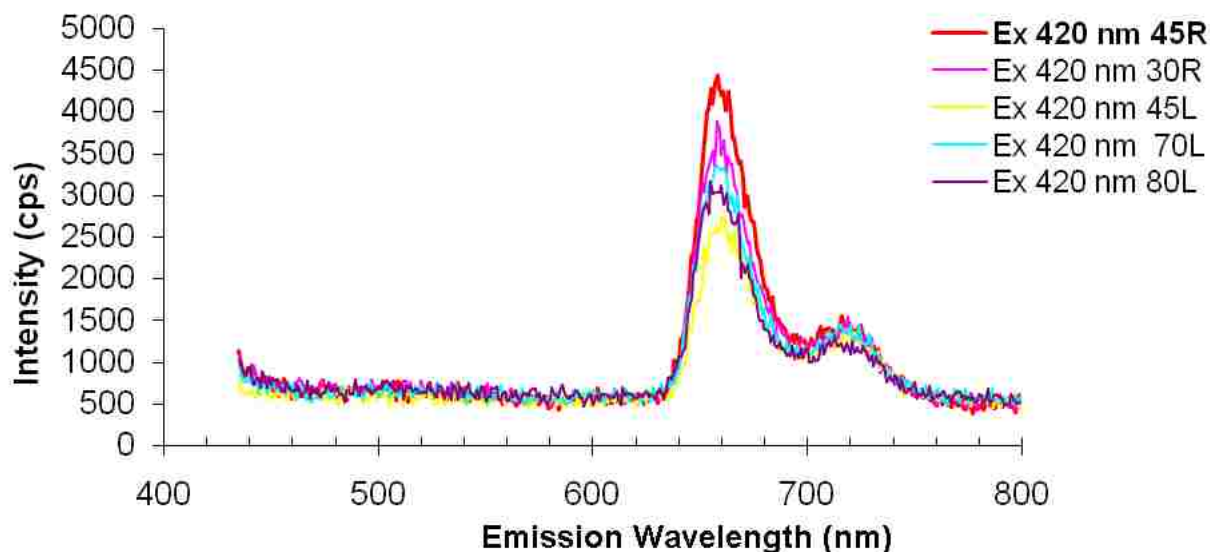
Figure 3.20: Emission spectra of monothiolated porphyrin in toluene chemisorbed on gold substrate excitated (Ex) at 420nm with different angles of incidence, both left (L) and right (R) as indicated. (Excitation and emission slit sizes : 5 nm respectively)

.
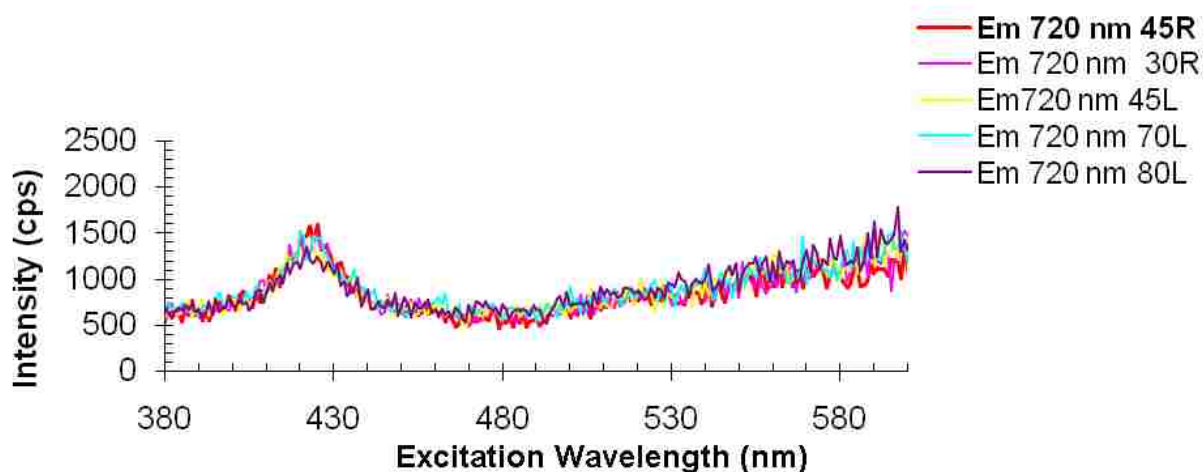
Figure 3.21: Excitation spectra of monothiolated porphyrin in toluene chemisorbed on gold substrate, emission (Em) at 720nm with different angle of incidence, both left (L) and right (R) as indicated. (Excitation and emission slit sizes : 5 nm respectively)

As mentioned above, the emission spectra of free base porphyrin exhibits two emission peaks at 659 and 720 nm. The excitation spectra of free base porphyrin obtained with reference to the two emission peaks are shown in Figure 3.21 and Figure 3.22, respectively. The fluorescence spectra (Excitation and Emission spectra) of free base porphyrin chemisorbed on gold substrate are in good agreement with the literature.[96,97] Both the excitation spectra obtained for individual emission peaks coincide with each other at the same excitation peak (420 nm)
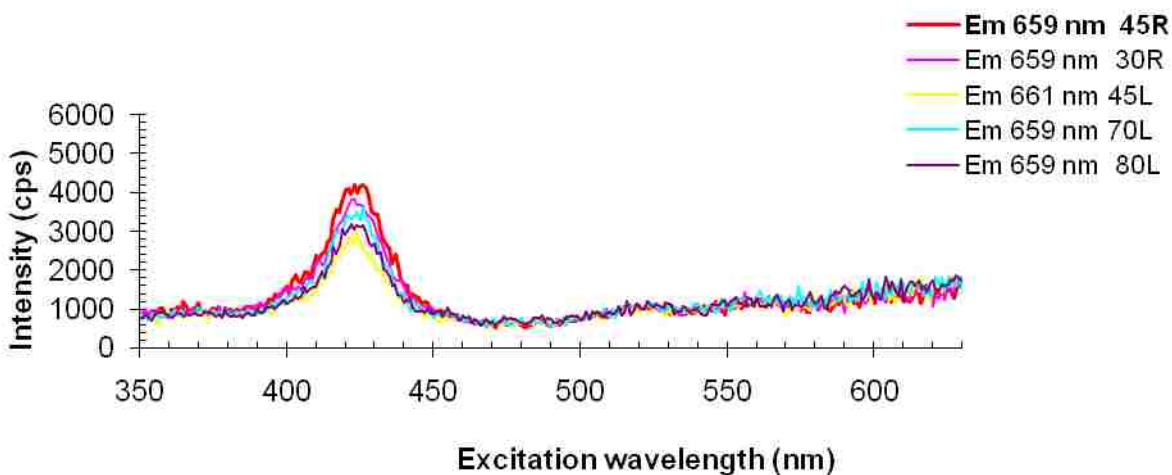
Figure 3.22: Excitation spectra of monothiolated porphyrin in toluene chemisorbed on gold substrate, emission (Em) at 659nm with different angle of incidence, both left (L) and right (R) as indicated. (Excitation and emission slit sizes : 5 nm respectively)

71

3.5.4.2 Characterization of Porphyrin Molecules on Gold

Figure 3.23 shows the normalized fluorescence spectra of free base porphyrins chemisorbed onto gold/mica substrates. The fluorescence emission of porphyrin in solution is reproduced on self-assembled porphyrin on gold. A gold electrode has no significant effect on the band gap energy of porphyrin molecules. Porphyrin molecules have strong interaction with photons including absorbance and fluorescence, as it has a core of π electrons inside the pyyrole ring. The fluorescence could originate through the π-π electron transitions. Porphyrin molecules may exhibit different fluorescence characteristics caused by their conformation and complex formation with the substrate.

Typical FL spectra of films of porphyrin materials show clear vibronic peaks (659 and 720 nm), well in agreement with the spectra (662 and 720 nm) of porphyrin solution but with a slight shift in the emission peak and decrease in FL intensity. The decrease in intensity could be attributed to the interaction of porphyrin molecules with the gold substrate. The molecular fluorescence is considered via electron-hole injection and assumed that the energy levels of emitting molecules are influenced by the substrate.

The emission spectra show a broad band in the visible range (640 to 740 nm) with two pronounced high energy peak at 659 and 720 nm respectively. The high energy peak could be due to the radiative recombination of a confined π-electron in the porphyrin molecules and a hole captured at a shallow acceptor level. The broad emission spectrum of free base porphyrin is reduced compared to the emission spectra of free base porphyrin in solution. This weak emission could be attributed to the metal cations forming a complex with the porphyrin molecules. The FL measurements of the same samples on different days showed similar fluorescence behavior except lower FL intensity. Therefore, it appears that porphyrin molecules form a stable monolayer on gold substrates.
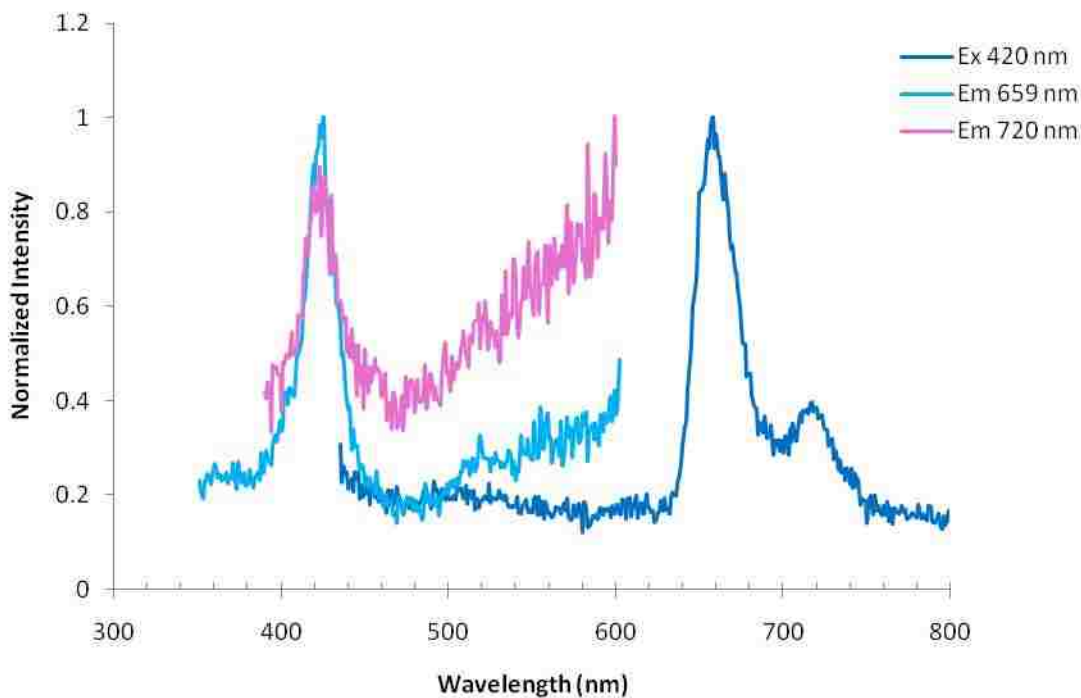
Figure 3.23: Normalized fluorescence spectra of self-assembled monolayer of monothiolated porphyrin on gold substrate showing excitation (Ex) and emission (Em) peaks respectively. (Excitation and emission slit sizes : 5 nm)

3.6 CONCLUSIONS AND FUTURE WORK

3.6.1 Conclusions

I have reported a fluorescence spectroscopic study of self-assembled monolayers of AOT capped CdS quantum dots on metal, insulator, and semiconductor substrates. Q-CdS adsorbed onto different substrates such as gold, GaAs, and mica has the same excitation wavelength. However, I observed a slight but systematic redshift of peaks in the emission spectra characteristics of spatially confined phonon interactions. The effects of relative quantum dot sizes, different substrates, and light intensity are reported in this study. As the sizes of the quantum dots decrease, the excitation peaks are slightly blue shifted. The increase in the emission peak could be attributed to higher radiative recombination of confined electrons in quantum dot and trapped charge carriers compared to free charge carriers. Finally, in the context

73

of engineering applications, the observation of electron-phonon interactions in self-assembled Q-CdS holds out the hope of developing a good top contact capable of forming a metal-molecule-quantum dot heterostructure. I have also reported a fluorescence spectroscopic study of self-assembled functionalized porphyrin molecules on gold electrodes. This fluorescence could be attributed to the recombination of the charge carriers immobilized in traps of different energy levels and through the π-π electron transitions. I obtained the band gap energy of porphyrin molecules and Q-CdS as ~ 2.95 eV and 3.35 to 3.45 eV, respectively from the excitation spectra.

3.6.2 Future Work

Although the optical properties of self-assembled Q-CdS and porphyrin have been studied using fluorescence spectroscopy in this work, there other parameters that should be investigated to understand the electron-phonon interactions in these materials. First, further investigation into electron transport in CdS quantum dots and conformational studies of porphyrin molecules will be needed. Second, fluorescence spectroscopic measurements with a detection rage in near IR wavelengths should be carried out. Third, analysis of the effect of capping ligands on the luminescence response of CdS quantum dots and the implementation of different metal substituent for free base porphyrin are required. Fourth, temperature dependence measurements on both Q-CdS and porphyrin based molecules should be made. Lastly, further investigation into the effect of size variation in Q-CdS particles adsorbed onto various substrates may prove useful for future HEM studies of this nature.

4. AFM STUDY OF CURRENT TRANSPORT THROUGH PORPHYRIN BASED MOLECULES

4.1 INTRODUCTION

In the most recent quarter century there has been a tremendously growing interest throughout the science-engineering community in the various aspects of nanoscience. Researchers past and present are working to better understand the structures of organic, inorganic, and biological materials by probing their chemical and physical properties on a molecular scale and by comparing the properties of a single molecule with those of an *ensemble or Avogadro's* number of molecules. Previously, information on the sub-micron scale was accessible by using only indirect techniques such as electron or X-ray diffraction or with electron microscopes which require a vacuum environment and specially prepared materials. Since the invention of scanning probe microscopy (SPM) in 1982 by Gerd Binning and Heinrich Rohrer of the IBM Zurich research group, it is possible to generate real-space images of surfaces with a resolution on the nanometer scale.[27]

Binning *et al.* examined the surface topography of (110) surfaces of $CaIrSn_4$ and Au by their new technique and in doing so presented fascinating possibilities for surface characterization using STM (Scanning Tunneling Microscopy). The operation of an STM system is straightforward in that it consists of essentially moving a metal tip over a conductive surface while maintaining a constant tunnel current between tip and surface (Figure 4.1). The displacements of the metal tip given by the voltages applied to the piezo-drives yield a topographic picture of the surface. Four years later in 1986, Binning and Rohrer were awarded the Nobel Prize in Physics for their invention which became the basis for practically all nanoscale electronic materials surface science. At that time, STM was proposed as a method by

which to measure forces as small as 10^{-18} Newtons (N). In further development of this concept, Binning and Rohrer invented a new type of microscope, the atomic force microscope (AFM), capable of investigating surfaces of insulating materials on an atomic scale.[81]
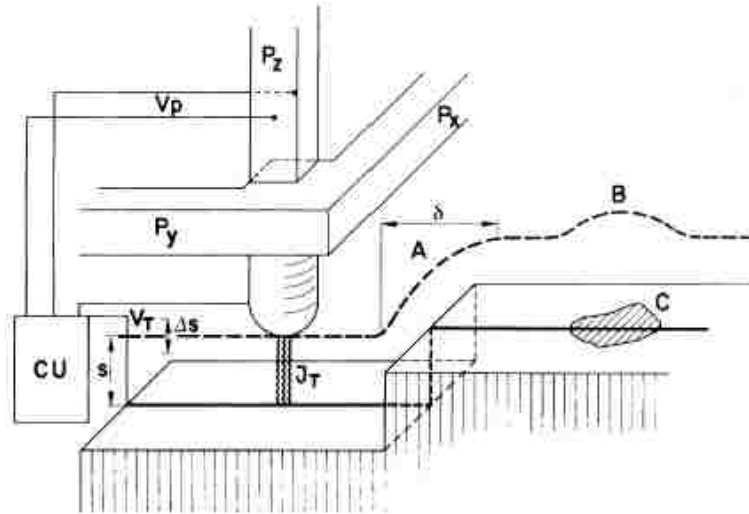
Figure 4.1: Schematic setup of STM showing the principle of operation. The piezodrivers P_x and P_y scan the metal tip M over the surface. The control unit (CU) applies the appropriate voltage V_p to Z-piezo P_z for constant tunnel current J_T at constant tunnel voltage V_T. Variation in tunnel distance s by Δs gives a measure of work function. Reprinted from [27]

4.2 BACKGROUND AND DEVELOPMENT OF AFM

In the still relatively brief history of AFM, the instrument has proven itself to be as versatile as it is essential to nanoscale materials characterization. For example, Marti *et al.* imaged highly oriented pyrolytic graphite (HOPG) surfaces covered with paraffin oil as well as investigated cleaved sodium chloride surfaces covered with an oil film. These studies revealed the hexagonal rings of carbon atoms and monoatomic steps, respectively.[82] They were able to image surfaces with atomic-level resolution even with a relatively crude AFM fabricated on a

screw with fine wires, epoxy, and a small fragment from a shattered diamond. Together, these images illustrated the capability of AFM for studying either conducting or nonconducting surfaces or even surfaces covered with liquids. Albrecht *et al.* demonstrated the capability of the AFM to image the surface of an electrically insulating solid in air with low-noise atomic resolution.[83] Kirk *et al.* developed the new concept of low-temperature atomic force microscopy (LTAFM).[84] The instrument consisted of a rigid compact design which included microfabricated force-sensing cantilevers, and it could easily be tailored for operation as a STM. They imaged 2H-MoS$_2$ surfaces both in air (at room temperature) and immersed in liquid helium at 4.2 K. LTAFM presented greater stability in tip, lever, and sample characteristics along with elimination of mechanical drift and improved signal-to-noise ratio.
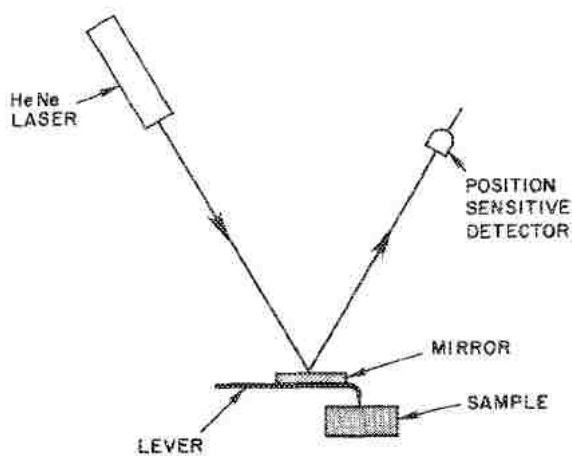
Figure 4.2: Schematic of cantilever deflection detection scheme. Reprinted with permission (Appendix A9)

A novel optical approach to AFM materialized from Meyer *et al.* in which a sensitive and simple optical method was introduced for detecting deflection of the cantilever.[85] Until then, AFM was based on sensing the forces between a sharp stylus and the surface of interest. Instead Meyer and colleagues employed a laser source along with a tungsten stylus-cantilever wire

(electrochemically etched from a sharp tip) with a minute mirror attached to cantilever's backside. A position sensitive detector (PSD) was also a part of the setup. In this approach, the cantilever displacement was measured by using the PSD to detect the deflection of a weak laser beam (HeNe) focused onto the cantilever and reflected off its backside with the help of the mirror as shown in Figure 4.2. This setup was placed in an ultrahigh vacuum (UHV) chamber while the laser source and the PSD were located outside of the UHV. The microscope was operated in the attractive (van der Waals) regime of the interaction potential, and the force gradient was measured by vibrating the cantilever and detecting the change in its amplitude as a function of tip-sample distance.

Further, the effect of van der Waals (vdW) interaction between sharp probes and the flat sample surfaces was analyzed by Hartmann.[86] Van der Waals forces arise from instantaneous moments of otherwise nonpolar atoms or molecules. Here, they derived a theory that describes vdW interaction based on mascroscopic dielectric properties. It was shown that the spatial resolution of force sensing solely depends on probe geometry and probe sample spacing. The magnitude of the force was determined by the dielectric permittivities of probe, sample, and surrounding media. It was computed that the polar immersion liquids considerably reduce vdW interactions and may cause a transition from attractive to repulsive interactions.

Goodman *et al.* calculated the attractive (vdW) forces that were expected between tips and samples in experiments using scanning probe microscopy (SPM).[87] SPM is the term used to describe the various forms of nanoscale surface related microscopies that emerged from the work of the 1986 Nobelists, previously discussed, of which AFM is one form. They concluded that an AFM should be operated with its tip touching the surface but with its cantilever deflected towards the surface. This configuration would cause the associated spring forces to counteract most of the attractive forces. They also computed the deformations produced at the tip and

sample by forces. Operating the AFM with the repulsive forces in the elastic regime avoids destroying the tip and sample while diminishing the associated problem of hysteresis. They found that in order to achieve nondestructive measurements, an AFM should be operated, if possible, in a purely attractive mode with small (but not negligible) repulsive force. They also suggested that more satisfactory measurements would be obtained in liquid environments due to the resultant reduction in the attractive forces.

Weisenhorn *et al.* showcased the AFM's capability in their work to image lipid Langmuir-Blodgett (LB) films with different surface charges and DNA with molecular-resolution.[88] The molecular arrangement of the lipids in the LB films agreed with known 3D crystal data to within 20% accuracy of their measurements and showed a clear difference from the molecular structure of their mica substrate. Depending on the rigidity of the underlying monolayer of the LB films, the increased applied force could scrape off the two films and image the underlying substrate structure. If the bottom film was covalently linked, an increased force would not have altered the films.

Within a decade of the discovery of AFM there was considerable interest in the electronic properties of single molecules wired into electronic circuits. To measure the electronic properties, at least two electrical contacts are required to reliably probe single (or more) molecules. Cui *et al.* developed a covalently bonded single molecule nanojunction which overcomes problems associated with mechanical non-bonded contacts.[26] They inserted n-alkanedithiols into a host matrix of the corresponding n-alkanethiol monolayer on Au(111). The protruding thiol moieties of the other end of dithiols were located by incubating the modified film with a suspension of gold nanoparticles. After removing the film from the solution, the assembly was rinsed to remove the nonbonded particles and imaged with a gold coated AFM tip under an oxygen free organic solvent. The electrical contact to the gold nanoparticles was made

through the gold coated tip. With this configuration they demonstrated that having a chemical bond between the molecule and both electrodes, which prevent washing away of nanoparticles during rinsing, is an essential condition to obtain reproducible and reliable *I-V* characteristics. The covalent bonding between the thiol and nanoparticles was established by introducing gold nanoparticles coated with and stabilized by ligands, mostly triphenylphosphine. These ligands are readily exchanged for alkanethiol ligands upon exposure to thiol in solution. The gold coated conductive AFM tips were used to probe the stabilized nanoparticles to obtain a good "metal-to-metal" electrical contact. They observed distinct families of *I-V* characteristics when alkanethiols were wired in a circuit. They also found that the decay constant (β) varies as a function of applied bias. The decay constant per methylene at zero bias was determined to be 0.57±0.03 and fell to about 0.47 when a bias of ±1 V was applied to the metal-molecule-metal assembly.

Another group at Minnesota, Wold *et al.,* characterized metal-molecule-metal heterostructures using a conducting AFM.[46] They characterized both alkyl and benzyl thiol SAMs on Au with gold coated AFM tips. I-V behaviors of these assemblies were probed as a function of SAM thickness and load applied to the AFM tip. Bilayer assembly was formed by putting alkanethiol coated tips in contact with alkanethiol SAMs on Au. They observed linear *I-V* traces over ±0.3 V, and the junction resistance increased exponentially with alkyl chain length for both monolayer and bilayer junctions; however, the junction resistance decreased with increasing load. The resistances obtained from the benzyl thiol assembly were lower by a factor of 10 compared to hexyl thiol SAMs of the same chain length. The junctions formed were able to sustain fields up to 2 x 10^7 V/cm before breakdown. They calculated the conductance decay constant (β) as 1.2 (~1.1Å^{-1}) per methylene unit for both monolayer and bilayer junctions.

As a pioneer, Engelkes *et al.* developed nanoscopic tunnel junctions by contacting Au-, Pt-, or Ag-coated AFM tips to SAMs of alkanethiol or alkanedithiol molecules on polycrystalline Au, Pt, or Ag substrates.[20]   *I-V* traces exhibited sigmoidal behavior and an exponential attenuation with increasing barrier width (length of the molecule), characteristic of nonresonant tunneling. For both alkanethiol and alkanedithiol junctions, resistances were larger when lower work function metals were used as electrodes. They observed the largest junction resistance for Ag contacts, smallest for Pt, and between these two for Au contacts. For all eighteen junction types, the average β value measured was 1.1 per carbon atom (or 0.88 Å^{-1}). The junction resistance was found to decrease with increasing electrode work function and increased applied bias. The same group also investigated the causes of variance in junction resistance in a metal-molecule-metal heterostructure formed by CP-AFM.[89]   Measurements were made on Au-decanethiol-Au monolayer junctions, and parameters such as substrate roughness, tip chemistry, presence of solvent, extended tip usage, tip radius, and applied load were taken into consideration. *I-V* traces exhibited variation in resistance over orders of magnitude, and appeared to be distributed log-normally, indicating that the variance stems from a parameter that affects the resistance exponentially. They considered that the variation could probably be caused by the effective change in the tunneling length of the junction. They observed larger resistance variation on rough substrates compared to flat surfaces, and this could be accounted for by the greater degree of torsional forces. Sensitivity of junction resistance was tested by chemically modified tips with ethanethiol or butanethiol. Measurements performed under cyclohexane were also observed to reduce variance by a factor of about 2-4. The junction resistance increased over the course of consecutive measurements for unmodified tips; however it remained same for modified tips. Therefore, they concluded that the variance could be due to the sensitivity of junction resistance to contact area.

Chen *et al.* presented a new method of controlling nanoscale structures of mixed SAMs on atomically flat Au(111) surfaces.[36] They proposed a new method for forming uniform mixed SAMs by coadsorption of asymmetrical and symmetrical disulfides. In order to compare the coadsorption results from thiol and disulfides, both thiols and disulfides were chosen in such a way they produce the same surface thiolates. The AFM images showed phase segregation in the mixed thiols with similar surface compositions, whereas mixed disulfides formed homogeneous SAMs on the Au(111).
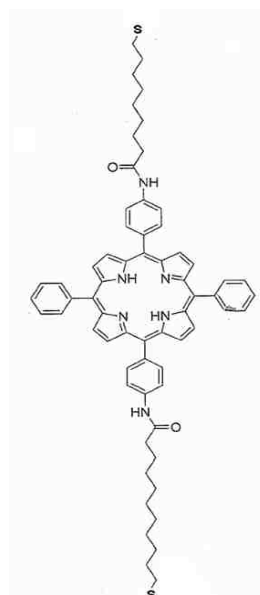
Figure 4.3: Schematic representation of dithiolated free base porphyrin molecule.

Synthetic tailorability of molecules enables them to functionalize with different linkage groups. The use of thiolated appendages leads to the formation of a chemisorbed monolayer of the corresponding thiolate to gold electrodes. Using this approach, electrocatalytic monolayers, with preselected architecture through the manipulation of the number and location of the appendages, may be formed. Porphyrins are readily attached to a gold surface via thiol linkers.[73-75] The rate of electron transfer between the electroactive surface and the porphyrin is one of the key factors that dictates suitability for molecular-based memory storage.[76] This rate depends on

the type and length of the linker connecting the thiol unit to the porphyrin. Different routes for the preparation of thiol derivatized porphyrins are available.[47] A schematic of dithiolated porphyrin is shown in Figure 4.3. To avoid "lie down" or "looped" monolayer dithiolated porphyrin SAM formation, the molecular chain is usually thiol protected using an acetyl group. It can be removed in situ and employed for the SAM deposition.

In this work, I am interested in inserting porphyrin based molecules into the defect sites of n-alkanethiol SAMs on gold surfaces to study the current transport behavior through this hybrid configuration. I use a CP-AFM to investigate the *I-V* behavior of porphyrin based molecules self-assembled on gold surface and to understand the electron transport phenomenon in porphyrin monolayers. The various test structures generally described in the literature to characterize many/few molecules are listed in Table 4.1.

Table 4.1: Test structures used to characterize groupings of many/few molecules (The definition of many versus few molecules depends upon the measurement technique and sample material under study)

Method	*Number of Molecules*	*Imaging Capability*
Nanopore	Many	No
Nanowire	Many	No
Break Junction	Few	No
STM	Few	Yes
CP-AFM	Few	Yes

Among the various techniques conductive probe-atomic force microscopy (CP-AFM) is able to characterize a few or individual molecules of interest. It also has imaging capability

which gives the topography of the molecules and is independent of current measurements (unlike in STM). The advantage of using CP-AFM compared to STM is listed in Table 4.2.

Table 4.2: A comparison between CP-AFM and STM measurements.

CP-AFM	*STM*
• Tip makes contact with molecule, no tunnel barrier between tip and sample	• Tunneling current from tip to molecule
• Topographic images scanned independent of transport measurements	• Topographic image includes both electronic and geometric properties of tip – surface system
• Possible to correlate force applied on the sample with transport measurement	• No force measurement
• Possible UHV	• Possible UHV

4.3 ATOMIC FORCE MICROSCOPY: THEORY OF OPERATION

An Atomic force microscope is a very high resolution type of scanning probe microscope with demonstrated resolution of fractions of a nanometer, several times better than the optical diffraction limit. It is being used to solve processing and materials problems in a wide range of technologies affecting the electronics, telecommunication, biological, chemical, and aerospace industries. By using AFM one can not only image the surface in atomic resolution but also measure the force at nano-Newton scale. In fact the physical properties that are measured with this apparatus, namely the interaction forces between a sharp conical tip and the sample surface,

allow investigations to be performed on electrical conductors as well as on semiconductors, organic, and biological materials.
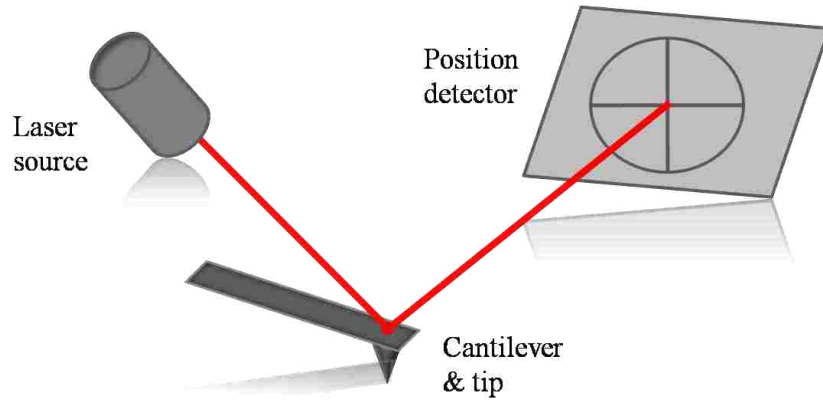
Figure 4.4: Representation of the basic principle of AFM with beam bounce deflection technique.

AFM investigates the surface of a sample with a sharp tip, with a terminal radius often less than 100 Å. The tip is located at the free end of an approximately 100μm long cantilever that has an elastic modulus which can reach tenths of N/m. Forces in the range of few pico-Newton between the sample surface and the tip cause deflections of the cantilever in the Angstrom spatial scale. A laser beam is focused on the back of the cantilever, right above the tip, and the reflected beam bounces off onto a position-sensitive photodetector (PSD) (Figure 4.4). Any changes in the cantilever position would reflect the laser position change in the PSD. This form of detection is very sensitive in that it measures displacements of light beams as small as 10 Å. The ratio of the path length between the cantilever and the detector to the length of the cantilever itself produces a mechanical amplification. As a result, the system can detect sub-Angstrom vertical deflections of the cantilever tip. The measured cantilever movements enable the software to generate a map of surface topography. If the tip were scanned

at a constant height, there would be risk that the tip would collide with the surface, causing damage. Hence, in most cases a feedback mechanism is employed to adjust the tip-to-sample distance and to maintain a constant force between the tip and the sample (Figure 4.5). The interaction forces in an AFM depend upon various factors, namely the number of atoms from the tip involved in the interaction, environment (gas, liquid or vacuum), tip deformation, and velocity dependent forces.
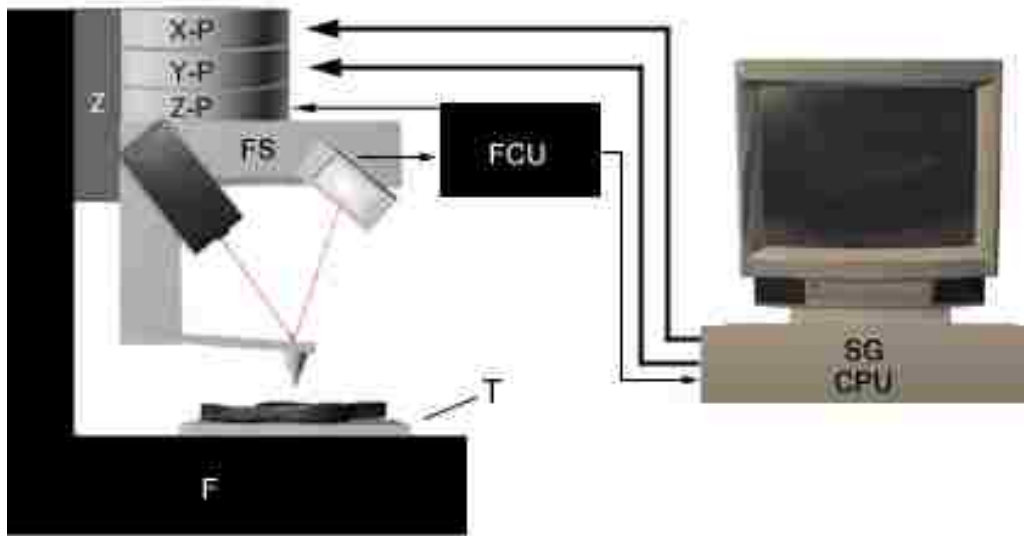
Figure 4.5: Schematics showing all the components and subsystems of an AFM. Z- coarse Z motion translator, T- coarse X-Y translation stage, X-P & Y-P –X and Y piezoelectric transducers, FS-force sensor, Z-P – Z piezoelectric ceramic, FCU-feedback control unit, SG-X-Y signal generator, CPU – computer, F-frame. Reprinted from [90]

4.3.1 Classification of Forces

The strongest forces between the probe and surface are the mechanical forces that occur when the atoms on the probe physically interact with the atoms on a surface. However, other forces between the probe and surface can have an impact on an AFM image. These are classified into long range and short range forces.

Long Range Forces

Van der Waals forces exists between every type of atom or molecule, and their roles are discussed here as long range forces.

1. Electrostatic forces: Insulating surfaces can store charge which can interact with charges on the probe or cantilever. Such forces can be so strong that they "bend" the cantilever when scanning a surface.

2. Capillary forces: The curvature at the contact between the tip and surface causes the condensation of vapor from the ambient including water from the air. Also surfaces exposed to the air environment are typically coated by a layer of water whose thickness depends on the relative humidity of the atmosphere and the nature of the surface.

Short Range Forces

1. Repulsive forces: The interatomic repulsion forces due to the overlap of two atoms which generates Columbic repulsion and involves the Pauli Exclusion Principle.

2. Covalent bonds: Interaction between two or more molecules interacting with the nuclei and also known as chemisorption.

3. Metallic bonding: Force originating from interaction between two or more metal atoms also known as physisorption.

4. Friction: Heterogeneous surfaces can have regions of varying hardness and friction. As the probe is scanned across a surface, the probe-surface interaction can change when moving from one region to another. Such changes in forces can give a "contrast" that is useful for differentiating between materials on a heterogeneous surface.

The contributions of the forces are on the basis of the Lennard-Jones potential:

$$\varepsilon(r) = -4\varepsilon_o \left[\left(\frac{\sigma}{r} \right)^6 - \left(\frac{\sigma}{r} \right)^{12} \right] \qquad (4.3.1)$$

where, ε_o is the potential energy at the minimum;

σ is the effective molecular diameter;

r is the interatomic distance.

The force, which is the negative gradient of energy plotted against distance, is shown in Figure 4.6. Two distance regimes are highlighted: 1) the *contact* regime, and 2) the *non-contact* regime. In the contact regime, the distance between the cantilever and the surface is only few Angstroms, and the interatomic force is repulsive. In the non-contact regime, the tip and the surface are apart by tens to hundreds of Angstroms, and the interatomic force is attractive (largely due to vdW interactions). Both modes of AFM are discussed in detail in the following sections.
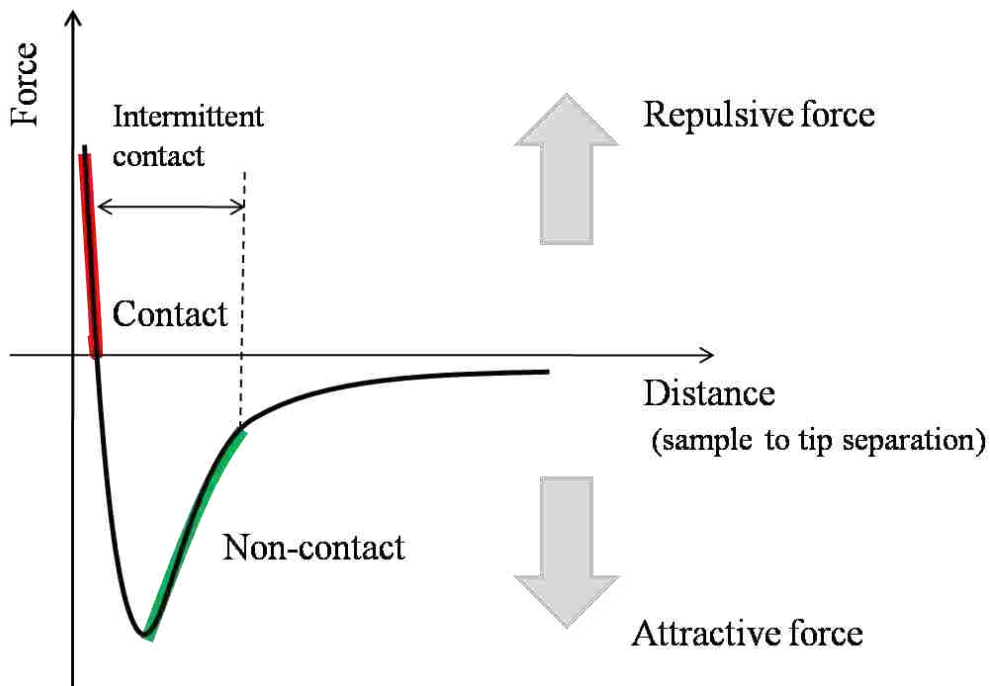
Figure 4.6: Interatomic force vs. distance curve.

4.3.2 Static Mode AFM

The static mode AFM is commonly known as the *contact mode* AFM. In the contact mode AFM, the tip and sample remain in close contact as the scanning proceeds (Figure 4.6). The tip is attached to the end of a cantilever with a spring constant lower than the effective spring constant holding the atoms of the sample together. As the scanner gently moves the tip across the sample surface (or the sample under the tip), the contact force causes the cantilever to bend in order to follow the topographic profile (Figure 4.7). Using very stiff cantilevers it is possible to exert large forces on the sample, and the sample surface is likely to get deformed; this may be also used in "nanolithography". A contact mode AFM can be operated in two principal modes—with and without feedback control—known as *constant force* and *constant height mode,* respectively.
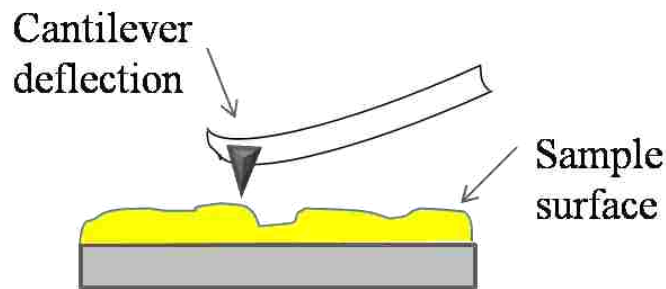
Figure 4.7: Schematic showing cantilever bending in contact mode AFM.

In *constant force mode*, the electronic feedback is switched on, and the positioning piezo, which moves the tip (or sample) in the Z direction, can respond to any changes in force which are detected. This piezo can then alter the tip-sample separation to restore the force to a pre-determined value. This mode usually enables the attainment of a faithful topographical image and hence the alternative name, *height mode*.

In *constant height mode*, the electronic feedback is switched off, and the distance between the tip and sample surface is fixed as it scans. This mode is used directly to provide the topographic data set for spatial variation of the cantilever deflections and to image very flat samples at high resolution. Often it is best to have a small amount of feedback-loop gain to avoid problems with thermal drift or the possibility of a rough sample damaging the tip and/or cantilever. This case is known as the *error signal mode*. The *error signal mode* may also be displayed even as feedback is switched on. This image will remove slow variations in topography but highlight the edges of features.

4.3.3 Dynamic Mode AFM

Dynamic mode is commonly known as vibrating mode AFM, in which the cantilever is operating in AC mode. In contact mode, the tip and the surface are in contact throughout the scan, and this could deform the sample surface. In order to overcome the problem of friction components during scanning and minimize the interacting forces, AFM cantilevers vibrate near (orders of ten to hundreds of Angstrom) the surface of a sample (Figure 4.8). The cantilever in an AFM can be vibrated using a piezoelectric ceramic. When the vibrating cantilever comes close to the sample surface, the amplitude and phase of the vibrating cantilever may change. The feedback unit keeps either the vibration amplitude or phase constant. Changes in the vibration amplitude or phase are easily measured, and the changes can be related to the force on the surface. Since the shear forces are eliminated, these modes are particularly useful for studying soft materials such as organic films and biomolecules. As a consequence of the oscillation of the cantilever, these modes do not suffer from tip or sample degradation effects which are predominant in contact AFM. However, the lateral resolution that can be reached is a few nanometers (much higher resolution) compared to the contact mode.
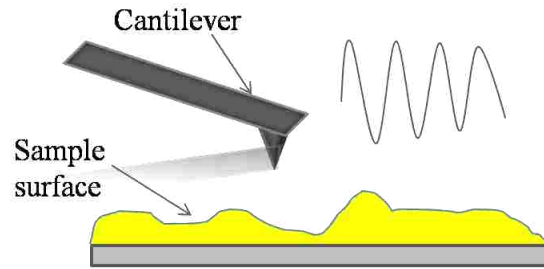
Figure 4.8: Schematic of vibrating mode AFM with tip-sample interactions affecting amplitude and phase swing.

4.3.3.1 Non-Contact Mode

In non-contact mode, the interaction between the tip and the sample is indicated on the force-distance curve shown in Figure 4.6. The cantilever must be oscillated above the surface of the sample at such a distance that it is no longer in the repulsive regime of the inter-molecular force curve. Further, cantilevers used here must be stiffer than those used for contact AFM because soft cantilevers can be pulled into contact with the sample surface. The thin layer of water contamination which exists on the surface of the sample will invariably form a capillary bridge between the tip and the sample and cause the tip to "jump-to-contact". The small force values and greater stiffness of cantilevers in this mode influences the force resolution and lateral resolution that can be achieved.

4.3.3.2 Tapping Mode

Tapping mode or intermittent mode is the next most common mode used in AFM. When operated in air or other gases, the cantilever is oscillated at its resonant frequency (often hundreds of kilohertz) and positioned above the surface so that it only taps the surface for a very small fraction of its oscillation period. The tapping mode regime is the region between the contact and non-contact mode in the force-distance curve plot (Figure 4.6). The cantilever is still in contact with the sample in the sense defined earlier, but the very short time over which this contact occurs means that lateral forces are dramatically reduced as the tip scans over the

91

surface. This mode may be a far better choice to image poorly immobilized or soft samples than contact mode AFM.

4.3.4 Applications of AFM

AFM can be used to image a variety of materials such as layered materials, ionic crystals, organic molecules, and biological samples. As discussed earlier in the background section of this chapter, AFM has been extensively used to image the surfaces of graphite and mica as well as organic molecules forming LB films and biological samples like DNA. In fact, an AFM tip can be coated with conducting materials or molecules and used in the formation of nanoscale junctions. These heterostructures or tunneling junctions can be used to study the electron transport mechanism in two terminal electronic devices. This method of forming metal-molecule-metal junctions and wiring in a circuit to measure the I-V characteristics of single molecules is commonly known as conductive probe-AFM (CP-AFM).

4.4 EXPERIMENTAL DETAILS

4.4.1 Chemicals and Materials

For our work high-purity water (Millipore purification system) was used in the preparation of all solutions. All chemicals were reagent or spectrographic grade and were used as received. In this work, gold substrate on mica and glass has been utilized. Before any process is done, the sample must be cleaned. Gold substrates were rinsed with toluene and then dried with a stream of nitrogen before the monolayer formation. Four primary forms of monolayer samples were prepared for this work. First, *n-alkanethiol monolayers on gold* were formed from 1mM alkanethiol (hexanethiol and octanethiol are used) solution in toluene. Second, *n-alkanedithiol monolayers on gold* were formed from 1mM alkanedithiol (hexanedithiol and octanedithiol) solution in toluene. Third, *mixed monolayers of alkanethiol on gold* were formed from 1mM

alkanethiol and alkanedithiol solution in toluene, respectively. Fourth, *functionalized porphyrin monolayers on gold* were formed from monothiolated phorphyrin molecules in toluene.
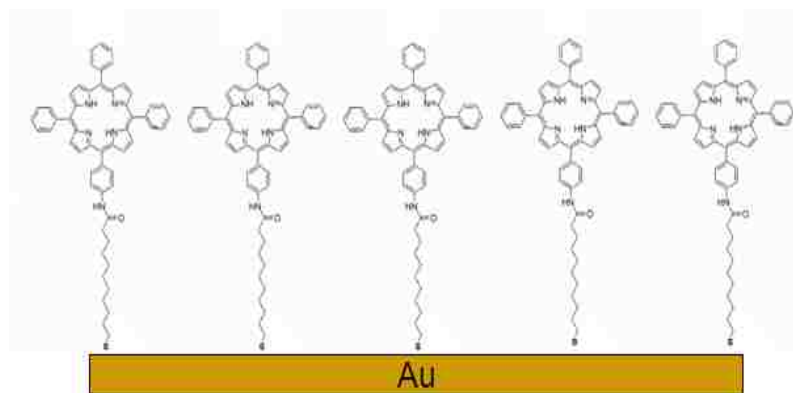
Figure 4.9: Schematic representation of SAM of monothiolated porphyrin on gold substrate.

Self assembled monolayers (SAMs) of alkanethiol and alkanedithiol were prepared by immersing freshly cleaned gold substrates in the respective alkyl solution for 12–14 hours. After immersion, the samples were removed from solution, rinsed with toluene at least three times, and then dried with a gentle stream of nitrogen. Mixed monolayer of alkyl chains were formed using two different techniques described as follows: *Technique I* – SAM of alkanethiol or alkanedithiol was prepared initially and transferred to alkanedithiol or alkanethiol solution to form the mixed monolayer of corresponding alkyl chains. *Technique II* - SAM of alkanethiol and corresponding alkanedithiol were prepared simultaneously from the mixed alkyl solution in toluene. SAM of porphyrins on gold (Figure 4.9) was formed from trityl protected monothiolated porphyrin molecules. The trityl groups were cleaved in ex-situ before the monolayer formation. All of the four different samples were allowed to sit in the respective molecular solution for 12–14 hours in order to form the respective monolayers. After immersion, the samples were rinsed with toluene at least three times and then dried with a gentle stream of nitrogen.

93

4.4.2 Characterization Techniques

Reflection-Absorption Infrared Spectroscopy: All reflection-absorption infrared spectroscopy (RAIRS) was performed with a Thermo Nicolet Nexus FT-IR model 670 ESP with a MCT (mercury-cadmium-telluride) detector as provided by Prof. Robin McCarley of the LSU Department of Chemistry. The instrument is equipped with a Versatile Reflection Attachment with Retro-Mirror Accessory (Harrick) in order to perform external reflection measurements. RAIRS is carried out using p-polarized light at a grazing incident angle of 86° with respect to the surface normal of the sample. Samples were deposited on a highly reflective gold substrate. Spectra were obtained using 512 scans at a resolution of 4 cm^{-1}. The purge time, to remove possible contamination from water and carbon dioxide vapor, was approximately 9 minutes. Baseline corrections and subtractions for water and carbon dioxide were performed using Omnic ESP Version 5.2a software. RAIRS was used to characterize the SAM of alkanethiols/alkanedithiols and to identify molecular adsorbates such as sulphur and methyl groups on gold. Bare gold prepared by UV-ozone cleaning immediately before use, under the same experimental setup as the samples, was used as the reference.

X-ray Photoelectron Spectroscopy: All X-ray Photoelectron Spectroscopy (XPS) was performed at the MC^2 Facility of the LSU Dept. of Mechanical Engineering, with an AXIS 165 High Performance Multi-Technique Surface Analysis (XPS/Auger). The samples were mounted on a sample holder and inserted into the ultra high vacuum experimental chamber. A p-polarized X-ray beam is made to impinge upon the sample surface at a fixed grazing angle. A mono (Al) X-ray gun was used with a 10 mA anode current and 15 kV anode voltage. The data acquisition spectra were observed over a range of 1200 eV to 0 eV, and individual components such as S (sulphur) 2p and C (carbon) 1s were obtained. Spectra are reported as photoelectron number (intensity) as a function of the binding energy (BE).

4.4.3 Conductive Probe - Atomic Force Microscopy

All of the current-voltage behaviors on SAM were obtained using an AFM from Pacific Nanotechnology, Inc (PNI). A schematic of CP-AFM circuit construction is shown in Figure 4.10. I have used a Keithley 4200-SCS Semiconductor Characterization System as the source from which to apply the required voltage bias and by which to measure the current through the metal-molecule-metal junction. A triax cable was used to connect the Keithley 4200-SCS to the AFM tip, as shown in Figure 4.11. Figure 4.12 shows the AFM scanner with the tip holder. A custom-designed ceramic piece obtained from PNI was used to isolate the AFM tip from the rest of the AFM scanner circuit (Figure 4.13). Ti/Pt coated ultra sharp conductive tips purchased from Mikro Mash were used to obtain all *I-V* measurements. *I-V* data are obtained by repeated cycling from small tip bias ranges ±0.8 V.
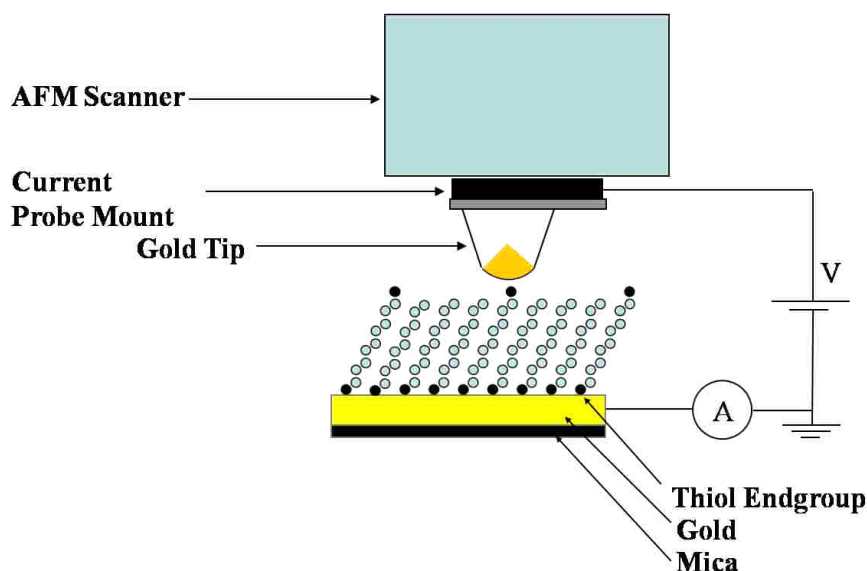
Figure 4.10: Schematic circuit of conductive probe AFM.

Figure 4.11: Circuit wiring of Keithley 4200-SCS.

Figure 4.12: AFM scanner showing the tip mounting region.

Figure 4.13: Ceramic probe substrate to isolate the AFM tip from the scanner circuitry.

Figure 4.14: Triax wiring with the AFM tip and sample.

Figure 4.15: Experimental setup of CP-AFM.

I-V measurements were carried out through direct contact between the AFM tip, and the molecule of interest without any tunneling barrier between the tip and the sample (Figure 4.14). Tailoring the force applied to the sample, corresponding transport measurements were obtained. On average the effective area of a CP-AFM tip is around 50 nm in diameter, and hence I am

attempting to probe a few molecules with this tip in the contact mode. Depending upon the tip contact, the electron transport measurement through the molecule varies. Lindsay and coworkers have measured the conductivity of alkanedithiols on gold.[43] Figure 4.15 shows the experimental setup of CP-AFM.

4.5 RESULTS AND DISCUSSION

4.5.1 Characterization of SAMs

In order to evaluate the contributions of molecular chain information and orientation, RAIRS measurements are made. Figure 4.16 shows the RAIRS spectrum for hexanethiol, hexanedithiol, octanethiol, and octanedithiol SAM on gold.

RAIRS spectra are reported as absorbance as a function of wave number. Absorbance peaks around the wave number $2800 - 2970$ cm^{-1} identify the presence of alkyl chains on the substrate. Peaks for thiol (S-H) and alkyl chains (C-H) are expected for dithiolated molecules. I observed peaks corresponding to alkyl chain groups, and this may be due to the orientation of the molecules as discussed earlier in the SAM deposition process. RAIRS spectra for mixed monolayer of the corresponding alkanethiol/dithiols are also obtained.

Absorbance peaks around $2580 - 2550$ cm^{-1} wave number indentifies the presence of thiol groups on the substrate. Figure 4.17 shows the RAIRS spectra of mixed monolayer for (A) Hexanethiol/hexanedithiol and for (B) Octanethiol/octanedithiol with absorbance peaks around 2550 cm^{-1} and 2970 cm^{-1} wave number.

Similar but nonetheless different absorbance peaks are identified with the porphyrin monolayer on gold. An absorbance peak around $1620 - 1475$ cm^{-1} signifies the presence of an aromatic ring. These data are shown in Figure 4.18, indicating peaks around 2930 and 1490 cm^{-1} for the monothiolated alkyl chain and aromatic ring (C=C) respectively. An absorbance peak around 2330 cm^{-1} indicates the possibility of a nitrogen group in the porphyrin molecule. All

98

these RAIRS spectra validate the reproducibility of these SAMs on gold. In general all the data

indicate that the alkyl chains in the film structure are identified.
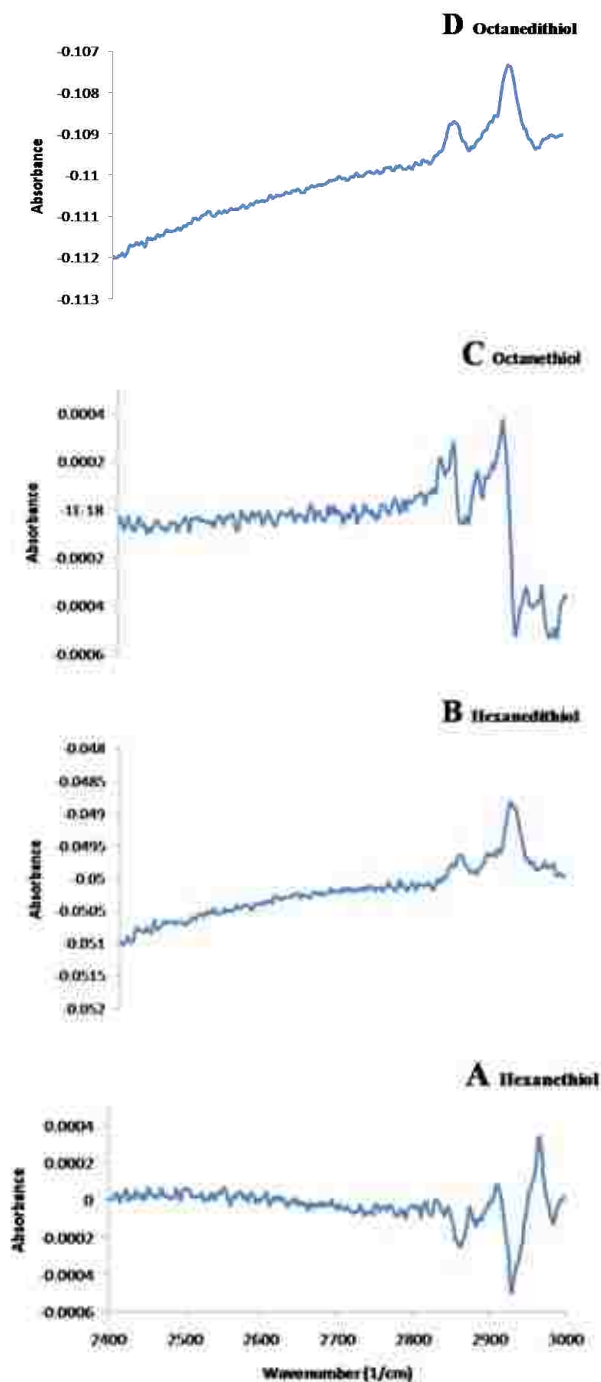
Figure 4.16: RAIRS spectra of SAM on Au (A) hexanethiol, (B) hexanedithiol, (C) octanethiol, and (D) octanedithiol.
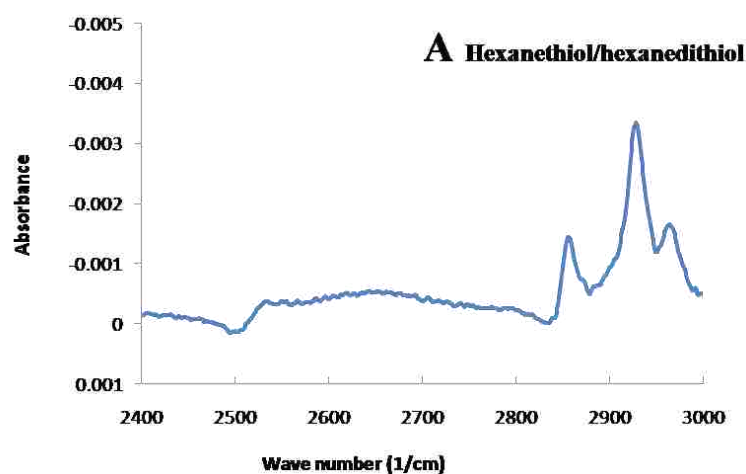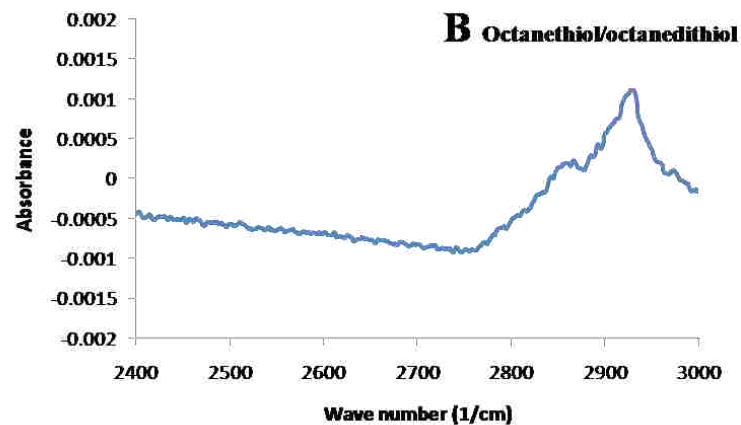
Figure 4.17: RAIRS spectra of mixed monolayer on Au (A) Hexanethiol/hexanedithiol, and (B) Octanethiol/octanedithiol.
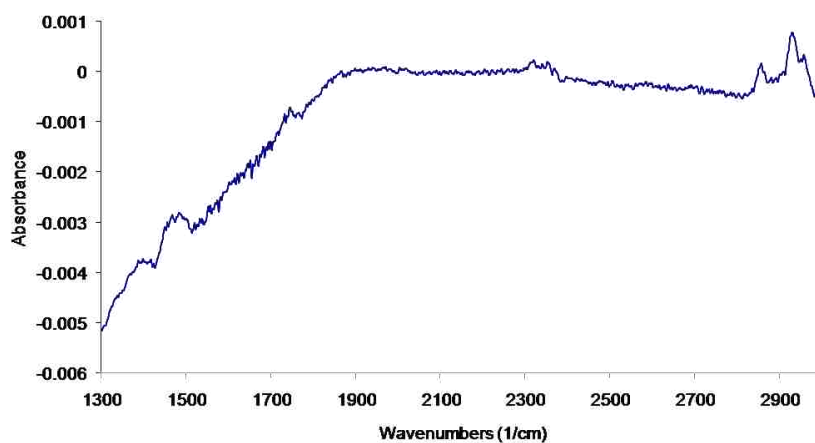
Figure 4.18: RAIRS spectrum of monothiolated porphyrin monolayer on gold.

100

XPS measurements are particularly well suited for identifying different chemical states. I have prepared two sets of samples from the Au/mica substrates annealed for 3 hours @ 400° C (M) and 8 hours @ 400° C (R). Binding energy (BE) is used to determine the presence of the required atoms in the SAMs. XPS spectra with photoelectron number intensity peaks around BE 283 – 285 eV and 163 – 165 eV were observed for carbon (1s) and sulphur (2p) atoms, respectively. Figure 4.19 and Figure 4.20 show the XPS spectra of hexanethiol on Au/mica annealed at 400 C for 3 hrs and 8 hours, respectively.

Figure 4.21 and Figure 4.22 shows the XPS spectra of hexanedithiol on Au/mica annealed at 400°C for 3 hrs and 8 hrs respectively.

Figure 4.19: XPS spectrum of hexanethiol SAM on Au/mica (M). Inset: carbon and sulphur peaks

Figure 4.23 and Figure 4.24 shows the XPS spectra of mixed monolayer of hexanethiol/hexanedithiol on Au/mica annealed at 400 C for 3 hours and 8 hours, respectively. The mixed monolayers were deposited using technique I as described earlier.

Figure 4.25 and Figure 4.26 show the XPS spectra of mixed monolayer hexanethiol/hexanedithiol on Au/mica annealed at 400 C for 3 hours and 8 hours, respectively. The mixed monolayers were deposited using technique II as described earlier.
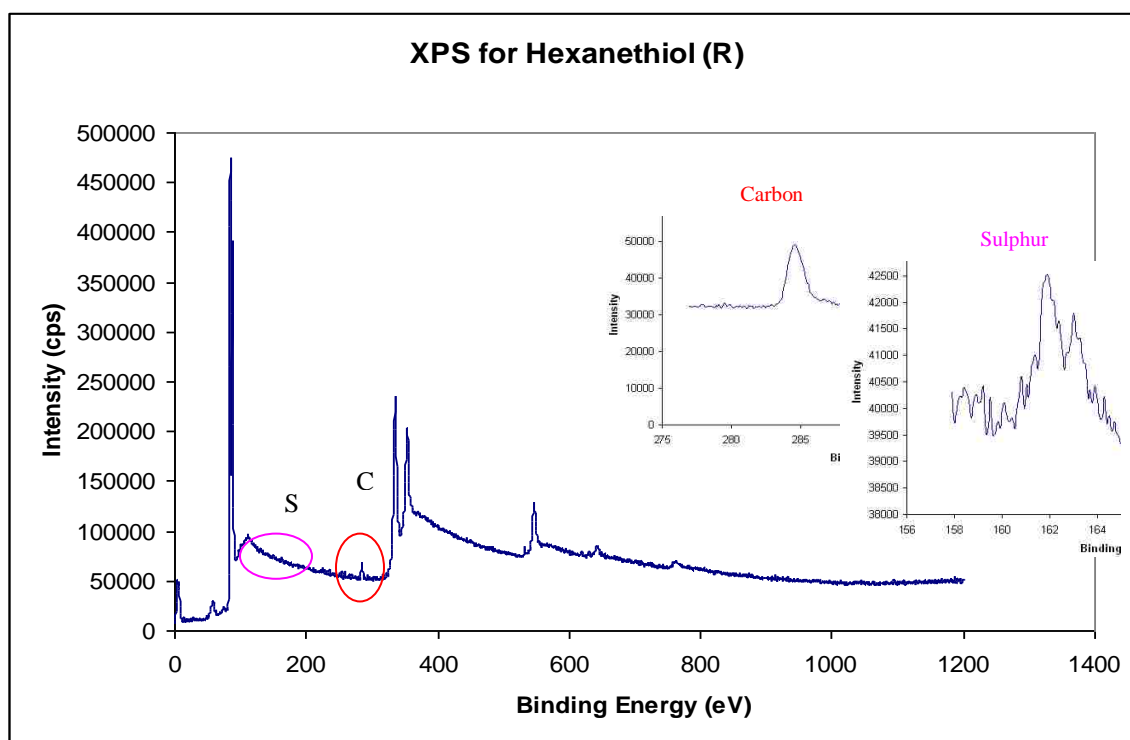
Figure 4.20: XPS spectrum of hexanethiol SAM on Au/mica (R). Inset: carbon and sulphur peaks

The XPS measurements on the alkanethiol and alkanedithiol samples confirm the presence of the SAM on Au/Mica. With the help of two sets of samples with different annealing conditions, I was able to observe higher intensity for the carbon peak with longer annealing time compared to the intensity with shorter annealing period. I believe that this result indicates the

deposition of more SAM molecules on the Au/mica substrates due to the larger surface area and larger grain boundaries. In Figure 4.20, I suspect that there may be some cross contamination in the sample preparation which could be the reason for the peak for sulphur. Moreover, I speculate that the peak for sulphur may be due to the random orientation of the thiol molecules on Au/Mica. As this is the only imperfection I found in the monolayer deposition, I consider this method of SAM formation to be a reproducible monolayer formation technique. Figure 4.27 shows the XPS spectrum of octanethiol SAM deposited on Au/mica without annealing.

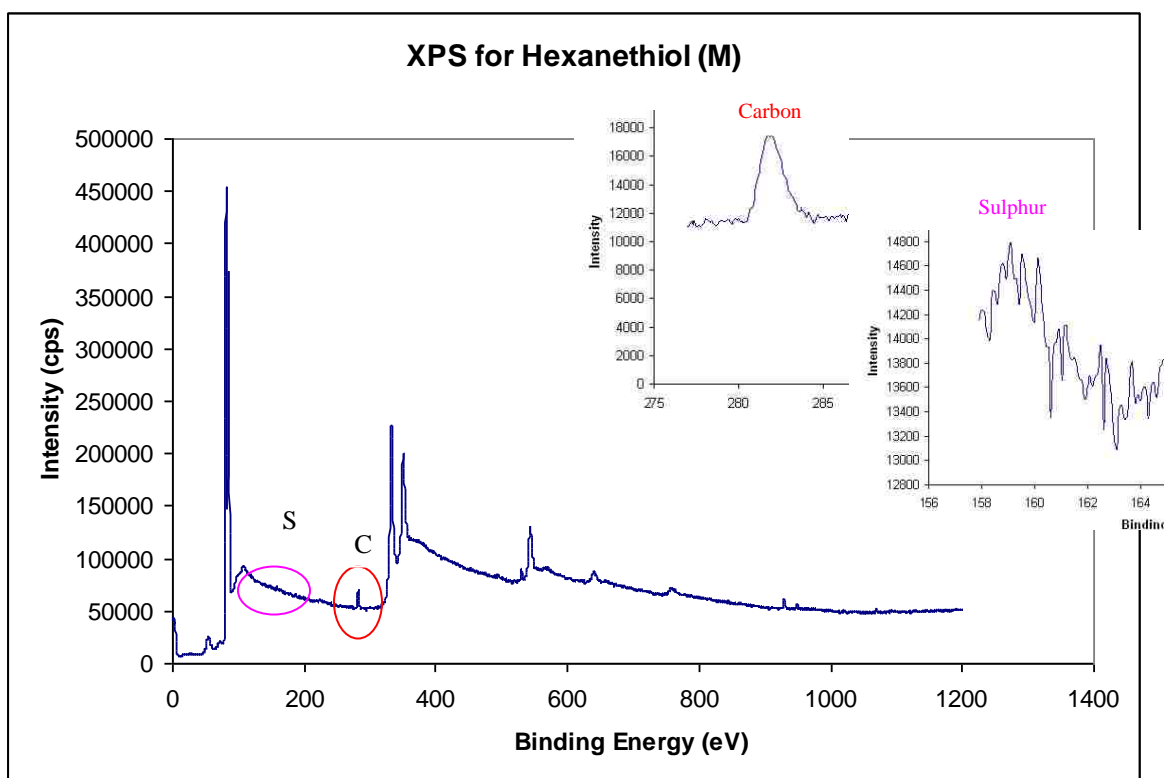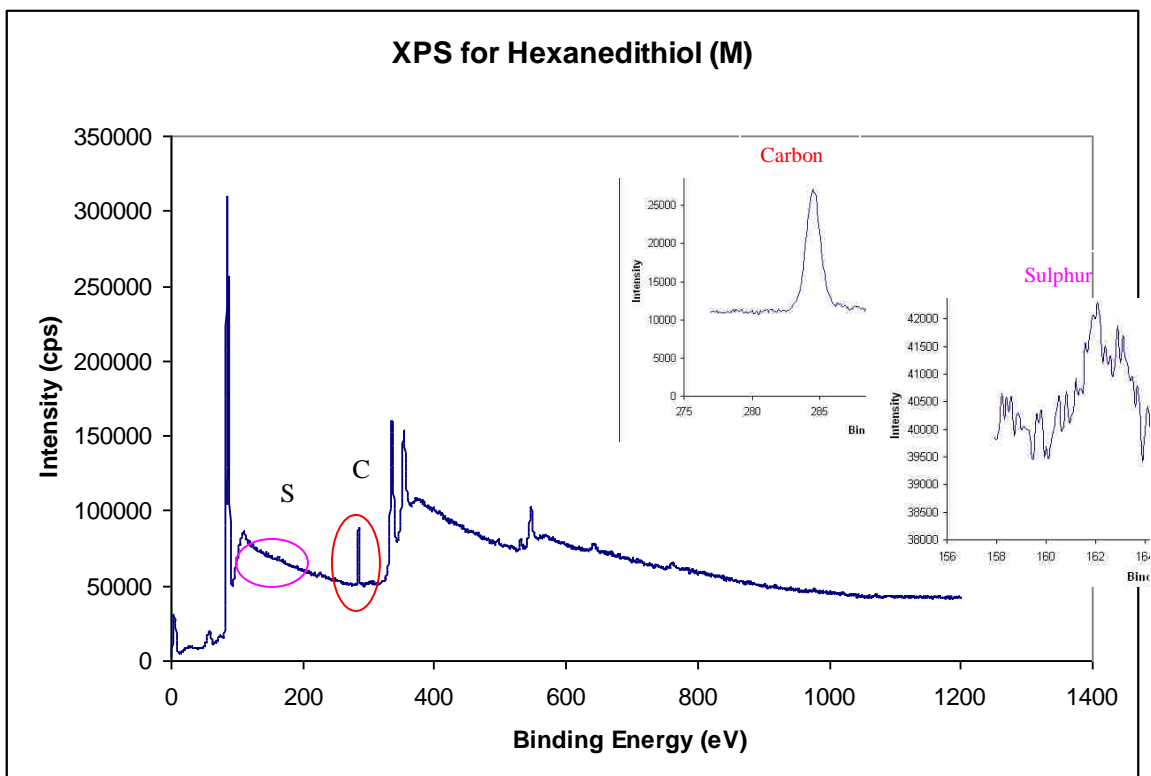Figure 4.21: XPS spectrum of hexanedithiol SAM on Au/mica (M). Inset: carbon and sulphur peaks

103
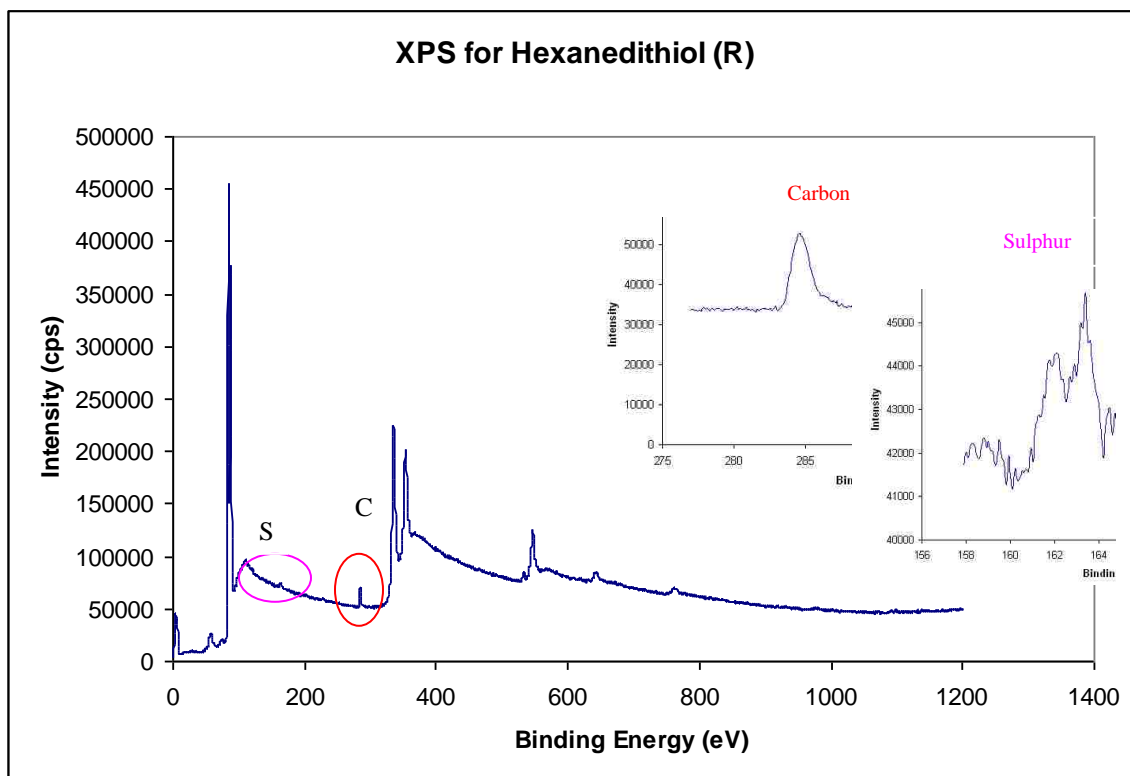
Figure 4.22: XPS spectrum of hexanedithiol SAM on Au/mica (R). Inset: carbon and sulphur peaks
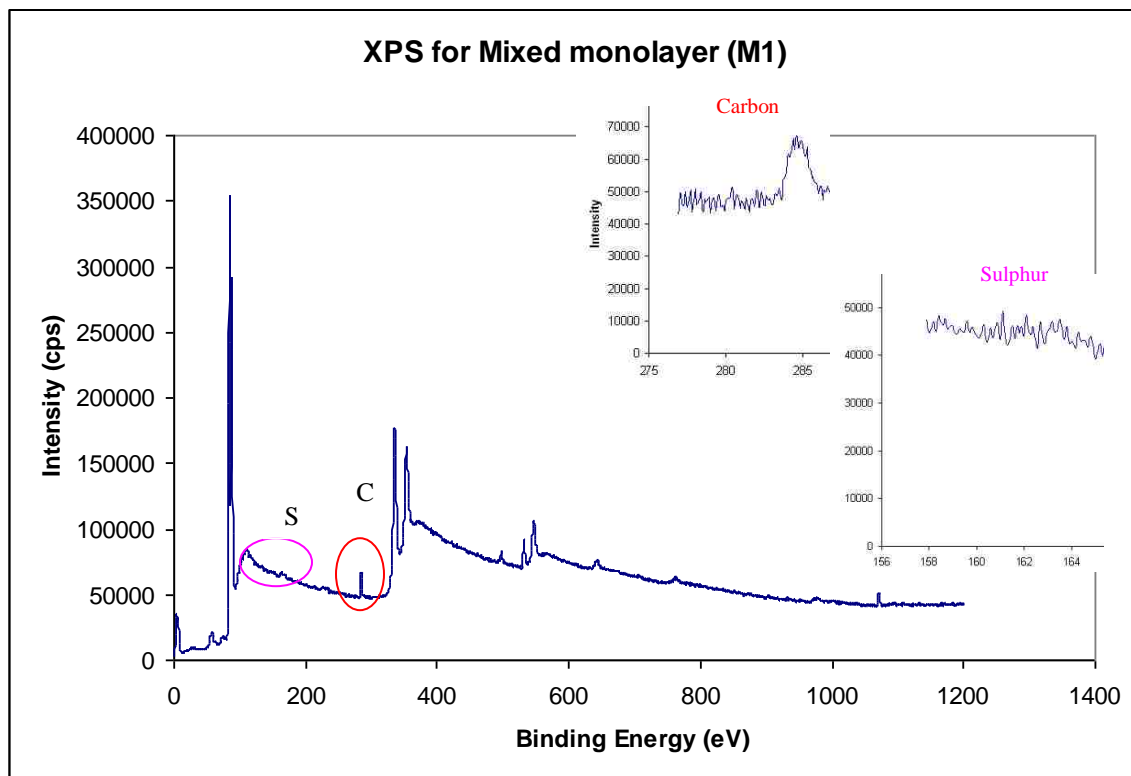
Figure 4.23: XPS spectrum of mixed monolayer of hexanethiol/hexanedithiol SAM on Au/mica (M) using SAM deposition technique I. Inset: carbon and sulphur peaks
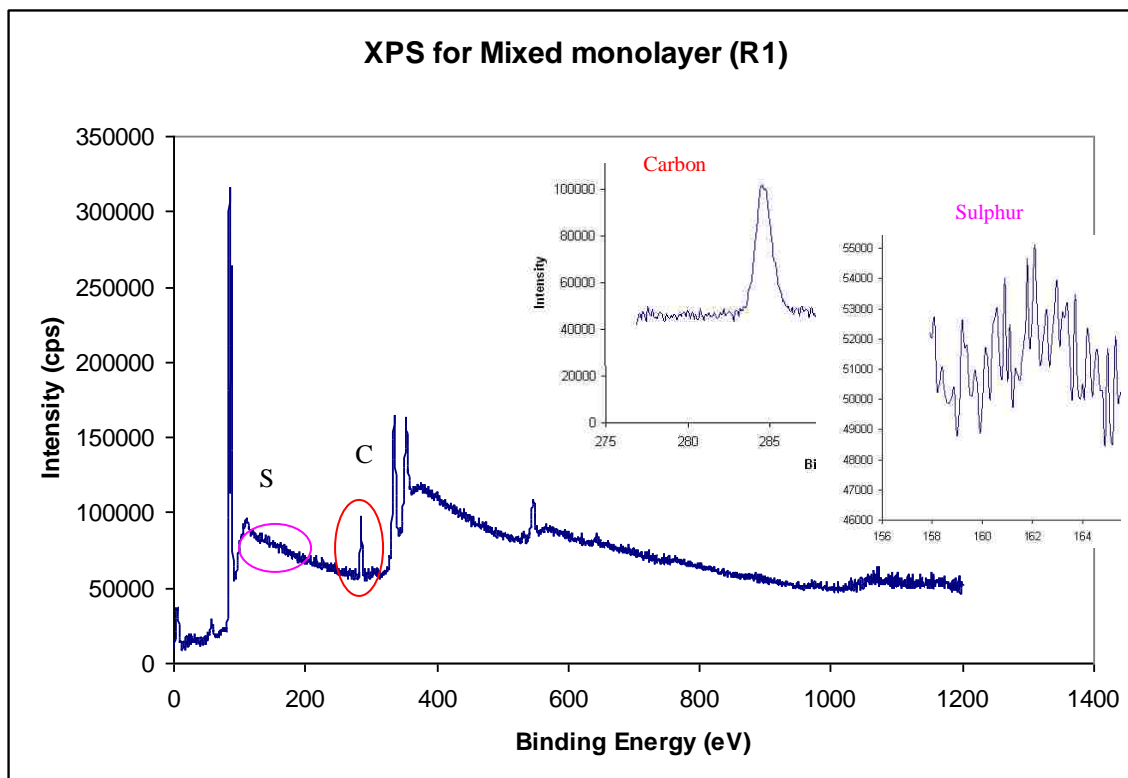
Figure 4.24: XPS spectrum of mixed monolayer of hexanethiol/hexanedithiol SAM on Au/mica (R) using SAM deposition technique I. Inset: carbon and sulphur peaks
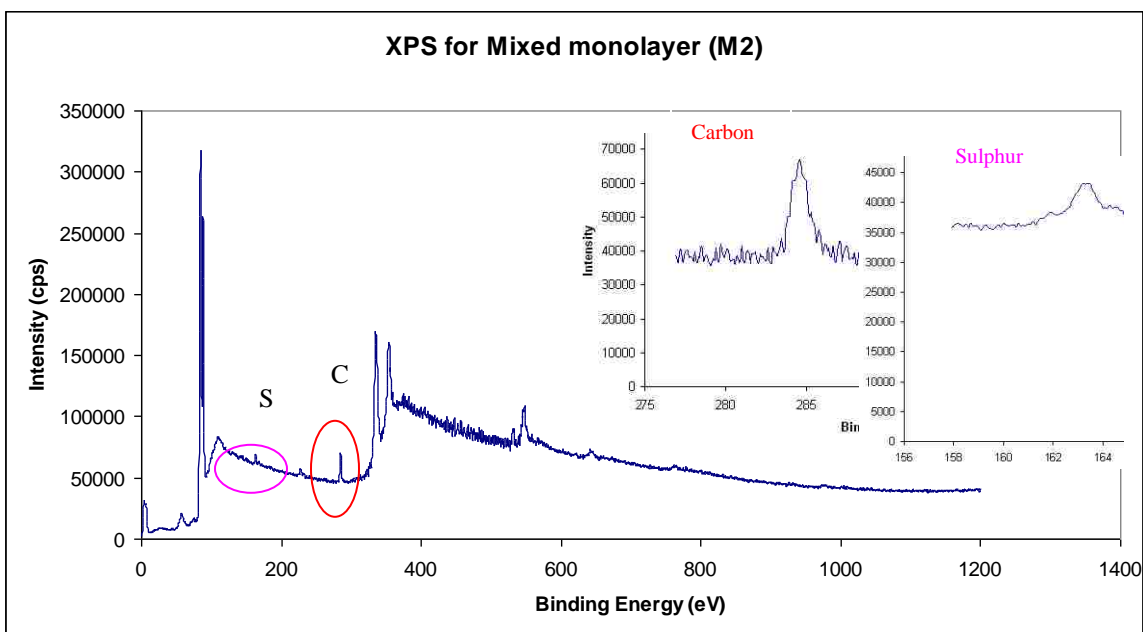
Figure 4.25: XPS spectrum of mixed monolayer of hexanethiol/hexanedithiol SAM on Au/mica (M) using SAM deposition technique II. Inset: carbon and sulphur peaks
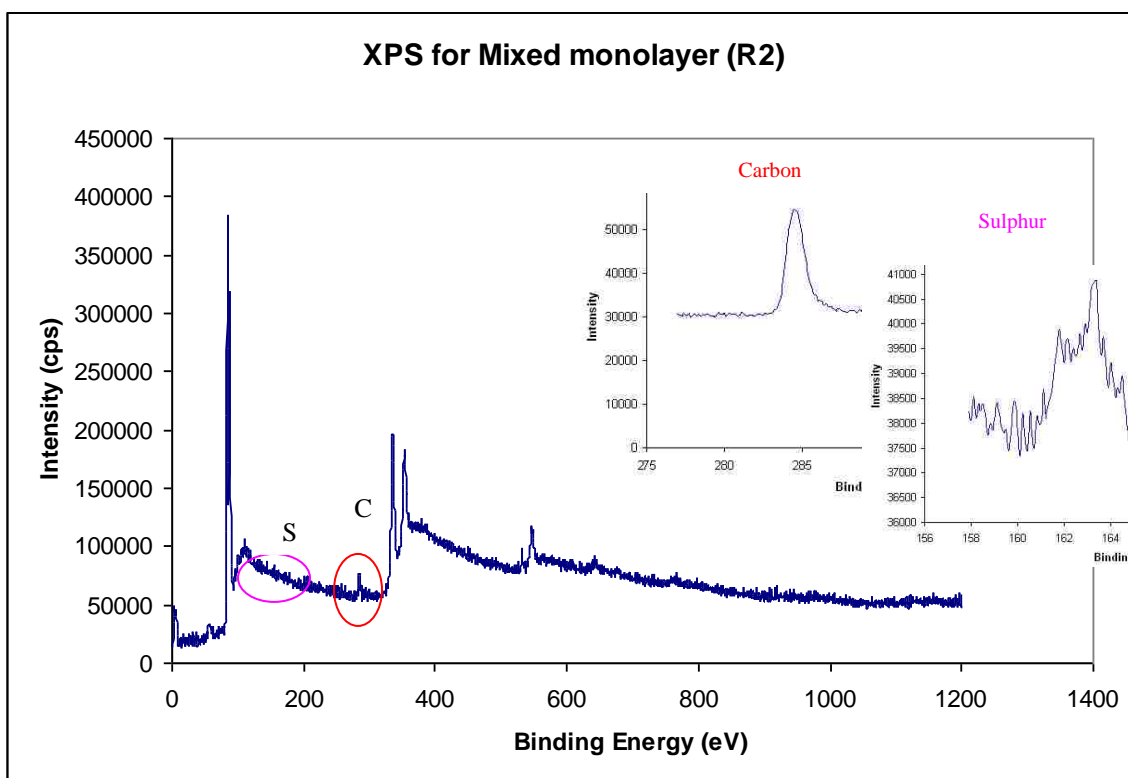
Figure 4.26: XPS spectrum of mixed monolayer of hexanethiol/hexanedithiol SAM on Au/mica (R) using SAM deposition technique II. Inset: carbon and sulphur peaks
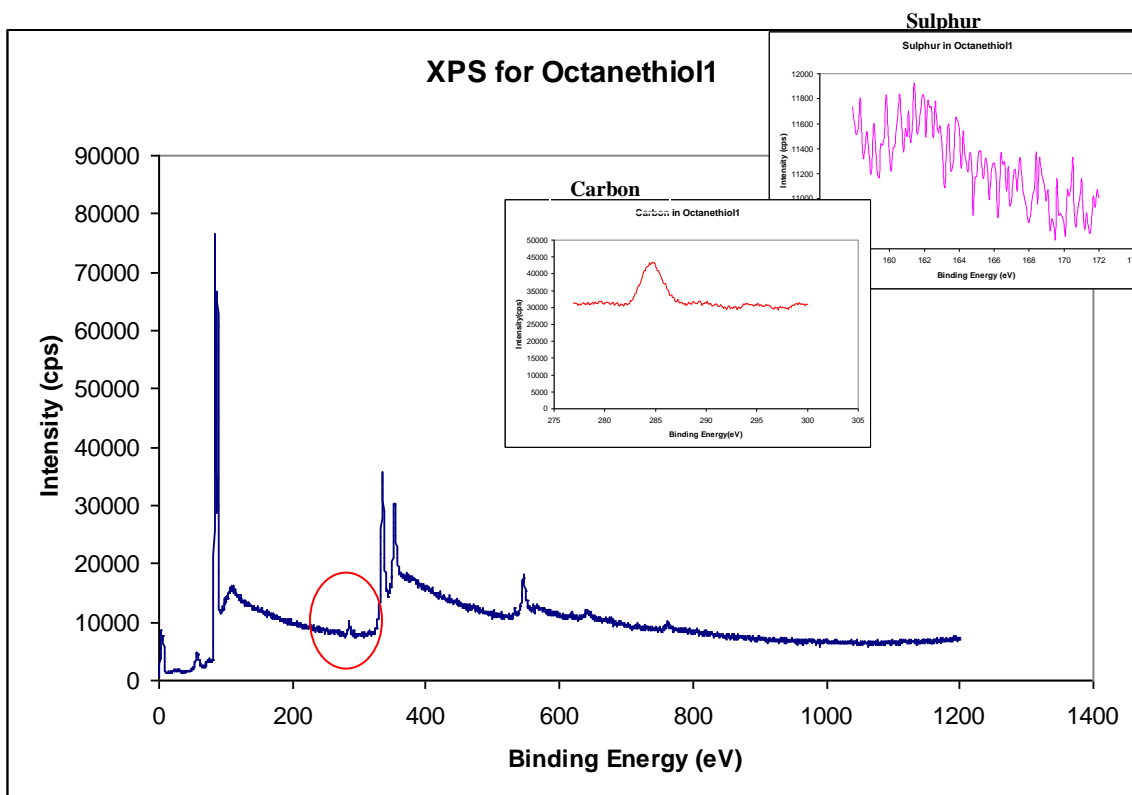
Figure 4.27: XPS spectrum of octanethiol SAM on Au/mica. Inset: carbon and sulphur peaks

4.5.2 Conductive AFM Results

Prior to current-voltage measurements, self-assembled molecules on gold were scanned by the AFM in tapping mode. Figure 4.28 shows the AFM scan of a SAM of octanedithiol on gold. Figure 4.29 shows distinct families of *I-V* curves of hexanethiol (C6) and octanethiol (C8) Au-alkanethiol-Pt junctions (absolute value of current is displayed).   *I-V* data for hexanethiol shows a three order of magnitude higher than octanethiol molecules. The average junction resistances with hexanethiol and octanethiol molecules were 4.6 MΩ and 12.3 GΩ respectively.

I have observed an exponential decrease in current with increasing barrier width (length of the molecule). The current magnitudes through hexanethiol and octanethiol junctions are in the range of nano and pico amperes, respectively. Therefore, I observed that the conduction

mechanism through alkanethiol is tunneling. Figure 4.30 shows the *I-V* traces of monothiolated porphyrin chemisorbed on Au/mica. *I-V* data observed illustrates a symmetric behavior for the applied bias between ± 0.8 V. The symmetrical *I-V* traces could be because of the symmetrical structure of the porphyrin. The variations in current values around ± 0.4 V are also symmetrical, and this could be accounted for by the complex and symmetric structure of porphyrin. The average junction resistance for a monothiolated porphyrin junction is approximately 6.4 GΩ. The current magnitude through the Au-porphyrin-Pt junction is observed in the order of pico-amperes (pA). Figure 4.31 shows the semilog plot of *I-V* traces of a metal-porphyrin-metal junction.
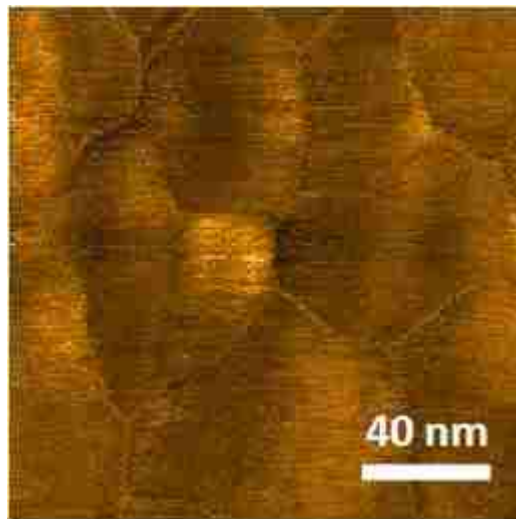
Figure 4.28: AFM scan of self-assembled octanedithiol on gold.

Effect of Surface Interaction on AFM Tips

SEM images of AFM tips illustrate the effect of surface interaction upon these tips. Figure 4.32 shows an SEM image of a Ti/Ir coated conductive probe prior to making contact with the molecules on the sample surface. Figure 4.33 shows an SEM image of a Ti/Ir coated

conductive probe after the tip is in contact with the sample surface and retracted. These SEM images clearly illustrate that the radius of curvature of the tip is changed drastically due to the impact of surface interactions. Damage may have been caused either by sample motion upward against the tip due to unstable mounting or by the contact area of the metal-molecule junction.

The fact that the contact resistance varies over orders of magnitude is very likely given the changes in contact area due to surface interactions. *I-V* traces could vary with the junction area, different materials used to build metal-molecule-metal junction, the barrier height (length of the molecules), and the type of barrier (type of molecular structure).
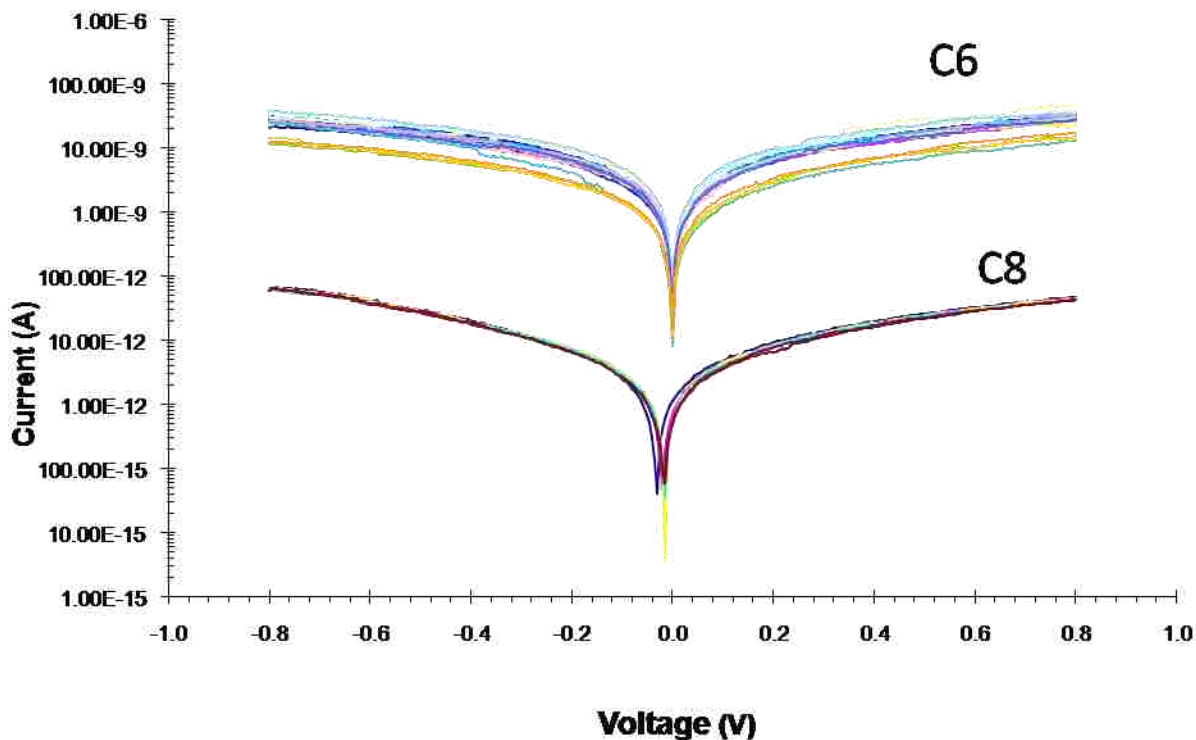
Figure 4.29: Log plot of *I-V* traces of C6, and C8 Au-alkanethiol- Pt junction.
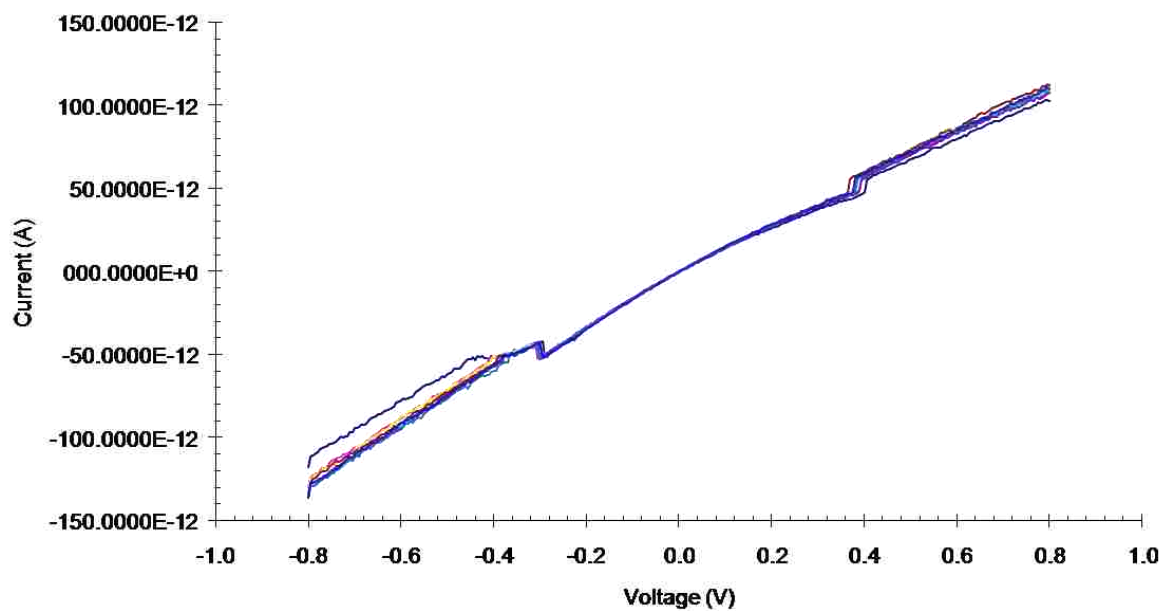
Figure 4.30: Current-voltage data on monothiolated porphyrin self-assembled on gold/mica.
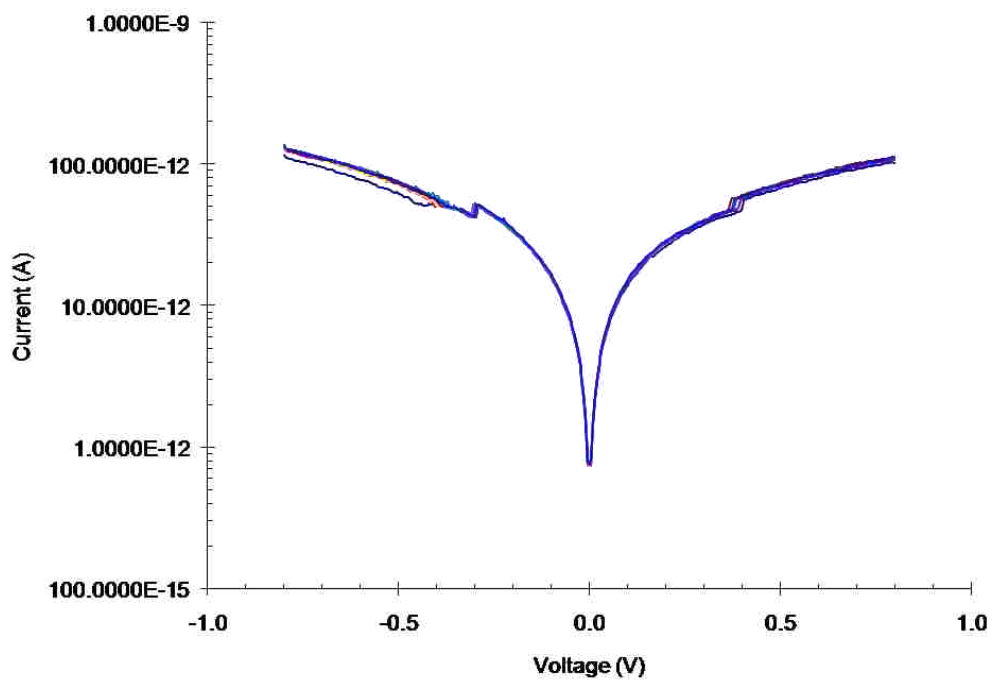
Figure 4.31: Log plot of *I-V* traces of Au-Porphyrin- Pt junction.
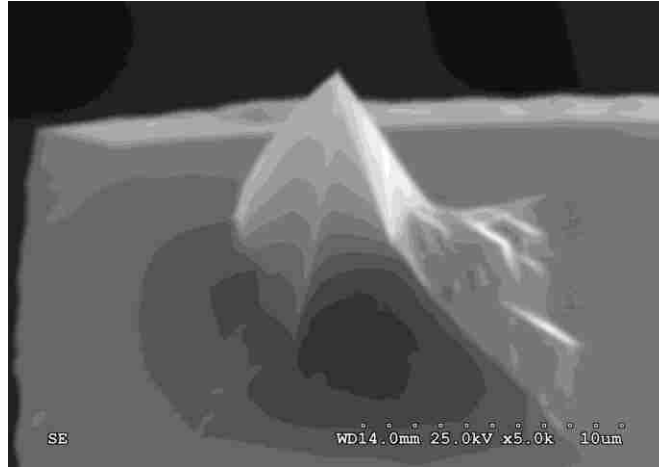
Figure 4.32: SEM image of Pt/Ir coated AFM probe.
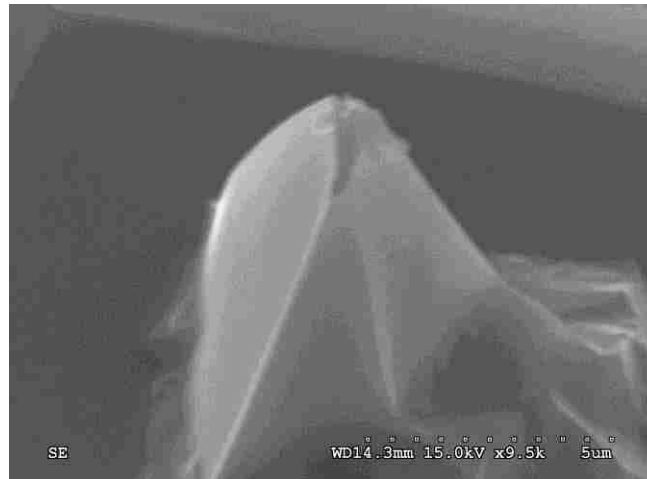
Figure 4.33: SEM image of Pt/Ir coated tip with deformations due to surface interactions.

Extensive usage of tips could be a reason for a change in the level of tip contamination. The variation in junction resistance, as seen in Figure 4.29 could also imply tip contamination and the effect of surface interaction on tip deformation. Although surface interaction on AFM tips is observed, the CP-AFM technique still provides a good method to measure junction

113

resistance if care is taken to reduce the effect of these interactions. For instance, in this work I have used the conductive tips for a limited number of times to establish the metal-molecule-metal junction. This degradation may be less likely in the case of surface modified AFM tips. These factors would have a stronger impact on the junction resistance than an increase in contact area.

4.5.3 General I-V Behavior

Figure 4.27 shows that current-voltage traces of Au- porphyrin-Pt junction behave sigmoidally according to the Simmons Equation[20] for tunneling through a square barrier,

$$I = \frac{qA}{4\pi^2\hbar^2 s^2}\{ (\phi - \frac{qV}{2}).\exp(-\frac{2s\sqrt{2m}}{\hbar}\sqrt{\phi - \frac{qV}{2}}) - (\phi + \frac{qV}{2}).\exp(-\frac{2s\sqrt{2m}}{\hbar}\sqrt{\phi + \frac{qV}{2}})\} \qquad \textbf{(4.1)}$$

where A is the junction area, s is the width of the barrier, m is the electron mass, and ϕ is the barrier height. In the low-bias regime, current is essentially linear with applied voltage and increases exponentially at higher applied voltages approaching $\phi/2$.

By using a contact area of ~50 nm in diameter, I conclude that the conduction mechanism through porphyrin is tunneling. Tunneling through porphyrin SAMs has been assumed to be "through-bond" tunneling. Based on the applied bias (V) as compared to barrier potential (ϕ), the tunneling through a SAM layer can be categorized into either direct (V < ϕ) or through-bond tunneling (V > ϕ). *I-V* traces indicate no obvious "through-bond" tunneling, thus determining that the barrier height is larger than the applied bias for $\phi > 0.8$ eV. This study is restricted to applied biases ± 0.8V. The transition from direct to through-bond tunneling requires higher bias. Having established tunneling as the conduction mechanism, I can now obtain the barrier height by comparing the experimental *I(V)* data with theoretical calculations from a tunneling model.

The *I-V* behavior of a porphyrin monolayer follows this general form and is shown in Figure 4.34. I obtained the potential barrier or energy gap of porphyrin (ø) as 2.52 eV from the theoretical model.

I-V Measurements of Porphyrin Molecule

Practical
Theoretical

Data: Append1_E
Model: MolecularJunctionIV
Weighting:
C   No weighting

Chi^2/DoF   = 5.4829E-23
R^2   = 0.98766

a   5.024E-15   ±0
q   1.6E-19±0
h   6.626E-34   ±0
m   9.1E-31±0
s   1.3E-9 ±0
phi   4.0605E-19   ±2.53E-22
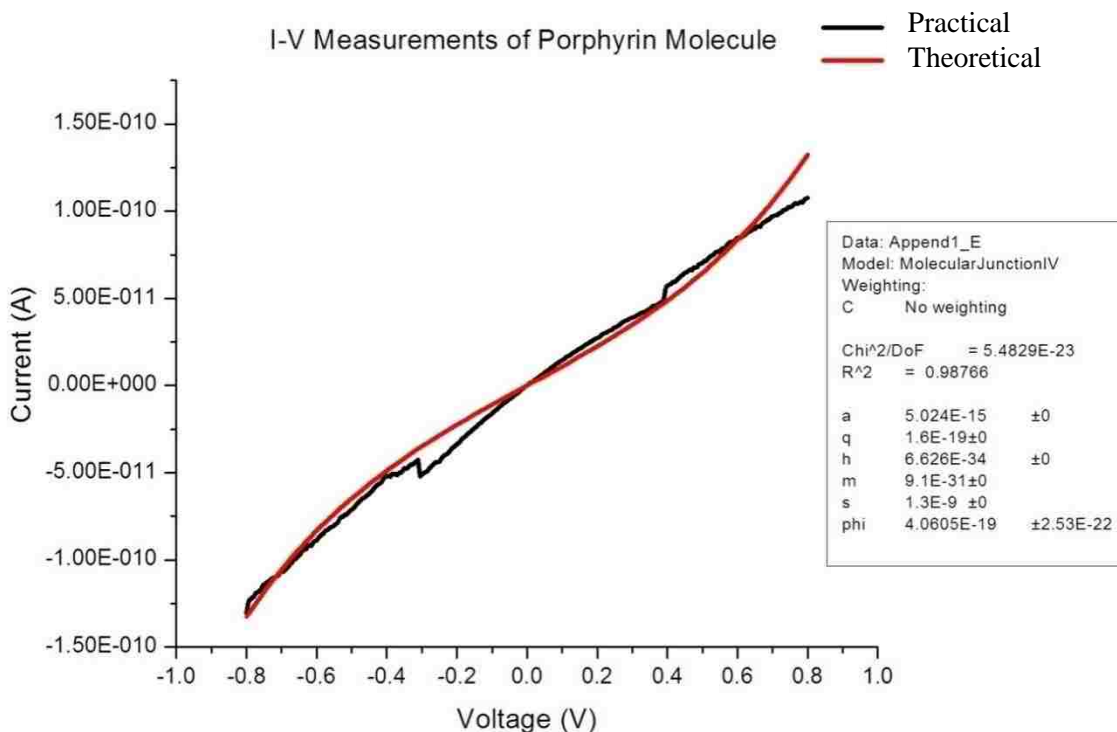
Figure 4.34: Theoretical prediction as per Eq 4.1 and experimental fit for the *I-V* trace of a Au-Porphyrin-Pt junction. Inset shows the fit parameters and obtained potential barrier.

4.6 CONCLUSIONS AND FUTURE WORK

4.6.1 Conclusions

Molecular tunneling junctions were formed using CP-AFM to contact SAMs on gold substrates. The electron transport mechanisms of single molecules have been studied using a CP-AFM. It has been demonstrated that extensive usage of tips has adverse effects on surface interactions. *I-V* traces of alkanethiols illustrate the change in average junction resistance with

respect to the barrier width (length of the molecule). Characterization and analysis of free base porphyrin as a potential component of hybrid electronic devices has been investigated. Current-Voltage characteristics of porphyrin behave sigmoidally according to the Simmons equation for tunneling through a square barrier. I also showed that the electron transport mechanism through porphyrin is direct tunneling for the applied bias levels. I obtained the barrier height of porphyrin as approximately 2.52 eV by comparing the experimental *I(V)* data with theoretical modeling data. The barrier height of porphyrin obtained by fluorescence measurements and CP-AFM study are 2.95 eV and 2.52 eV, respectively. The difference in the barrier height of porphyrin could be due to the area of contact in CP-AFM.

4.6.2 Future Work

CP-AFM has been used in this work to study the materials characteristics and resultant effects upon electron transport in a metal-molecule-metal system. The average tip contact area resulted in contact to several molecules in the host matrix. There are, in fact, more parameters to be investigated in order to more closely study the *I-V* characteristics of single porphyrin molecules. First, the transition from direct to through-bond tunneling requires higher bias. Second, on average the effective area of a CP-AFM tip is around 50 nm in diameter, and attempting to probe a single molecule with this tip in contact mode would result in measuring the electron transport through the molecule of interest as well as that of the surrounding host matrix. Since the exchange of molecules is most active at SAM defect sites, substrate step edges, and substrate vacancy islands, a mixed monolayer of SAM (direct self-assembly) molecules of porphyrin with a dithiol functional group can be inserted into the isolating host matrix. This would allow one to fine tune the area under study. Third, immobilizing functionalized nanoparticles on the mixed monolayer, allows the terminal thiol group of the porphyrin chain to anchor with the nanoparticles. This forms a metal-molecule-metal junction that can be probed

using CP-AFM. The functionalized nanoparticles used to anchor the molecules could form a cluster, and contact more than one molecule. The adhesive force between the sample and the tip could be controlled by imaging under toluene or other organic solvents. This enables measurement of the single molecule transport mechanism without a tunneling barrier. Fourth, instead of free base porphyrin, metal substituted porphyrin derivatives can be used to form the metal/ metallic-porphyrin-derivatives/metal hetereojunction and investigate using CP-AFM. Study of the electron transport mechanism of metallic-porphyrin could lead to different electronic properties such as switches, negative differential resistance, and memory elements.

.

BIBILIOGRAPHY

1. F. Sawano, I. Terasaki, H. Mori, T. Mori, M. Watanabe, N. Ikeda, Y. Nogami, and Y. Noda, Nature , 2005, 437, 522-524.

2. Z. Shen, P. E. Burrows, V. Bulovic, S. R. Forrest, M. E. Thompson, Science, 1997, 276, 2009-2011.

3. C. Li, W. Fan, B. Lei, D. Zhang, S. Han, T. Tang, X. Liu, Z. Liu, S. Asano, M. Meyyappan, J. Han and C. Zhou, App. Phy. Lett, 2004, 84, 1949-1951.

4. Z. Liu, A. A. Yasseri, J. S. Lindsey, D. F. Bocian, Science, 2003, 302, 1543-1545.

5. G. Eres and J.W. Sharp, J. Appl. Phys., 1993, 74, 7241-7450.

6. M. A. Reed and T. Lee, "Molecular Nanoelectronics", 2003, 6, 153-173.

7. A. Aviram and M. A. Ratner, Chem. Phys. Lett., 1974, 29, 277-283.

8. G. Cuniberti, G. Fagas, and K. Richter, Introducing Molecular Electronics: A Brief Overview, Lect. Not. Phys., 2005, 680, 1.

9. A. S. Gyorgyi, Science, 1941, 93, 609-611.

10. R. P. Feynman, *Engineering and Science*, 1960, 23, 22-36.

11. James R. Heath and Mark A. Ratner, Physics Today, 2003, 43-49.

12. J. Gu, S. Tanaka, Y. Otsuka, H. Tabata, and T. Kawai, App. Phys. Lett., 2002, 80, 688-690.

13. J. Gu, L. Cai, S. Tanaka, Y. Otsuka, H. Tabata, and T. Kawai, J. App. Phys., 2002, 92, 2816-2820.

14. J. Koo, H. Lee, Y. Ha, Y. Choi, Y. Kim, Thin Solid Films, 2003, 123-127.

15. T. Tsujioka and H. Kondo, App. Phys. Lett., 2003, 83, 937-939.

16. H.L. Kwok and J.B. Xu, IEE Proc.-Nanobiotechnol., 2004, 151, 48-52.

17. C. Nogues, S. R. Cohen, S. S. Daube and R. Naaman, Phys. Chem. Chem. Phys., 2004, 6,4459-4466.

18. G. E. Moore, Electronics, 1965, 38 (8).

19. Images obtained from the Jobin Yvon Horiba, Inc:
http://www.jobinyvon.com/usadivisions/Fluorescence/product/flogcat.pdf

20. V. B. Engelkes, J. M. Beebe, and C. D. Frisbie, J. Am. Chem. Soc., 2004, 126, 14287-14296.

21. M. D. Porter, T. B. Bright, D. L. Allara, and C. E. D. Chidsey, J. Am. Chem. Soc., 1987, 109, 3559-3568.

22. Y. Chen and Z. Rosenzweig, Anal. Chem., 2002, 74, 5132-5138.

23. J. G. Kushmerick, D. B. Holt, J. C. Yang, J. Naciri, M. H. Moore, and R. Shashidhar, Phys. Rev. Lett., 2002, 89, 086802(4).

24. S. Yasutomi, T. Morita, Y. Imanishi, and S. Kimura, Science, 2004, 304, 1944-1947.

25. M. A. Reed, J. Chen, A. M. Rawlett, D. W. Price, and J. M. Tour, Appl. Phys. Lett., 78, 3735-3737.

26. X. D. Cui, A. Primak, X. Zarate, J. Tomfohr, O.F. Sankey, A. L. Moore, T. A. Moore, D. Gust, L. A. Nagahara, and S. M. Lindsay, J. Phys. Chem. B, 2002, 106, 8609-8614.

27. G. Binning, H. Rohrer, Ch. Gerber, and E. Weibel, Phys. Rev. Lett., 1982, 49, 57-61.

28. C.K. Chiang, Y.W. Park, A.J. Heeger, H. Shirakawa, E. J. Louis, and A. G. MacDiarmid, J. Chem. Phys., 1978, 69, 5098-5104.

29. M.A. Reed, Proc. IEEE, 1999, 87, 652-658.

30. S. Lodha and D. B. Janes, Appl. Phys. Lett., 2004, 85, 2809-2811.

31. A. Balandin, K. L. Wang, N. Koukin and S. Bandyopadhyay, Appl. Phys. Lett., 2000, 76, 137-139.

32. K. M. Roth, N. Dontha, R. B. Dabke, D. T. Gryko, C. Clausen, J. S. Lindsey, D. F. Bocian, and W. G. Kuhr, 2000, J. Vac. Sci. Technol. B, 18, 2359-2364.

33. C. Li, D. Zhang, X. Liu, S. Han, T. Tang, C. Zhou, W. Fan, J. Koehne, M. Meyyappan, A. M. Rawlett, D. W. Price, and J. M. Tour, Appl. Phys. Lett., 2003, 83, 645-647.

34. A. Salomon, D. Cahen, S. Lindsay, J. Tomfohr, V. B. Engelkes, and C. D. Frisbie, Adv. Mater., 2003, 15, 1-10.

35. J. Yang, C. Lee, S. Yau, C. Chang, C. Lee, and J. Leu, J. Org. Chem., 2000, 65, 871-877.

36. S. Chen, L. Li, C. L. Boozer, and S. Jiang, J. Phys. Chem. B, 2001, 105, 2975-2980.

37. M. T. Cygan, T. D. Dunbar, J. J. Arnold, L. A. Bumm, N. F. Shedlock, T. P. Burgin, L. Jones II, D. L. Allara, J. M. Tour, and P. S. Weiss, J. Am. Chem. Soc., 1998, 120, 2721-2732.

38. B. A. Mantooth and P. S. Weiss, Proceedings of the IEEE, 2003, 91, 1785-1802.

39. J. M. Beebe, V. B. Engelkes, J. Liu, J. Gooding, P. K. Eggers, Y. Jun, X. Zhu, M. N. Paddon-Row, and C. D. Frisbie, J. Phys. Chem. B, 2005, 109, 5207 – 5215.

40. D. Li, B. I. Swanson, J. M. Robinson, and M.. A. Goffbauer, J. Am. Chem. Soc., 1993, 115, 6975-6980.

41. C. A. Hacker, J. D. Batteas, J. C. Garno, M. Marquez, C. A. Richter, L. J. Richter, R. D. vanZee, and C. D. Zangmesiter, Langmuir, 2004, 20, 6195-6205.

42. O. Cavalleri, G. Gonella, S. Terreni, M. Vignolo, L. Foleano, A. Morgante, M. Canepa, and R. Rolandi, Phys. Chem. Chem. Phys., 2004, 6, 4042-4046.

43. X. D. Cui, A. Primak, X. Zarate, J. Tomfohr, O. F. Sankey, A. L. Moore, T. A. Moore, D. Gust, G. Harris, and S. M. Lindsay, Science, 2001, 294, 571-573.

44. W. Wang, T. Lee, and M. A. Reed, Physical Review B, 2003, 68, 035416(7).

45. W. Wang, T. Lee, M. A. Reed, M. P. Stewart, J. J. Hwang, and J. M. Tour, Superlattices and Microstructures, 2003, 33, 217-226.

46. D. J. Wold and C. D. Frisbie, J. Am. Chem. Soc., 2001, 123, 5549-5556.

47. J. Zak, H. Yuan, M. Ho, L. K. Woo, and M. D. Porter, Langmuir, 1993, 9, 2772-2774.

48. M. A. Reed, C. Zhou, C. J. Muller, T. P. Burgin, and J. M. Tour, Science, 1997, 278, 252-254.

49. J. Reichert, R. Ochs, D. Beckmann, H. B. Weber, M. Mayor, and H. V. Lohneysen, Phys. Rev. Lett., 2002, 88, 176804(4).

50. C. Zhou, M. R. Deshpande, M. A. Reed, L. Jones II and J. M. Tour, Appl. Phys. Lett., 1997, 71, 611-613.

51. J. Chen, W. Wang, J. Klemic, M. A. Reed, B. W. Axelrod, D. M. Kaschak, A. M. Rawlett, D. W. Price, S. M. Dirk, J. M. Tour, D. S. Grubisha, D. W. Bennett, "Molecular wires, switches, and memories", Molecular Electronics II, Ann. N.Y. Acad. Sci., 2002, 960, 69-99.

52. J. Chen, W. Wang, M. A. Reed, M. Rawlett, D. W. Price, and J. M. Tour, Appl. Phys. Lett., 2000, 77, 1224-1226.

53. K. A. Fletcher, S. O. Fakayode, M. Lowry, S. A. Tucker, S. L. Neal, I. W. Kimaru, M. E. McCarroll, G. Patonay, P. B. Oldham, O. Rusin, R. M. Strongin, and I. M. Warner, Anal. Chem., 2006, 78, 4047 – 4068.

54. S. Sapra and D. D. Sarma, Electronic Structure and Spectroscopy of Semiconductor Nanocrystal, Solid State and Structural Chemistry Unit, Indian Institute of Science, Bangalore, India, 1-51.

55. L. M. peter, D. J. Riley, E. J. Tull and K. G. U. Wijayantha, Chem. Commun., 2002, 1030-1031.

56. J. Chen and C. Zhu, Analytica Chimica Acta, 2005, 546, 147-153.

57. R. Kho, C. L. Torres-Martinez, and R. K. Mehra, J. Colloid and Interface Science, 2000, 227, 561-566.

58. S. F. Wuister, and A. Meijerrink, J. Luminescence, 2003, 105, 35-43.

59. Y. Chan, J. S. Steckel, P. T. Snee, J. M. Caruge, J. M. Hodgkiss, D. G. Nocera, and M. G. Bawendi, App. Phys. Lett., 2005, 86, 73102(3).

60. A. Mews, A. V. Kadavanich, U. Banin, and A. P. Aliviasatos, Physical Review B, 1996, 53, 13242-13245.

61. K. Sookal, L. H. Hanus, H. J. Ploehn, and C. J. Murphy, Advanced Materials, 1998, 10, 1083-1087.

62. E. P. A. M. Bakkers, E. Reitsma, J. J. Kelly, and D. Vanmaekelbergh, J. Phys. Chem. B, 1999, 103, 2781-2788.

63. J. Li and J. Xia, Physical Review B, 2000, 62, 12613-12616.

64. Yu. P. Rakovich, A. G. Rola, M. V. Stepikhova, M. I. Vasilevskiy, M. J. M. Gomes, M. V. Artemyev, W. Jantsch, W. Heiss, and G. Prechtl, Mat. Res. Soc. Symp. Proc., 2000, 571, 69-74.

65. S. Sapra, J. Nanda, D. D. Sarma, F. Abed El-Al and G. Hodes, Chem. Commun., 2001, 2188-2189.

66. A. Kuhnle, T. R. Linderoth, B. Hammer and F. Besenbacher, Nature, 2002, 415, 891-893.

67. G. Gonnella, S. Terreni, D. Cvetko, A. Cossaro, L. Mattera, O. Cavalleri, R. Rolandi, A. Morgante, L. Floreano, and M. Canepa, J. Phys. Chem. B, 2005, 109, 18003-18009.

68. S. Ogawa, F. F. Fan, and A. J. Bard, J. Phys. Chem., 1995, 99, 11182-11189.

69. M. Pope, H. P. Kallmann, and P. Magnante, J. Chem. Phys., 1963, 38, 2042-2043.

70. W. Helfrich and W. G. Schneider, Phys. Rev. Lett., 1965, 14, 229-231.

71. W. Helfrich and F. R. Lipsett, J. Chem. Phys., 1965, 43, 4368-4376.

72. C. D. Dimitrakopoulos and D. J. Mascaro, IBM J. Res. & Dev., 2001, 45, 11-27.

73. D. T. Gryko, C. Clausen, K. M. Roth, N. Dontha, D. F. Bocian, W. G. Kuhr, and J. S. Lindsey, J. Org. Chem., 2000, 65, 7345-7355.

74. D. T. Gryko, F. Zhao, A. A. Yasseri, K. M. Roth, D. F. Bocian, W. G. Kuhr, and J. S. Lindsey, J. Org. Chem., 2000, 65, 7356-7362.

75. C. Clausen, D. T. Gryko, R. B. Dabke, N. Dontha, D. F. Bocian, W. G. Kuhr, and J. S. Lindsey, J. Org. Chem., 2000, 65, 7363-7370.

76. C. Clausen, D. T. Gryko, A. A. Yasseri, J. R. Diers, D. F. Bocian, W. G. Kuhr, and J. S. Lindsey, J. Org. Chem., 2000, 65, 7371-7378.

77. J. Li, D. Gryko, R. B. Dabke, J. R. Diers, D. F. Bocian, W. G. Kuhr, and J. S. Lindsey, J. Org. Chem., 2000, 65, 7379-7390.

78. F. J. Kampas, K. Yamashita and J. Fajer, Nature, 1980, 284, 40-42.

79. J. A. Strickland, L. G. Marzilli, K. M. Gay, and W. D. Wilson, Biochemistry, 1988, 27, 8870-8878.

80. A. D. Schwab, D. E. Smith, B. Bond-Watts, D. E. Johnson, J. Hone, A. T. Johnson, J. C. de Paula, and W. F. Smith, Nano Letters, 2004, 4, 1261-1265.

81. G. Binning, C. F Quate, and Ch. Gerber, Phys. Rev. Lett., 1986, 56, 930-934.

82. O. Marti, B. Drake, and P.K. Hansma, Appl. Phys. Lett., 1987, 51, 484-486.

83. T. R. Albrecht and C. F. Quate, J. Appl. Phys., 1987, 62, 2599-2602.

84. M. D. Kirk, T. R. Albrecht, and C. F. Quate, Rev. Sci. Instrum., 1988, 59, 833-835.

85. G. Meyer and N. M. Amer, Appl. Phys. Lett., 1988, 53, 1045-1047.

86. U. Hartmann, Physical Review B, 1991, 43, 2404-2407.

87. F. O. Goodman and N. Garcia, Physical Review B, 1991, 43, 4728-4731.

88. A. L. Weisenhorn, M. Egger, F. Ohnesorge, S. A. Gould, S.P. Heyn, H. G. Hansma, R. L. Sinsheimer, H. E. Gaub, and P. K. Hansma, Langmuir, 1991, 7, 8-12.

89. V. B. Engelkes, J. M. Beebe, and C. D. Frisbie, J. Phys. Chem., 2005, 109, 16801-16810.

90. Images obtained from the Pacific Nanotechnology, Inc:
    http://www.pacificnanotech.com/afm-tutorial_afm-instrumentation.html

91. M. Strukelj, R. H. Jordan, and A. Dodabalapur, J. Am. Chem. Soc., 1996, 118, 1213-1214.

92. A. Chattopadhyay, and H. Raghuraman, Current Science, 2004, 87, 175-180.

93. C. Beaufils, C. Alexopoulos, M. P. Petrakai, A. D. Tselepis, N. Coudevylle, M. Sakarellos-Daitsiotis, C. Sakarellos, and M. Thong Cung, Peptide Science, 2006, 88, 362- 372.

94. N. C. Maiti, M. Ravikanth, S. Mazumdar, and N. Periasamy, J. Phys. Chem., 1995, 99, 17192-17197.

95. S. Prathapan, T. E. Johnson, and J. S. Lindsey, J. Am. Chem. Soc., 1993, 115, 7519-7520.

96. R. Nishitani, H. Liu, A. Kasuya and H. Iwasaki, J. Physics: Conference Series, 2007, 61, 879-883.

97. H. W. Liu, Y. Ie, R. Nishitani, Y. Aso, and H. Iwasaki, Physical Review B, 2007, 75, 115429(5).

98. T. Arockiadoss, N.S. Sundaram, F.P. Xavier, S. Thiruvengadam, T. Daniels-Race, Marybabu, "Development of Collagen Based Organic Semiconductor", AVS 52 International Symposium, Boston, MA, USA, October 30 – November 4, 2005.

APPENDIX A: PERMISSION TO USE COPYRIGHTED MATERIAL

A1.

From: Jones, Jennifer (ELS-OXF) [mailto:J.Jones@elsevier.co.uk]
Sent: Monday, June 25, 2007 9:36 AM
To: sthiru@cct.lsu.edu
Cc: USJCS (ELS-ORL)
Subject: RE: Requesting permission

ELSEVIER

Dear Sathish Thiruvengadam

We hereby grant you permission to reprint the material detailed below at no charge **in your thesis** subject to the following conditions:

1.   If any part of the material to be used (for example, figures) has appeared in our publication with credit or acknowledgement to another source, permission must also be sought from that source. If such permission is not obtained then that material may not be included in your publication/copies.

2.   Suitable acknowledgment to the source must be made, either as a footnote or in a reference list at the end of your publication, as follows:

   "This article was published in Publication title, Vol number, Author(s), Title of article, Page Nos, Copyright Elsevier (or appropriate Society name) (Year)."

3.   Your thesis may be submitted to your institution in either print or electronic form.

4.   Reproduction of this material is confined to the purpose for which permission is hereby given.

5.   This permission is granted for non-exclusive world **English** rights only. For other languages please reapply separately for each one required. Permission excludes use in an electronic form other than submission. Should you have a specific electronic project in mind please reapply for permission

6.   This includes permission for UMI to supply single copies, on demand, of the complete thesis. Should your thesis be published commercially, please reapply for permission.

Yours sincerely

Jennifer Jones
Rights Assistant

Your future requests will be handled more quickly if you complete the online form at www.elsevier.com/permissions

A2.

From: Giorgos Fagas [mailto:gfagas@tyndall.ie]
Sent: Tuesday, July 25, 2006 6:17 AM
To: sthiru@cct.lsu.edu
Subject: re: citation reference- addendum

Dear Sathish,

Many thanks for your note. I would be glad if you used the figure as you inquire. You may wish, however, to get also permission from the Springer editors who have the copyright (for further info and inquiries you may check the website http://www.springer.com/east/home/contact?SGWID=5-40103-0-0-0).

The citation should read

G. Cuniberti, G. Fagas, and K. Richter, Introducing Molecular Electronics: A Brief Overview, Lect. Not. Phys. 680, 1 (2005)

Unfortunately, the original high-quality copy is difficult to retrieve from the labyrinth of my archives. In any case, I attach another copy that it will hopefully do.

Best regards and all the best with completing your thesis,
Giorgos Fagas

A3.

ok with me
best
mark

At 05:54 PM 6/21/2007, you wrote:

Dear Sir/Madam,
I am Sathish Thiruvengadam, graduate student from Louisiana State University, Louisiana, USA. I am currently working on hybrid electronics regime and in the verge of completing my thesis chapters. I read the book cited: **Molecular Nanoelectronics, edited by Mark A. Reed and Takhee Lee, 2003.** I would like to use the table 1. Possible conduction mechanisms of page 89 in this book for my thesis literature review chapter. Kindly looking forward to get your permission to use is table in my thesis.

Looking forward to hearing from you. Thanks in advance for your time and consideration

Sincerely,
Sathish Thiruvengadam

A4.

ok

At 06:04 PM 6/21/2007, you wrote:

Dear Sir/Madam
I am Sathish Thiruvengadam, graduate student from Louisiana State University, Louisiana, USA. I am currently working on hybrid electronics regime and in the verge of completing my thesis chapters. I read the article cited: **M. A. Reed, C. Zhou, C. J. Muller, T. P. Burgin, and J. M. Tour, Science, 1997, 278, 252-254** (attached here). I would like to use the Figure 3 of page 253 in this article for my thesis literature review chapter. Kindly looking forward to get your permission to use is table in my thesis.
Looking forward to hearing from you. Thanks in advance for your time and consideration

Sincerely,
Sathish Thiruvengadam

A5.

From: Wilson Laura [mailto:Laura.Wilson@oxon.blackwellpublishing.com] **On Behalf Of** Journals Rights
Sent: Monday, June 25, 2007 5:47 AM
To: sthiru@cct.lsu.edu
Subject: FW: Citation requst

Thank you for your email request. Permission is granted for you to use the material below for your thesis/dissertation subject to the usual acknowledgements and on the understanding that you will reapply for permission if you wish to distribute or publish your thesis/dissertation commercially.

Best wishes
Laura Wilson.

Permissions Controller
Wiley-Blackwell
PO Box 805
9600 Garsington Road
Oxford
OX4 2ZG
United Kingdom

Fax: 00 44 1865 471150

Permission requests can now be sent to journalsrights@oxon.blackwellpublishing.com

A6.

June 25, 2007

Sathish Thiruvengadam
Graduate Research Assistant
Electrical and Computer Engineering
Louisiana State University

Ref # 5155

Thank you for your permission request dated June 25, 2007. We are pleased to grant you a non-exclusive, non-transferable permission, English rights, limited to **print and electronic format**, provided you meet the criteria outlined below. Permission is for a one-time use and does not include permission for future editions, updates, databases, translations, or any other matters. Permission must be sought for each additional use. This permission does not include the right to modify APS material.

Please print the required copyright credit line on the first page that the material appears: "Reprinted (abstract/excerpt/figure) with permission from [FULL REFERENCE CITATION] as follows: authors names, journal title, volume number, page number and year of publication. Copyright (YEAR) by the American Physical Society.

The following language must appear somewhere on the website: "Readers may view, browse, and/or download material for temporary copying purposes only, provided these uses are for noncommercial personal purposes. Except as provided by law, this material may not be further reproduced, distributed, transmitted, modified, adapted, performed, displayed, published, or sold in whole or part, without prior written permission from the American Physical Society."

Provide a hyperlink from the reprinted APS material (the hyperlink may be embedded in the copyright credit line). APS's link manager technology makes it convenient and easy to provide links to individual articles in APS journals. For information, see: http://publish.aps.org/linkfaq.html

You must also obtain permission from at least one of the authors for each separate work, if you haven't done so already. The author's name and address can be found on the first page of the published Article.

Use of the APS material must not imply any endorsement by the American Physical Society.

Permission is granted for use of the following APS material only:
- Fig. 1a, Phys Rev. Lett., Vol. 89, 086802 (2002)

Permission is limited to the single title specified or single edition of the publication as follows:
- Thesis

If you have any questions, please refer to the Copyright FAQ at: http://forms.aps.org/author/copyfaq.html or contact me at assocpub@aps.org.

Sincerely,

Eileen LaManca
Marketing Assistant

A7.

From: PS Weiss [mailto:stm@psu.edu]
Sent: Thursday, June 21, 2007 6:09 PM
To: sthiru2@lsu.edu
Subject: Re: Request for citation
Yes, you may use those figures.
Do you need higher quality versions?

Yours,
Paul

Paul S. Weiss
Distinguished Professor of Chemistry and Physics
104 Davey Laboratory
The Pennsylvania State University
University Park, PA   16802-6300, USA
+1 (814) 865-3693 voice & messages
+1 (814) 863-5516 fax
stm@psu.edu
http://www.nano.psu.edu/
+1 (814) 865-7817 staff assistant, Stephen Bumbarger, sxb10@psu.edu
ACS Nano, Editor-in-Chief
editor@nano.psu.edu

A8.

From: sarma.dd@gmail.com [mailto:sarma.dd@gmail.com] On Behalf Of D. D. Sarma
Sent: Saturday, June 23, 2007 6:18 AM
To: sthiru2@lsu.edu
Subject: Re: citation request

Dear Mr. Sathish Thiruvengadam,

We have no problem if you use these figures in your thesis.

Wishing you the very best with your thesis submission,

D. D. Sarma

A9.

From: Karen Gonda [mailto:gonda@us.ibm.com]
Sent: Friday, June 22, 2007 3:53 PM
To: sthiru2@lsu.edu
Subject: IBM Copyright Permission #12956

Dear Mr. Thiruvengadam:

With the understanding that use will be tailored as described in your June 22, 2007 submission
below, your request to use IBM copyrighted material has been approved. The permission
agreement below provides the terms and conditions of this approval.

Thank you for contacting IBM.

Karen Gonda
IBM Corporation
External Submissions
extsub@us.ibm.com
https://www-01.ibm.com/contact/submissions/extsub.nsf/copyright

**INTERNATIONAL BUSINESS MACHINES CORPORATION (IBM) ARMONK, NEW
YORK 10504**

PERMISSION TO REPRINT IBM COPYRIGHTED PUBLICATIONS
IBM grants permission to Sathish Thiruvengadam to reproduce the following in his thesis:

1) Figures 2, 3 and 5 on pg. 279: Aviram and Ratner, Chem. Phys. Lett., 1974, 29 (2), 277-283
2) Figure 1 on pg. 1045: Gerhard Meyer and Nabil M. Amer, Appl. Phys. Lett., 1988, 53 (12),
1045-1047.

APPENDIX B: ADDITIONAL INFORMATION CONCERNING AFM AND FLUORESCENCE

B1. Scanning Probe Microscopy

The scanning probe technique, including both STM and CP-AFM, has been an invaluable tool in the characterization of hybrid electronic properties.[34] Direct measurements of electronic behavior of single molecules can be resolved using scanning probe microscopy. Macroscopic analytical methods such as ellipsometry, FTIR, and XPS have been successfully used to characterize the average film compositions of mixed systems, whereas these real-space techniques offer a molecular scale view of the surface structure. Recent STM investigations have yielded molecular resolution images of both single composition (Figure 1) and mixed composition (Figure 2) SAMs.[38]
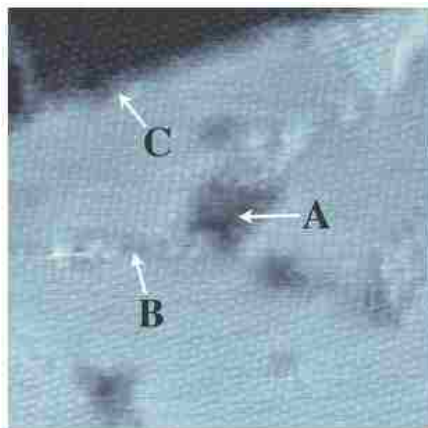

Figure 1: Topographic STM image (250 Å x 250 Å) of a decanethiolate SAM on Au{111}. Inherent defects including (A) substrate vacancies; (B) domain boundaries; and (C) step edges. Reprinted with permission (Appendix A7)
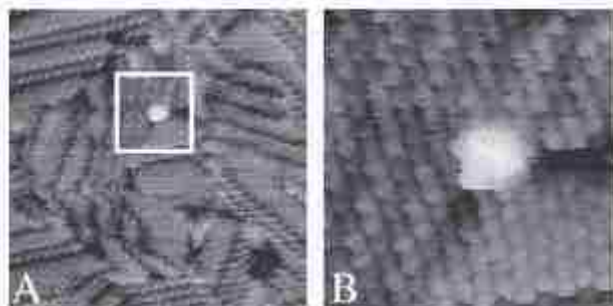
Figure 2: Topographic STM images (200 Å x 200 Å) of a molecular switch molecule inserted in a dodecanethiolate SAM. Reprinted with permission (Appendix A7)

In these images, the positions of the individual molecules can be located and differentiated. This is the beginning of using the imaging a surface to help determine the geometry and chemistry for a specific molecule. Cygan *et al.* showed that molecules can be imbedded in self-assembled n-alkanethiolate films where these SAMs chemically and electrochemically isolate the underlying substrates from their surroundings.[37] The researchers found that molecules of interest (conjugated organic oligomers) can be inserted into alkanethiolate SAMs on Au(111) at film defects such as domain boundaries and step edges without disturbing the overall system. They used a microwave frequency alternating current STM (ACSTM) to make conductivity measurements and found that the inserted conjugated organic oligomers molecule showed greater intensity of conductance compared to the SAM of the dodecanethiolate lattice.

Researchers at the Weizmann Institute characterized single strands of DNA (ssDNA) using conducting AFM.[17] They adapted the technique from Cui *et al*. who developed a method (Figure 3) for measuring the conductivity if single molecules.[26] In this approach, they have used thiolated ssDNA oligomers to form SAMs on gold substrates after hybridization. Reproducible AFM conductivity measurements were obtained in intermittent-contact mode, and significant differences were observed between conductivity in single and double-stranded DNA.

132

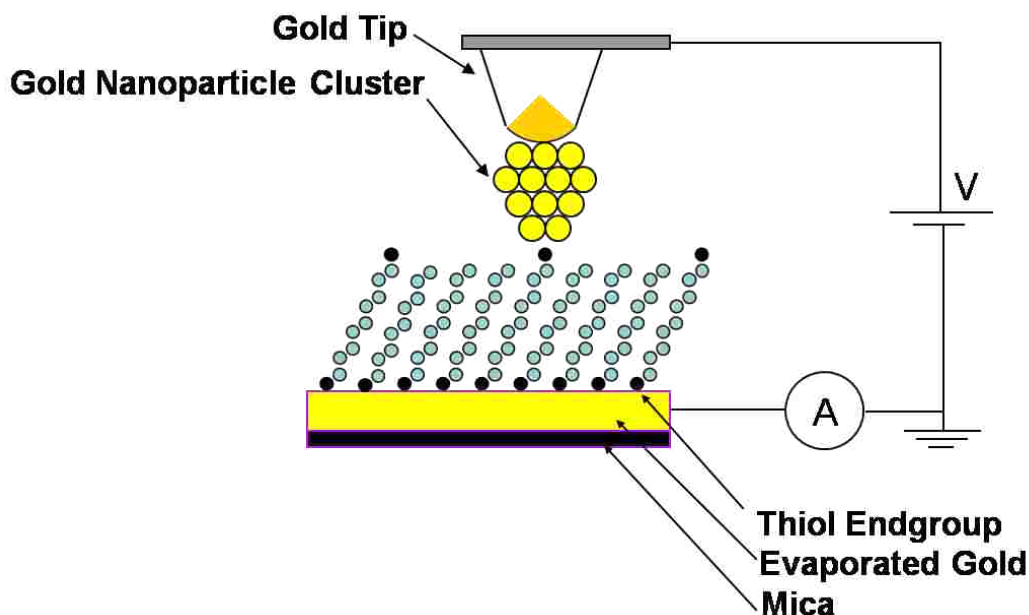More details about the characterization of complex structures using CP-AFM were discussed in Chapter 4.

Figure 3: Schematic layout of the single-molecule contact.

B2. Spectroscopy

Spectroscopy is a characterization technique which helps to study the interaction between radiation (electromagnetic radiation, or light, as well as particle radiation) and matter and to measure these interactions. A plot of the interaction is referred to as a spectrogram, or informally, a spectrum. Spectroscopy is often used in physical and analytical chemistry for the identification of substances with the help of the spectrum emitted from or absorbed by them. The most common type of spectroscopic method used to characterize novel materials is fluorescence spectroscopy. Fluorescence spectroscopy uses higher energy photons to excite a sample, which will then emit lower energy photons. This technique can be used to understand the electron-phonon interactions in colloidal quantum dots and to study how vibrational and

electronic modes are coupled in these systems. Fluorescence spectroscopy has been employed to gain insight into analyte binding and dynamics. It is a very useful technique for investigating molecular dynamic, molecular association, and microstructure within organized media. There are several groups that have employed fluorescence spectroscopy to observe the fluorescence properties of conjugated complexes.[53]

B3. Ellipsometric Film-Thickness Measurements

Ellipsometry was used as a preliminary method to determine the thicknesses of the molecular films. A Rudolph Research AutoFL ellipsometer (Rudolph Instruments), as provided with permission by Prof. David Spivak of the LSU Department of Chemistry, was used to measure the alkyl chain thickness excited with a laser source at 632.8 nm immediately after removal from the SAM deposition process. The complex refractive index for organic film is assumed to be 1.45 (the imaginary part of the complex refractive index equals zero).

Table 1: Molecular thickness for SAM adsorbed on gold.

S. No.	Hexanethiol (Å)	Octanethiol (Å)
1	10.1	12.2
2	8.5	13.0
3	7.7	12.2
4	7.7	13.0
5	9.3	13.0
6	6.9	9.8
7	6.9	10.7
Average Molecular Length	8.16 ± 1.12	11.98 ± 1.2

Optical ellipsometry is applied as a convenient and precise means of determining the average monolayer thickness of the films. The self-assembled monolayers of alkanethiols are formed in toluene solution. The estimated average molecular length of hexanethiol and octanethiol are 8.16 ± 1.12 Å, and 11.98 ± 1.2 Å respectively. These data are shown in Table 1.

VITA

    Sathish Thiruvengadam was born in 1981 in Salem in Tamil Nadu, a southern state of India. He finished his bachelor of engineering in electronics and communication engineering at the Kumaraguru College of Engineering, affiliated to Bharathiyar University, India, in May 2002. He is currently a candidate for the degree of Master of Science in Electrical Engineering in the department of Electrical and Computer Engineering at Louisiana State University.